Ore Geology Reviews 77 (2016) 279–311

Contents lists available at ScienceDirect

Ore Geology Reviews

journal homepage: www.elsevier.com/locate/oregeorev

Economic minerals of the Kovdor baddeleyite-apatite-magnetite deposit, Russia: mineralogy, spatial distribution and ore processing optimization

G.Yu. Ivanyuk [a,b], A.O. Kalashnikov [b,*], Ya.A. Pakhomovsky [a,b], J.A. Mikhailova [a,b], V.N. Yakovenchuk [a,b], N.G. Konopleva [a], V.A. Sokharev [c], A.V. Bazai [a,b], P.M. Goryainov [b]

[a] Nanomaterials Research Centre, Kola Science Centre, Russian Academy of Sciences, 14 Fersman Street, Apatity, Murmansk Region 184209, Russia
[b] Geological Institute, Kola Science Centre, Russian Academy of Sciences, 14 Fersman Street, Apatity, Murmansk Region 184209, Russia
[c] JSC "Kovdorskiy GOK", 5 Sukhachova Street, Kovdor, Murmansk Region 184141, Russia

ARTICLE INFO

Article history:
Received 16 September 2015
Received in revised form 12 February 2016
Accepted 15 February 2016
Available online 19 February 2016

Keywords:
Phoscorite
Carbonatite
Magnetite
Apatite
Baddeleyite
3D mineralogical model

ABSTRACT

The comprehensive petrographical, petrochemical and mineralogical study of the Kovdor magnetite-apatite-baddeleyite deposit in the phoscorite–carbonatite complex (Murmansk Region, Russia) revealed a spatial distribution of grain size and chemical composition of three economically extractable minerals — magnetite, apatite, and baddeleyite, showing that zonal distribution of mineral properties mimics both concentric and vertical zonation of the carbonatite-phoscorite pipe.

The marginal zone of the pipe consists of (apatite)-forsterite phoscorite carrying fine grains of Ti–Mn–Si–rich magnetite with ilmenite exsolution lamellae, fine grains of Fe–Mg-rich apatite and finest grains of baddeleyite, enriched in Mg, Fe, Si and Mn. The intermediate zone accommodates carbonate-free magnetite-rich phoscorites that carry medium to coarse grains of Mg–Al-rich magnetite with exsolution inclusions of spinel, medium-grained pure apatite and baddeleyite. The axial zone hosts carbonate-rich phoscorites and phoscorite-related carbonatites bearing medium-grained Ti–V–Ca-rich magnetite with exsolution inclusions of geikielite–ilmenite, fine grains of Ba–Sr–Ln-rich apatite and comparatively large grains of baddeleyite, enriched in Hf, Ta, Nb and Sc. The collected data enable us to predict such important mineralogical characteristics of the multicomponent ore as chemical composition and grain size of economic and associated minerals, presence of contaminating inclusions, etc. We have identified potential areas of maximum concentration of such by-products as scandium, niobium and hafnium in baddeleyite and REEs in apatite.

1. Introduction

Phoscorites belong to a rare type of igneous rocks in relation to carbonatite magmatism. They predominantly consist of forsterite, magnetite, apatite and carbonates. Phoscorite and carbonatite igneous complexes may host important deposits of Fe, Cu, Nb, PGE, REE, P and Zr (Wall and Zaitsev, 2004): Phalaborwa (South Africa), Sokli (Finland), Catalão (Brasil), Mt. Weld (Australia). The Kovdor phoscorite–carbonatite pipe hosting the Kovdor magnetite-apatite-baddeleyite deposit is a typical example of such deposits. Currently the open pit mine "Zhelezniy" located at the Kovdor deposit produces about 5.7 Mt/year of magnetite concentrate, 2.7 Mt/year of apatite concentrate and 10,000 t/year of baddeleyite concentrate (Eurochem, 2014; Khramov, 2014). The deposit has been mined as an open pit since 1962. Today it is owned by JSC "Kovdorskiy GOK", part of Eurochem Corporation. Resources of Russian A + B + C1 categories (approximately corresponding to measured resources in JORC classification) amount to 267 Mt, while the resources of C2 category (approximate equivalent of indicated resources) are 219.7 Mt at grades (average for all categories) of 27 wt.% Fe_{total}, 6.8 wt.% P_2O_5 and 0.17 wt.% ZrO_2 (Khramov, 2014).

The Kovdor deposit is mineralogically diverse. This, on the one hand, gives a long-term outlook, but exploration becomes more complicated, on the other hand. This required a detailed and systematic 3D mineralogical mapping (Kalashnikov et al., 2012; Ivanyuk et al., 2013; Mikhailova et al., 2015), as modern economic conditions call for an advanced and more precise extraction technology for different elements. Development of the Kovdor deposit is an example of the most efficient use of complex mineral resources. But the modern economy requires an advanced and more precise elements recovery technology. One of significant concentration problems is the irregular distribution of Mg and Mn in magnetite. Other problems are variation of magnetite grain size, different gauge microinclusions (spinel or/and ilmenite group minerals, quintinite). In addition, characterization of the spatial distribution of

* Corresponding author.
E-mail addresses: ivanyuk@geoksc.apatity.ru (G.Y. Ivanyuk), kalashnikov@geoksc.apatity.ru (A.O. Kalashnikov), pakhom@geoksc.apatity.ru (Y.A. Pakhomovsky), ylya_korchak@mail.ru (J.A. Mikhailova), yakovenchuk@geoksc.apatity.ru (V.N. Yakovenchuk), konoplyova55@mail.ru (N.G. Konopleva), victor.sokharev@eurochem.ru (V.A. Sokharev), bazai@geoksc.apatity.ru (A.V. Bazai), pgor@geoksc.apatity.ru (P.M. Goryainov).

http://dx.doi.org/10.1016/j.oregeorev.2016.02.008
0169-1368/

other potentially economic components (e.g., scandium in baddeleyite, Kalashnikov et al., 2016) could improve efficiency of the mine. There are no fast and inexpensive methods for real-time assaying of chemical composition, grain-size distribution and inclusions of the ore minerals in each exploration block. The necessity for rather accurate forecast of the ore minerals properties became another reason for mineralogical mapping. An idea about geological, mineralogical and metallurgical mapping of the Kovdor deposit was suggested by Riko et al. (1987) and Krasnova and Kopylova (1988), who compiled a geological model and designed a mapping program for complex ores with different processing and metallurgical properties. This resembles a concept of geometallurgical units (Lotter et al., 2003). However, the political and economic crisis in the late USSR put those plans on shelf. Our study is the further development of this idea.

We have introduced the 3D mineralogical mapping approach in our previous papers. Mikhailova et al. (2015) presented new petrographic and geological data and compiled all previous borehole data. The authors proposed a new classification of rocks for the phoscorite–carbonatite series. Based on these data, zonation and rock relationships were identified at the Kovdor deposit. Here we present a model of spatial distribution of properties of recoverable minerals — magnetite, apatite and baddeleyite. These minerals have been thoroughly described in numerous articles (Rimskaya-Korsakova, 1950, 1963; Rimskaya-Korsakova and Dinaburg, 1964; Rimskaya-Korsakova et al., 1968, 1979; Kurbatova, 1974; Kopylova et al., 1980, 1985) and summary monographs (Kukharenko et al., 1965; Ternovoy et al., 1969; Kapustin, 1980; Rimskaya-Korsakova and Krasnova, 2002; Wall and Zaitsev, 2004; Afanasyev, 2011). However, all these works are based on the data obtained from optical microscopic observations and conventional wet chemical or emission spectrometry assays. Ivanyuk et al. (2002) published representative electron-microprobe data on most Kovdor minerals, yet those remained unstructured and rather few for every mineral. Therefore, this study is devoted to results of modern systematic investigation of the deposit. About 60 microprobe analyses of XYZ-coordinated baddeleyite samples from deep levels of the Kovdor phoscorite–carbonatite pipe were published by Polyakov and Polezhaeva (1991), and we used some of them in this work.

2. Geological setting

The Kovdor alkaline ultramafic massif is situated in the southwest of the Murmansk Region, Russia (Fig. 1). It consists of peridotite, foidolite, phoscorite, carbonatite and the related metasomatic rocks (Kukharenko et al., 1965; Ivanyuk et al., 2002; Krasnova et al., 2004; Afanasyev, 2011). The Kovdor massif is a central-type multiphase volcano–plutonic complex that intruded into the Archean granite-gneiss at 376–380 Ma (U–Pb and Th–Pb data on zircon, baddeleyite, apatite and calcite) (Bayanova et al., 1997; Amelin and Zaitsev, 2002; Rodionov et al., 2012). At the western contact of the diopsidized peridotite with foidolite, a concentrically zoned phoscorite–carbonatite pipe intrudes the massif (Fig. 1) and is a host to the Kovdor baddeleyite-apatite-magnetite deposit (Fig. 2). Carbonatite is a magmatic rock, where more than 50% of the volume is represented by carbonates; and phoscorite is a magnetite-olivine-apatite-carbonate (predominantly calcite) rock associated with carbonatites (Le Maitre, 2002). The classification of phoscorites, based on the schemes by Streckeisen (1974) and Yegorov (1993) and the International Union of Geological Sciences recommendation (Le Maitre, 2002), is introduced in Mikhailova et al. (2015). Modal compositions of the studied phoscorite–carbonatite series are shown in Fig. 3.

The rocks of the Kovdor phoscorite–carbonatite complex form natural series with the significant content of apatite and magnetite, which first gradually increases due to the earlier forsterite and then decreases due to development of carbonates (Rimskaya-Korsakova, 1963; Ternovoy, 1977; Dunaev, 1982; Ivanyuk et al., 2013; Mikhailova et al., 2015). As a result, the phoscorite–carbonatite pipe has a clear concentric zonation (from margins to the center, Fig. 2): the marginal zone consists of forsterite-dominant and apatite-forsterite phoscorites (F and AF fields in Fig. 3); the intermediate zone comprises low-calcite magnetite-rich phoscorites (M, MF, MA and MAF fields in Fig. 3); the inner (axial) zone includes calcite-rich phoscorites (CA, CM, CMA, CMF, CAF and CMAF fields in Fig. 3) and phoscorite-related carbonatites (red points in the carbonatite half of the Fo-Ap-Mag-Cb tetrahedron in Fig. 3). Logical calculation of the phoscorite name, based on percentage of carbonates, magnetite, apatite and forsterite is presented in Supplementary Material 1. Magnetite–dolomite-(phlogopite)-serpentine rock is a metasomatic rock after peridotite or forsterite-rich phoscorite. The magnetite–dolomite-(phlogopite)-serpentine rock constitutes a small ore body (so called “Eastern Satellite”) in the east of the Kovdor phoscorite–carbonatite pipe and several clusters within the main ore body (Fig. 2). Veins of calcite carbonatite (blue points in the carbonatite half of Fo-Ap-Mag-Cb tetrahedron in Fig. 3) intersect the entire pipe and host rocks. The northeast-trending linear zone of dolomite carbonatite veins (Fig. 2) extends from the central part of the pipe to the Eastern Satellite (Ivanyuk et al., 2013; Mikhailova et al., 2015).

3. Samples and methods

For this study we have collected 546 samples of phoscorites (mainly), carbonatites and host rocks from 108 holes drilled within the Kovdor phoscorite–carbonatite complex (Mikhailova et al., 2015). Thin polished sections of these samples were petrographically analyzed under a microscope to estimate texture, mineral relations and grain size, and to determine the scope of electron microscopic study. Grain size of the minerals was estimated with Image Tool 3.0 as a mean equivalent circle diameter.

We have conducted our studies with the LEO-1450 scanning electron microscope featuring the Röntek energy-dispersive microanalyzer (at Geological Institute of the Kola Science Center, Russian Academy of Sciences (GI KSC RAS), Apatity) to obtain BSE-images of the key regions and fulfill the preliminary analysis of all minerals found (including fluorine in apatite). Chemical composition of minerals was measured in the MS-46 Cameca electron microprobe (GI KSC RAS) operating in WDS-mode at 20 kV and 20–30 nA. Beam diameter varied from 1 to 10 μm (depending on mineral stability). The used standards and limits of accuracy for each measured elements are shown in Table 1. For statistical investigation, values of analyses below the limit of accuracy are recognized as ten times less than the limit.

Chemical analyses of rocks used for mineralogical prognosis were performed in analytical laboratory of JSC “Kola Geological Informational Laboratory Center”(Apatity, Murmansk Region, Russia) using conventional wet chemical method for SiO_2, TiO_2, MgO, CaO, K_2O, Na_2O, Al_2O_3, Fe_{total}, $Fe_{magnetic}$, P_2O_5, ZrO_2, S_{total} and CO_2. In total, we analyzed 1846 drillcore intervals, averaging 16 m length, from 180 exploration drill holes, totaling 30,213 m and representing the entire deposit.

Statistical studies were carried out using STATISTICA 8.0 (StatSoft). For statistics, values of analyses below the limit of accuracy (Table 1) are recognized as values ten times less than the limit. Geostatisical studies were conducted by GEOMIX (JSC “VIOGEM”, Belgorod, Russia). Interpolation was performed by ordinary Kriging. Phoscorite types were named according to the main minerals: A — apatite, C — carbonate, F — forsterite and M — magnetite. The respective abbreviation for names of rock-forming minerals is included in denomination of a rock if the content of such mineral exceeds 10 mod %. Within the phoscorite–carbonatite series, the rocks with carbonate content exceeding 50 mod % received the denomination of “phoscorite-related carbonatites”, while the remaining rocks are named “phoscorites” (Mikhailova et al., 2015). The automatic naming of rocks of phoscorite–carbonatite series were carried out by logical evaluation in Microsoft Excel spreadsheet (Supplementary Data 1).

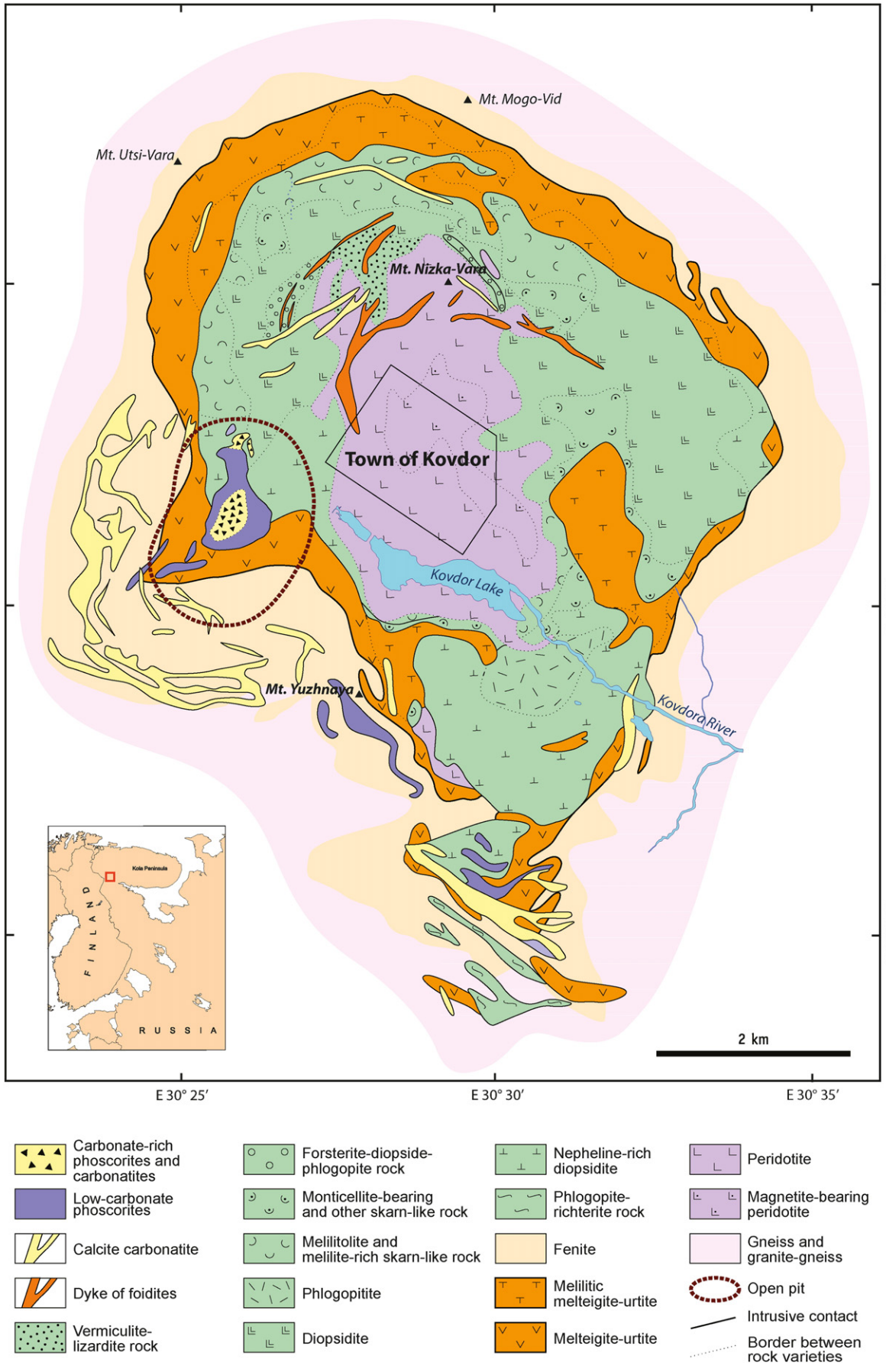

Fig. 1. Geological map of the Kovdor alkaline ultramafic massif (after Afanasyev and Pan'shin, with modification of Mikhailova et al. (2015)).

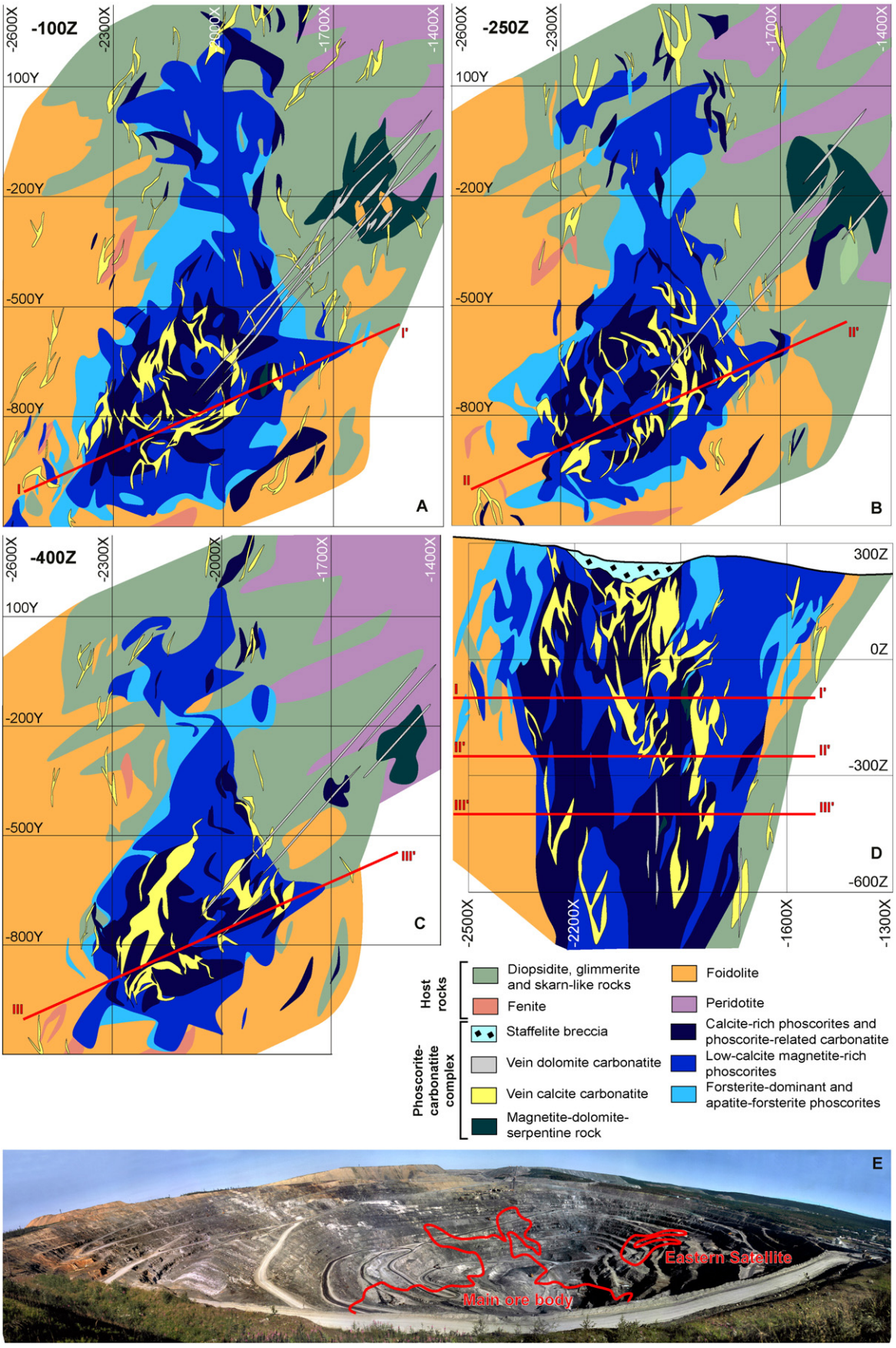

Fig. 2. Geological maps of levels −100 m (a), −250 m (b), and −400 m (c), Y axis shows the North; a cross-section (d), and a general view of the open pit (e) of the Kovdor baddeleyite-apatite-magnetite deposit.

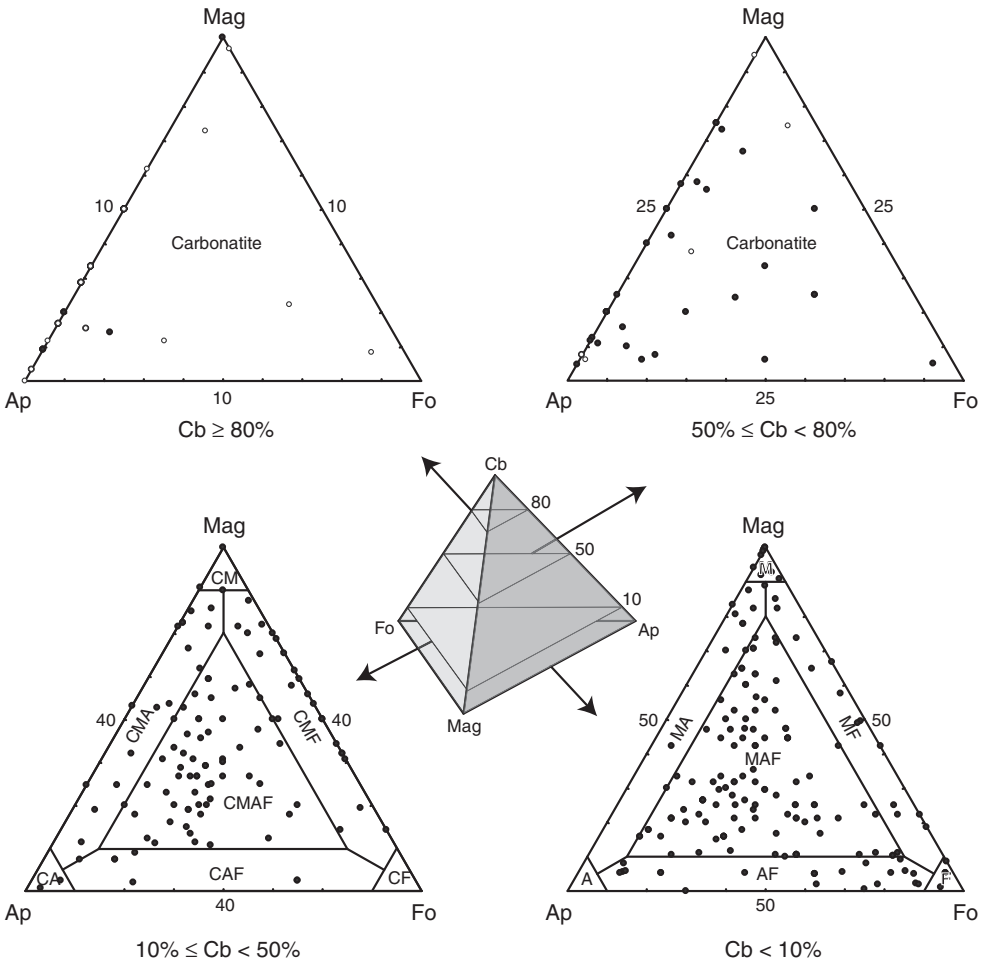

Fig. 3. Classification of the phoscorite–carbonatite rocks (Mikhailova et al., 2015). Ap — apatite, Fo — forsterite, Mag — magnetite, Cb — carbonates (calcite and dolomite). Points are rocks located within the corresponding tetrahedron segment (according to carbonate content) projected onto the bottom plane of every segment. Black points correspond to phoscorites (Cb < 50 mod %) and phoscorite-related carbonatite (Cb > 50 mod %), open points correspond to the vein carbonatites. MAF, MF, MA, AF, CAF, CMAF etc. are types of phoscorite in accordance with content of the rock-forming minerals (C — carbonate, M — magnetite, A — apatite, F — forsterite).

4. Magnetite

Magnetite is an accessory mineral of foidolite, diopsidite, phlogopitite and dolomite carbonatite. It is an accessory or minor rock-forming mineral of forsteritite, apatite-forsterite phoscorite and calcitic carbonatite veins. It is also a main mineral of all other types of phoscorites and carbonatites (Fig. 4, Tables 2-3, Supplementary Data 2). Morphology, anatomy, grain size and chemical composition of magnetite and related (oxy)-exsolution products correspond to concentric zoning of the phoscorite–carbonatite pipe (Ivanyuk et al., 2013; Mikhailova et al., 2015).

In foidolites magnetite occurs as small (with the mean equivalent circle diameter of 0.2 mm), irregularly shaped grains and skeletal crystals in the interstices of grains in rock-forming silicates. In these rocks, magnetite content reaches 30 mod % (on average, 2 mod %). It carries inclusions of most common titanite and ilmenite, occasional calcite and pyrrhotite, and, in its turn, forms inclusions (and intergrowths) in calcite, nepheline, diopside, phlogopite and titanite.

In diopsidite and phlogopitite accessory or rock-forming magnetite (up to 70 mod %, on average 10 mod %) forms small, irregular grains (up to 70 modal %) in interstices of rock-forming silicates and larger poikilitic crystals that accommodate mineralized fractures and poikilitic inclusions of surrounding minerals (mainly forsterite, phlogopite, pyrrhotite and baddeleyite). Magnetite grains carry (oxy)-exsolution inclusions of common ilmenite–geikielite and rare ulvöspinel:

$$\underset{\text{Mg-Ti-rich magnetite}}{20\,Fe_{2.4}Mg_{0.3}Ti_{0.3}O_4} + O_2 \rightarrow \underset{\text{Magnetite}}{16\,Fe_3O_4} + \underset{\text{Geikielite}}{6MgTiO_3},$$

$$\underset{\text{Ti-rich magnetite}}{20\,Fe_{2.7}Ti_{0.3}O_4} + O_2 \rightarrow \underset{\text{Magnetite}}{16\,Fe_3O_4} + \underset{\text{Ilmenite}}{6FeTiO_3},$$

$$\underset{\text{Ti-rich magnetite}}{2\left(Fe^{3+}_{0.5}Fe^{2+}_{0.5}\right)\left(Fe^{2+}Fe^{3+}_{0.5}Ti_{0.5}\right)O_4} \rightarrow \underset{\text{Magnetite}}{Fe_3O_4} + \underset{\text{UlvÐspinel}}{Fe_2TiO_4}.$$

Thin ilmenite–geikielite lamellae are oriented accordingly along the magnetite planes {111} and {100}, forming characteristic rectangular lattice in all other sections (Gaydukova et al., 1984; Krasnova and Krezer, 1995). Ulvöspinel forms thin exsolution lamellae oriented along plane {100} of host magnetite crystals. Magnetite itself usually forms inclusions in phlogopite, diopside, calcite and dolomite as well as close intergrowths with diopside, phlogopite, calcite, apatite, baddeleyite and pyrrhotite. Mean equivalent circle diameter of magnetite grains in these rocks is about 1 mm (Table 2).

In phoscorites and phoscorite-related carbonatites, accessory or rock-forming magnetite (up to 95 mod %, on average, 29 mod %) occurs mainly as large (up to 15 cm in diameter) irregular poikilitic crystals with numerous poikilitic inclusions of surrounding minerals (first of

Table 1
Parameters of microprobe analyses.

Element	Limit of accuracy, wt.%	Standards for WDS analyses
F*	0.5	
Na_2O	0.1	Lorenzenite
MgO	0.1	Pyrope
Al_2O_3	0.05	Pyrope
SiO_2	0.05	Diopside
P_2O_5	0.05	Fluorapatite
CaO	0.03	Diopside
Sc_2O_3	0.02	Thortveitite
TiO_2	0.02	Lorenzenite
V_2O_3	0.1	Metallic vanadium
Cr_2O_3	0.02	Chromite
MnO	0.01	Synthetic $MnCO_3$
FeO	0.01	Hematite
CoO	0.01	Metallic cobalt
NiO	0.01	Metallic nickel
ZnO	0.01	Synthetic ZnO
SrO	0.1	Celestine
ZrO_2	0.1	Synthetic $ZrSiO_4$
Nb_2O_5	0.05	Metallic niobium
BaO	0.05	Barite
La_2O_3	0.05	Synthetic $LaCeS_2$
Ce_2O_3	0.05	Synthetic $LaCeS_2$
Nd_2O_3	0.1	Synthetic $LiNd(MoO_4)_2$
HfO_2	0.2	Metallic hafnium
Ta_2O_5	0.05	Metallic niobium

* Fluorine measured by EDS method.

all, apatite, forsterite and baddeleyite) and rock fragments (Fig. 4a). Such inclusions (up to 60% of the grain volume) can be distributed uniformly (in the most minerals) or predominantly in peripheral zone of magnetite crystals (baddeleyite). Numerous fractures, filled with calcite, dolomite and phlogopite, split magnetite poikilitic crystals. Broadly speaking, well-shaped crystals are not typical for magnetite, although its small grains often have a comparatively regular shape (Fig. 4b). Besides, magnetite poikilitic crystals obtain regular mirror-surfaced faces at points of contact with calcite or dolomite veinlets. Phoscorite-related carbonatites carry perfect magnetite crystals (up to 20 cm in diameter) of octahedral {111}, rhombic dodecahedral {110} and rare tetragonal trioctahedral {311} and hexahedral {100} forms (Chernysheva and Gaydukova, 1973; Ivanyuk et al., 2002, 2013; Krasnova et al., 2004; Mikhailova et al., 2015).

Magnetite poikilitic crystals usually contain fine inclusions of ilmenite–geikielite and/or spinel being the result of high-temperature (about 600 °C) (oxy)-exsolution of Ti-rich (see above) and/or Mg–Al-rich magnetite:

$$4\underset{\text{Mg-Al-rich magnetite}}{\left(Fe^{2+}_{0.75}Mg_{0.25}\right)\left(Fe^{3+}_{1.50}Al_{0.50}\right)O_4} \rightarrow \underset{\text{magnetite}}{3F_3O_4} + \underset{\text{spinel}}{MgAl_2O_4}.$$

Both ilmenite and geikielite form rectangular trellis of thin lamellae (see Fig. 4b) as described above and rare irregularly shaped perthite-like inclusions in magnetite. Sometimes ilmenite lattice coexists with separate isometric geikielite inclusions. Spinel renders rounded grains, octahedral, needle-like and fusiform crystals with orientation similar to that of the magnetite host crystal (Rimskaya-Korsakova, 1950; Gaydukova et al., 1984). Often, spinel crystals group in rectangular lattice, chains and spots (Fig. 4c and d). Baddeleyite is a characteristic satellite of exsolution spinel, forming prismatic inclusions within its crystals (Fig. 16e).

Within the phoscorite–carbonatite pipe, (apatite)-forsterite phoscorites of the marginal zone, carbonate-rich phoscorites and phoscorite-related carbonatites of the axial zone contain magnetite with inclusions of ilmenite–geikielite, while carbonate-free magnetite-rich phoscorites of the intermediate zone predominantly contain magnetite with exsolution inclusions of spinel (Figs. 5 and 6). In carbonate-bearing phoscorites of the intermediate zone, magnetite grains are frequently distinguished by an unusual zoning — spinel-impregnated core and ilmenite–geikielite-rich marginal zone.

At final stages of the magnetite exsolution in carbonatites and carbonate-rich phoscorites, quintinite can form instead of spinel at 400–200 °C (Ivanyuk et al., 2012):

$$8\underset{\text{Mg-Al-rich magnetite}}{\left(Mg_{0.5}Fe^{2+}_{0.5}\right)\left(Fe^{3+}_{1.75}Al_{0.25}\right)O_4} + H_2CO_3 + 8H_2O \rightarrow \underset{\text{Magnetite}}{6Fe_3O_4}$$

$$+\underset{\text{Quintinite}}{Mg_4Al_2(CO_3)(OH)_{12}\cdot 3H_2O} + \S\, O_2.$$

Quintinite-2*H* also replaces spinel to form full pseudomorphs after the latter within magnetite matrix (Fig. 4d):

$$4\underset{\text{Spinel}}{MgAl_2O_4} + H_2CO_3 + 8H_2O \rightarrow \underset{\text{Quintinite}}{Mg_4Al_2(CO_3)(OH)_{12}\cdot 3H_2O} + 3Al_2O_3.$$

In addition to inclusions in magnetite, a comparatively high-temperature quintinite-2*H* forms well shaped crystals growing on magnetite in voids. These crystals can be then incrusted by crystals of a low-temperature quintinite-2*H*1*c*, quintinite-2*H*3*c* and quintinite-1*M* (Krivovichev et al., 2010a, 2010b; Krivovichev et al., 2012; Zhitova et al., 2010). In addition to quintinite, grains of Mg–Al-rich magnetite can contain unusual polymineral inclusions (Fig. 4e) of spinel, clinochlore, dolomite, calcite, magnesite, eitelite, shortite, burbankite, khanneshite, nyerereite and northupite, with their concentration increasing with depth (Mikhailova et al., 2002, 2015).

Aside from the above-mentioned magnetite poikilitic oikocrysts carrying crystal nuclei (chadacrysts) and (oxy)-exsolution inclusions, there are small homogenous rounded grains and octahedral crystals of magnetite that associate with the poikilitic crystals (Fig. 4a). The youngest generation of magnetite is represented by the secondary dispersive grains formed during serpentinization of phlogopite and forsterite:

$$\underset{\text{Forsterite}}{MgFeSiO_4} + H_2O + \tfrac{1}{2}O_2 \rightarrow \underset{\text{Serpentine}}{Mg_3Si_2O_5(OH)_4} + \underset{\text{Magnetite}}{Fe_3O_4} + SiO_2.$$

Magnetite grain size analysis is a challenge even in thin sections as the presence of both large poikilitic crystals and tiny satellite grains results in a bi-modal distribution on the corresponding histograms. Quantity of satellite grains is ten to hundred times greater than that of large poikilitic crystals, though the total area of poikilitic crystals in thin sections is usually larger (Fig. 7). Therefore, mean grain size was estimated as a mean equivalent circular diameter of grains with larger total area (Mercus, 2009). This approach revealed a clear trend towards increasing size of magnetite grains in magnetite-rich rocks, especially in magnetitite and magnetite-apatite phoscorite of the intermediate zone of the phoscorite–carbonatite pipe (Table 2, Fig. 8). Within this zone, magnetite grains vary widely and randomly in size, becoming smaller and uniform as the depth increases.

Vein carbonatites are characterized by varying magnetite morphology. In apatite- and phlogopite-rich regions, it forms irregular to well-shaped poikilitic crystals in interstices of the minerals, while regions dominated by carbonate accommodate rounded grains and well-shaped octahedral crystals (of up to 3 cm in diameter) of magnetite with minor rhombic dodecahedral faces (Ivanyuk et al., 2002). All the crystals contain exsolution lamellae of ilmenite (predominant) or geikielite similar to those found in phoscorite-related carbonatites. Poikilitic inclusions in magnetite grains are apatite, phlogopite, dolomite, calcite, baddeleyite, pyrochlore and pyrrhotite. Mean equivalent circle diameter of magnetite grains is 0.6 mm in calcite carbonatites and 1.2 mm in dolomite carbonatites.

In magnetite–dolomite-phlogopite-serpentine rock, magnetite forms irregular porous poikilitic crystals with mineralized fractures, numerous inclusions of early minerals (phlogopite, baddeleyite, apatite, calcite, dolomite, pyrochlore and sphalerite) and fragments of surrounding rock. Magnetite grains also invariably contain exsolution

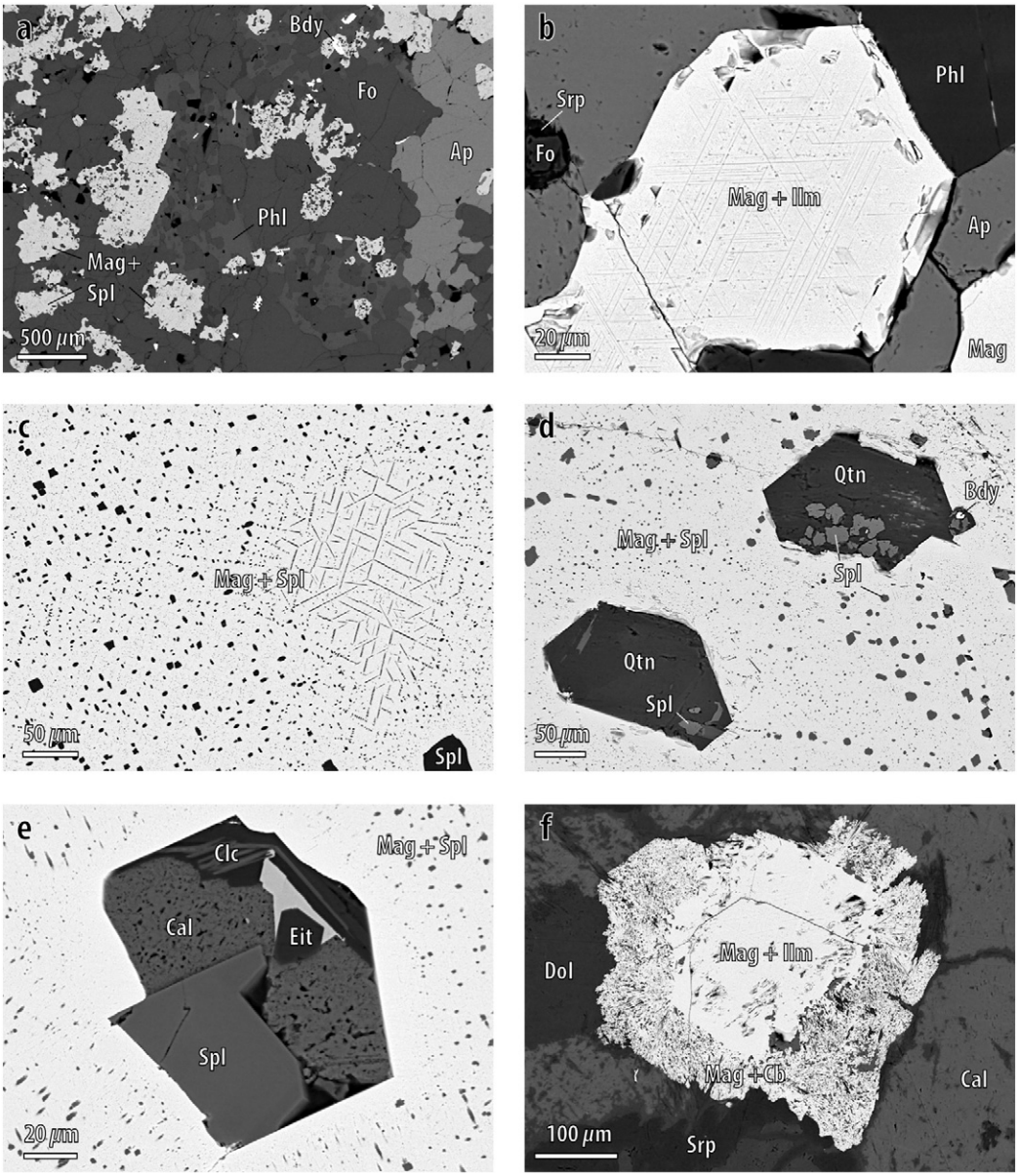

Fig. 4. BSE-images of magnetite poikilitic crystals with inclusions of surrounding minerals and exsolution products: a — magnetite-apatite-forsterite phoscorite 907/35.8; b — phlogopitized phorsteritite 916/330.2; c — magnetite-apatite-forsterite phoscorite 996/208.2; d — calcite–magnetite-forsterite phoscorite 957/118.5; e — apatite-forsterite phoscorite 981/183.1; f — magnetite–dolomite-phlogopite-serpentine rock 970/93.1. Ap — apatite, Bdy — baddeleyite, Cal — calcite, Clc — clinochlore, Dol — dolomite, Eit — eitelite, Fo — forsterite, Ilm — ilmenite, Mag — magnetite, Phl — phlogopite, Qtn — quintinite, Spl — spinel, Srp — serpentine.

inclusions of spinel and ilmenite–geikielite similar to those occurring in phoscorites. There is characteristic rectangular lattice of thin ilmenite–geikielite lamellae filled with carbonates instead of leached magnetite as well as fine intergrowths of magnetite and calcite (Fig. 4f). Occasionally, there can be box-like crystals of magnetite filled with fine-grained magnetite-carbonate aggregate. Mean equivalent circle diameter of magnetite grains in this rock is 2 mm.

Generalized data on chemical composition of magnetite in phoscorites and carbonatites are given in Tables 2 and 3. Content of FeO_{total} in this mineral reveals minor variations of 87–93 wt.%. The impurities include Mg, Ti, Mn, Al, Ca, V, Cr, Si, Zn, Ni and Sc that replace iron according to the three main patterns of iso- and heterovalent isomorphism: $Fe^{2+} \leftrightarrow (Mg, Mn, Zn, Ca)^{2+}$; $Fe^{3+} \leftrightarrow (Al, V, Cr, Sc)^{3+}$; $2Fe^{3+} \leftrightarrow Fe^{2+} + (Ti, Si)^{4+}$. Average magnetite composition of the Kovdor phoscorite–carbonatite complex corresponds to $Fe^{3+}{}_{1.00}(Fe^{3+}{}_{0.90}Fe^{2+}{}_{0.80}Mg_{0.22}\ Ti_{0.03}Al_{0.02}Mn_{0.02}Ca_{0.01})_{\Sigma 2.00}O_4$.

Magnesium is the main impurity found in magnetite (on average, 4 wt.% MgO or 0.2 *a.p.f.u.*). The maximum content of magnesium in magnetite is recorded in calcite–magnetite-forsterite phoscorite (6 wt.% MgO or 0.33 *a.p.f.u.*), the lowest concentration is recorded in vein carbonatite, magnetite–dolomite-phlogopite-serpentine rock, forsteritite and surrounding foidolites, diopsidite and phlogopitite. According to Volotovskaya (1952, 1958) and Mikhailova et al. (2015), the rocks of the Kovdor phoscorite–carbonatite complex form the following natural series (from earlier to later, and from marginal to axial within the phoscorite–carbonatite pipe): forsterite-dominant phoscorite (F) — apatite-forsterite phoscorite (AF) — forsterite-apatite-magnetite phoscorites (MF, MA, MAF) — calcite–magnetite–apatite-forsterite phoscorites and phoscorite-related carbonatites (CMF, CAF, CMAF) — calcite–magnetite–apatite phoscorites and phoscorite-related carbonatites (CM, CA, CMA) — calcitic vein carbonatite — dolomitic vein carbonatite. In this rock sequence, the

Table 2
Grain size and chemical composition of magnetite (mean ± SD/min–max).

Rock (number of analyses)	Content, modal %	D_{eq}, mm	MgO	Al_2O_3	SiO_2	CaO	Sc_2O_3	TiO_2	V_2O_3	Cr_2O_3	MnO	FeO_{total}	ZnO
Foidolite (22)	2 ± 6	0.2 ± 0.3	2 ± 2	0.5 ± 0.3	0.3 ± 0.8	0.2 ± 0.3	<0.02	2 ± 1	0.2 ± 0.3	0.1 ± 0.2	0.5 ± 0.3	89 ± 3	<0.01
	0–30	0.01–0.90	<0.10–5.74	<0.05–1.49	<0.05–3.42	<0.03–1.44		0.10–4.62	<0.10–1.21	<0.02–1.10	<0.01–1.38	84.54–94.66	
Diopsidite (61)	12 ± 17	1 ± 1	2 ± 2	0.2 ± 0.3	0.1 ± 0.2	0.1 ± 0.2	<0.02	3 ± 4	0.09 ± 0.07	1 ± 4	0.7 ± 0.8	87 ± 6	0.03 ± 0.05
	0–70	0.02–5.50	<0.10–7.41	<0.05–1.74	<0.05–0.91	<0.03–0.78		0.13–19.77	<0.10–0.36	<0.02–23.77	<0.01–3.73	62.29–93.15	<0.01–0.14
Phlogopitite (17)	5 ± 7	0.8 ± 0.8	2 ± 1	0.4 ± 0.8	0.04 ± 0.08	0.1 ± 0.1	<0.02	1 ± 2	0.13 ± 0.06	<0.02	0.5 ± 0.8	90 ± 4	<0.01
	0–20	0.01–2.30	0.20–5.86	<0.05–3.17	<0.05–0.22	<0.03–0.40		0.25–9.28	<0.10–0.21		0.06–3.47	76.17–92.27	
F (17)	5 ± 3	0.3 ± 0.1	3 ± 2	0.4 ± 0.5	0.0 ± 0.1	0.1 ± 0.1	<0.02	1 ± 1	0.12 ± 0.08	0.1 ± 0.1	0.5 ± 0.2	89 ± 3	0.01 ± 0.02
	1–8	0.20–0.45	0.43–5.85	<0.05–1.44	<0.05–0.49	<0.03–0.38		0.12–4.05	<0.10–0.33	<0.02–0.43	<0.01–0.75	83.22–91.79	<0.01–0.07
AF (42)	5 ± 2	0.3 ± 0.2	4 ± 1	0.5 ± 0.6	0.1 ± 0.1	0.1 ± 0.1	0.00 ± 0.02	2 ± 1	0.11 ± 0.06	0.2 ± 0.4	0.6 ± 0.2	87 ± 2	0.02 ± 0.03
	0–8	0.07–0.90	0.79–6.69	<0.05–2.80	<0.05–0.81	<0.03–0.57	<0.02–0.11	<0.02–5.80	<0.10–0.34	<0.02–1.50	0.27–1.32	82.17–91.54	<0.01–0.10
MF (40)	47 ± 22	4 ± 5	5 ± 1	0.6 ± 0.4	0.1 ± 0.1	0.00 ± 0.01	0.00 ± 0.01	1 ± 1	0.09 ± 0.04	<0.02	0.6 ± 0.1	86 ± 2	0.00 ± 0.02
	15–85	0.08–20.00	1.84–7.26	<0.05–1.60	<0.05–0.44	<0.05–0.46	<0.02–0.05	0.30–5.60	<0.10–0.19		0.24–1.01	78.71–91.11	<0.01–0.11
MAF (249)	30 ± 16	3 ± 2	5 ± 1	0.7 ± 0.5	0.0 ± 0.1	0.1 ± 0.2	0.00 ± 0.01	1.0 ± 0.6	0.10 ± 0.04	0.00 ± 0.04	0.5 ± 0.1	86 ± 2	0.00 ± 0.02
	10–70	0.09–12.00	<0.10–8.53	<0.05–4.14	<0.05–1.40	<0.03–0.55	<0.02–0.19	<0.02–7.48	<0.10–0.28	<0.02–0.55	<0.01–1.01	77.71–92.99	<0.01–0.16
MA (42)	70 ± 13	5 ± 4	4 ± 2	0.5 ± 0.4	0.03 ± 0.06	0.1 ± 0.2	<0.02	0.9 ± 0.2	0.11 ± 0.05	<0.02	0.5 ± 0.1	88 ± 3	<0.01
	40–85	0.5–14.00	0.70–7.63	<0.05–1.78	<0.05–0.23	<0.03–0.58		0.49–1.48	<0.10–0.24		0.13–0.75	83.43–92.62	
M (29)	91 ± 2	11 ± 9	5 ± 2	0.7 ± 0.4	0.02 ± 0.05	0.1 ± 0.1	0.01 ± 0.02	0.9 ± 0.5	0.11 ± 0.04	<0.02	0.5 ± 0.1	86 ± 4	0.00 ± 0.01
	80–95	0.40–25.00	1.46–7.81	<0.05–1.74	<0.05–0.16	<0.03–0.45	<0.02–0.05	0.38–2.84	<0.10–0.22		0.29–0.74	66.23–91.70	<0.01–0.07
CMAF (151)	26 ± 11	2 ± 2	5 ± 2	0.6 ± 0.5	0.02 ± 0.06	0.2 ± 0.2	0.00	1.2 ± 0.8	0.12 ± 0.06	0.1 ± 0.4	0.5 ± 0.2	87 ± 3	0.00 ± 0.02
	10–55	0.01–10.00	<0.10–7.87	<0.05–3.42	<0.05–0.50	<0.03–0.99	<0.02–0.04	<0.02–4.71	<0.10–0.30	<0.02–5.16	0.03–1.46	65.89–92.44	<0.01–0.11
CMF (51)	39 ± 15	4 ± 3	6 ± 2	0.9 ± 0.6	0.1 ± 0.1	0.1 ± 0.2	0.00	0.9 ± 0.5	0.11 ± 0.04	0.1 ± 0.6	0.6 ± 0.1	85 ± 2	0.01 ± 0.03
	15–60	0.30–14.00	1.96–8.81	<0.05–2.32	<0.05–0.69	<0.03–0.77	<0.02–0.02	<0.02–3.18	<0.10–0.24	<0.02–4.29	0.30–0.92	79.06–90.89	<0.01–0.17
CAF (21)	4 ± 2	1 ± 2	3 ± 1	0.2 ± 0.3	0.1 ± 0.1	0.1 ± 0.2	<0.02	1 ± 2	0.11 ± 0.08	0.6 ± 0.8	0.6 ± 0.4	87 ± 5	0.02 ± 0.04
	2–8	0.04–4.00	<0.10–5.25	<0.05–0.96	<0.05–0.28	<0.03–0.60		<0.02–6.11	<0.10–0.23	<0.02–2.27	<0.01–1.79	68.45–92.80	<0.01–0.14
CMA (52)	46 ± 22	4 ± 6	5 ± 2	0.5 ± 0.4	0.01 ± 0.04	0.1 ± 0.2	0.00 ± 0.01	1.0 ± 0.7	0.11 ± 0.06	<0.02	0.5 ± 0.1	87 ± 2	0.00 ± 0.02
	11–79	0.40–25.00	0.99–8.11	<0.05–1.92	<0.05–0.22	<0.03–1.01	<0.02–0.04	0.30–4.02	<0.10–0.25		0.19–0.79	81.61–92.83	<0.01–0.08
CA (7)	3 ± 3	1 ± 1	3 ± 2	0.2 ± 0.3	<0.05	0.3 ± 0.2	<0.02	0.7 ± 0.5	0.11 ± 0.08	<0.02	0.4 ± 0.2	89 ± 2	0.02 ± 0.03
	1–6	0.26–2.60	<0.10–6.02	<0.05–0.89		<0.03–0.64		<0.02–1.28	<0.10–0.21		0.19–0.65	86.18–92.09	<0.01–0.06
CM (4)	77 ± 10	1.5 ± 0.8	5 ± 1	0.5 ± 0.1	0.03 ± 0.07	0.1 ± 0.2	<0.02	1.2 ± 0.3	0.12 ± 0.05	<0.02	0.61 ± 0.09	87 ± 1	<0.01
	70–84	0.90–2.00	3.83–5.83	0.42–0.69	<0.05–0.14	<0.03–0.33		0.82–1.38	<0.10–0.18		0.50–0.70	85.52–88.20	
Phoscorite-related carbonatite (71)	9 ± 8	2 ± 2	4 ± 2	0.4 ± 0.4	0.0 ± 0.1	0.2 ± 0.2	<0.02	1 ± 1	0.12 ± 0.08	0.00	0.5 ± 0.2	88 ± 3	0.01 ± 0.02
	1–35	0.15–12.00	<0.10–7.36	<0.05–2.12	<0.05–0.80	<0.03–0.79		<0.02–10.79	<0.10–0.37	<0.02–0.03	0.06–1.68	82.59–92.66	<0.01–0.11
Vein carbo-natite (86)	3 ± 3	1 ± 1	2 ± 2	0.2 ± 0.3	0.02 ± 0.06	0.3 ± 0.2	<0.02	1.1 ± 0.9	0.16 ± 0.08	0.00 ± 0.01	0.3 ± 0.2	89 ± 2	0.02 ± 0.05
	0–15	0.03–9.00	0.20–8.14	<0.05–1.67	<0.05–0.42	<0.03–0.92		0.08–4.59	<0.10–0.33	<0.02–0.13	<0.01–0.71	83.39–92.84	<0.01–0.35
Mag–Dol–Phl–Srp rock (85)	27 ± 23	2 ± 1	3 ± 2	0.3 ± 0.3	0.1 ± 0.2	0.1 ± 0.1	<0.02	0.9 ± 0.5	0.12 ± 0.07	0.02 ± 0.09	0.4 ± 0.2	89 ± 3	0.01 ± 0.02
	2–80	0.10–5.20	<0.10–7.53	<0.05–1.53	<0.05–0.89	<0.03–0.81		0.08–2.61	<0.10–0.38	<0.02–0.69	<0.01–0.81	83.81–93.01	<0.01–0.13

A — apatite, F — forsterite, M — magnetite, C— carbonates (calcite and dolomite); D_{eq} — mean equivalent circular diameter of grains.
"<n" refers to value below limit of accuracy.

Table 3
Magnetite formulae (atoms per formula unit) calculated on the basis of $Me^{2+}Me^{3-4+}{}_2O_4$ (mean ± SD/min–max).

Rock	Fe^{2+}	Mg	Mn	Ca	Zn	Fe^{3+}	Al	Ti	Si	V	Cr	Sc
Foidolite	0.9 ± 0.1	0.10 ± 0.09	0.02 ± 0.01	0.01 ± 0.01	–	1.86 ± 0.08	0.02 ± 0.02	0.05 ± 0.03	0.01 ± 0.03	0.00 ± 0.01	0.00 ± 0.01	–
	0.69–1.08	0.00–0.32	0.00–0.04	0.00–0.06		1.64–1.95	0.00–0.07	0.00–0.13	0.00–0.13	0.00–0.04	0.00–0.03	
Diopsidite	0.94 ± 0.09	0.1 ± 0.1	0.02 ± 0.02	0.00 ± 0.01	–	1.8 ± 0.2	0.01 ± 0.01	0.1 ± 0.1	0.00 ± 0.01	0.00	0.0 ± 0.1	–
	0.66–1.04	0.00–0.39	0.00–0.12	0.00–0.03		0.96–1.98	0.00–0.08	0.00–0.52	0.00–0.03	0.00–0.01	0.00–0.69	
Phlogopitite	0.92 ± 0.07	0.10 ± 0.08	0.02 ± 0.02	0.00 ± 0.01	–	1.9 ± 0.1	0.02 ± 0.03	0.03 ± 0.06	0.00	0.00	–	–
	0.70–0.99	0.01–0.32	0.00–0.11	0.00–0.02		1.36–1.98	0.00–0.14	0.01–0.25	0.00–0.01	0.00–0.01		
F	0.87 ± 0.08	0.15 ± 0.09	0.01 ± 0.01	0.00 ± 0.01	–	1.89 ± 0.07	0.02 ± 0.02	0.04 ± 0.03	0.00	0.00	0.00	–
	0.69–1.02	0.02–0.32	0.00–0.02	0.00–0.02		1.72–1.99	0.00–0.06	0.00–0.11	0.00–0.02	0.00–0.01	0.00–0.01	
AF	0.81 ± 0.08	0.22 ± 0.08	0.02 ± 0.01	0.00 ± 0.01	–	1.88 ± 0.07	0.02 ± 0.02	0.04 ± 0.03	0.00 ± 0.01	0.00	0.00 ± 0.01	–
	0.67–0.97	0.05–0.35	0.01–0.04	0.00–0.02		1.66–1.98	0.00–0.12	0.00–0.16	0.00–0.03	0.00–0.01	0.00–0.04	
MF	0.75 ± 0.08	0.27 ± 0.08	0.02	0.00	–	1.90 ± 0.06	0.03 ± 0.02	0.03 ± 0.03	0.00	0.00	–	–
	0.63–0.90	0.10–0.39	0.01–0.03	0.00–0.02		1.66–1.96	0.00–0.07	0.01–0.16	0.00–0.02	0.00–0.01		
MAF	0.74 ± 0.08	0.27 ± 0.08	0.02	0.00 ± 0.01	–	1.91 ± 0.04	0.03 ± 0.02	0.03 ± 0.02	0.00	0.00	0.00	0.00
	0.56–1.05	0.00–0.44	0.00–0.03	0.00–0.02		1.52–2.00	0.00–0.18	0.00–0.20	0.00–0.05	0.00–0.01	0.00–0.02	0.00–0.01
MA	0.8 ± 0.1	0.2 ± 0.1	0.01	0.00 ± 0.01	–	1.92 ± 0.02	0.02 ± 0.02	0.03 ± 0.01	0.00	0.00	–	–
	0.61–0.97	0.04–0.40	0.00–0.02	0.00–0.02		1.86–1.96	0.00–0.07	0.01–0.04	0.00–0.01	0.00–0.01		
M	0.72 ± 0.09	0.28 ± 0.09	0.02	0.00	–	1.92 ± 0.03	0.03 ± 0.02	0.02 ± 0.01	0.00	0.00	–	–
	0.58–0.92	0.08–0.42	0.01–0.02	0.00–0.02		1.83–1.97	0.00–0.07	0.01–0.08	0.00–0.01	0.00–0.01		
CMAF	0.76 ± 0.09	0.25 ± 0.08	0.02	0.01 ± 0.01	–	1.90 ± 0.05	0.03 ± 0.02	0.03 ± 0.02	0.00	0.00	0.00 ± 0.01	–
	0.57–1.00	0.00–0.42	0.00–0.04	0.00–0.04		1.70–1.98	0.00–0.14	0.00–0.13	0.00–0.02	0.00–0.01	0.00–0.15	
CMF	0.67 ± 0.08	0.33 ± 0.08	0.02	0.00 ± 0.01	–	1.91 ± 0.05	0.04 ± 0.02	0.02 ± 0.01	0.00	0.00	0.00 ± 0.02	
	0.53–0.88	0.11–0.46	0.01–0.03	0.00–0.03		1.73–2.00	0.00–0.09	0.00–0.08	0.00–0.03	0.00–0.01	0.00–0.12	
CAF	0.85 ± 0.08	0.17 ± 0.07	0.02 ± 0.01	0.00 ± 0.01	–	1.88 ± 0.09	0.01 ± 0.01	0.04 ± 0.04	0.00	0.00	0.02 ± 0.02	–
	0.71–1.00	0.00–0.29	0.00–0.05	0.00–0.02		1.65–2.00	0.00–0.04	0.00–0.15	0.00–0.01	0.00–0.01	0.00–0.07	
CMA	0.8 ± 0.1	0.3 ± 0.1	0.02	0.01 ± 0.01	–	1.92 ± 0.04	0.02 ± 0.02	0.03 ± 0.02	0.00	0.00	–	–
	0.56–0.97	0.06–0.43	0.01–0.02	0.00–0.04		1.74–1.98	0.00–0.08	0.01–0.11	0.00–0.01	0.00–0.01		
CA	0.9 ± 0.1	0.1 ± 0.1	0.01 ± 0.01	0.01 ± 0.01	–	1.95 ± 0.03	0.01 ± 0.01	0.02 ± 0.01	–	0.00	–	–
	0.68–0.97	0.00–0.32	0.01–0.02	0.00–0.03		1.92–1.99	0.00–0.04	0.00–0.04		0.00–0.01		
CM	0.75 ± 0.06	0.26 ± 0.05	0.02	0.00 ± 0.01	–	1.91 ± 0.01	0.02	0.03 ± 0.01	–	0.00	–	–
	0.69–0.81	0.21–0.32		0.00–0.01		1.89–1.92	0.02–0.03	0.02–0.04		0.00–0.01		
Phoscorite-related carbonatite	0.8 ± 0.1	0.2 ± 0.1	0.01 ± 0.01	0.01 ± 0.01	–	1.91 ± 0.07	0.02 ± 0.02	0.03 ± 0.04	0.00	0.00	–	–
	0.60–1.11	0.00–0.40	0.00–0.05	0.00–0.03		1.41–2.00	0.00–0.09	0.00–0.29	0.00–0.03	0.00–0.01		
Vein carbonatite	0.88 ± 0.09	0.13 ± 0.08	0.01	0.01 ± 0.01	0.00	1.92 ± 0.05	0.01 ± 0.01	0.03 ± 0.02	0.00	0.00	–	–
	0.58–1.04	0.01–0.42	0.00–0.02	0.00–0.04	0.00–0.01	1.73–1.98	0.00–0.07	0.00–0.13	0.00–0.02	0.00–0.01		
Mag–Dol–Phl–Srp rock	0.9 ± 0.1	0.2 ± 0.1	0.01 ± 0.01	0.00 ± 0.01	–	1.93 ± 0.03	0.01 ± 0.01	0.02 ± 0.01	0.00 ± 0.01	0.00	0.00	–
	0.61–1.02	0.00–0.40	0.00–0.03	0.00–0.03		1.82–1.99	0.00–0.06	0.00–0.07	0.00–0.03	0.00–0.01	0.00–0.02	

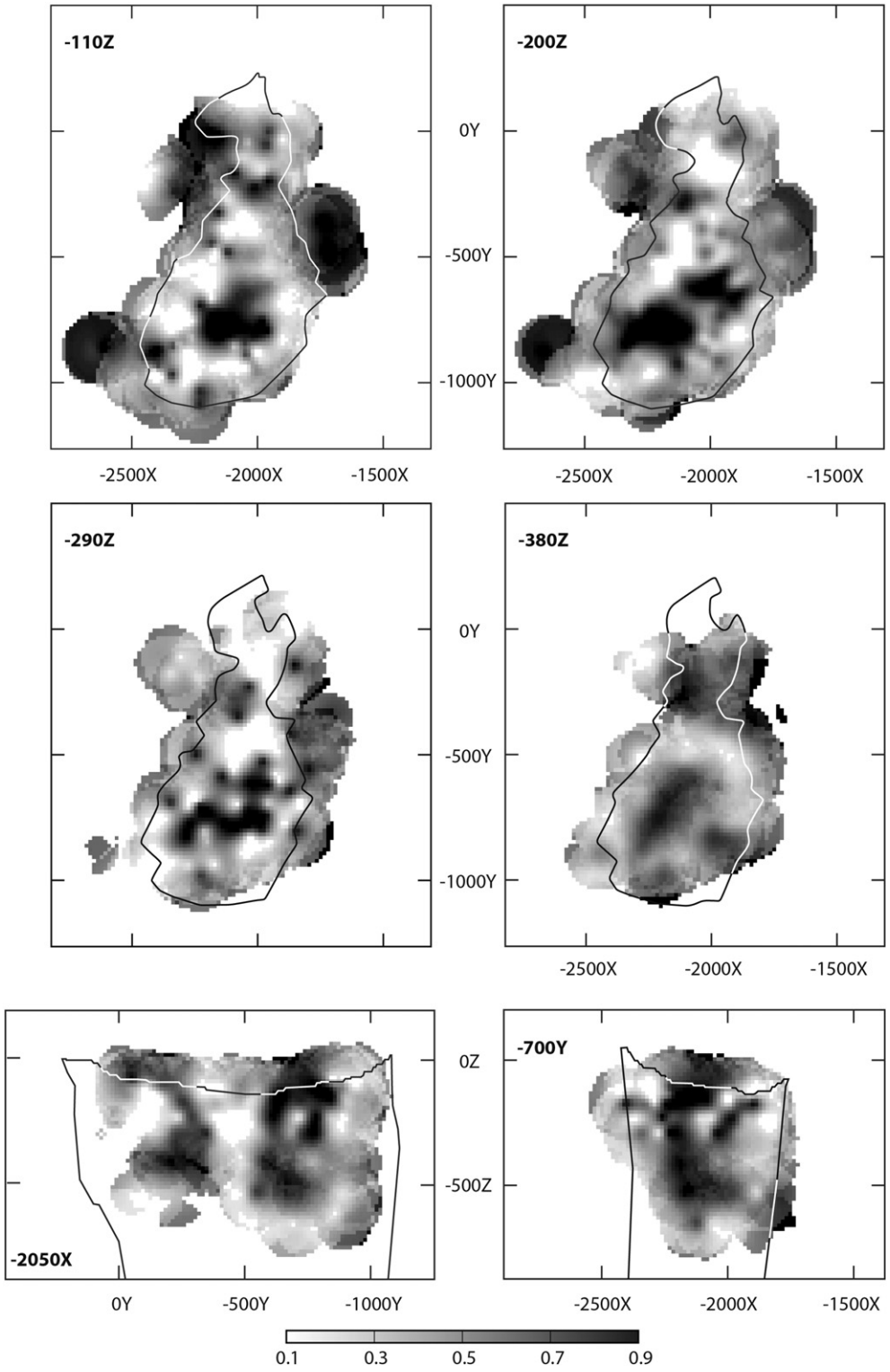

Fig. 5. Distribution of magnetite with exsolution inclusions of spinel. Solid lines show the phoscorite–carbonatite pipe boundary.

average magnesium content in magnetite increases significantly from early (apatite)-forsterite phoscorites (3.5 wt.% MgO) to intermediate carbonate-free magnetite-rich phoscorites (4.8 wt.% MgO), after which – in late carbonate-rich phoscorites and carbonatites – its content slightly drops (to 4.6 wt.% MgO). Similarly, magnetite with higher alumina content occurs predominantly in carbonate-free magnetite-rich phoscorites (0.7 wt.% Al_2O_3 or 0.03 *a.p.f.u.*), while younger carbonate-rich phoscorites and carbonatites and especially earlier (apatite)-forsterite phoscorites contain magnetite with lower content of Al_2O_3 (0.6 and 0.5 wt.% Al_2O_3, correspondingly).

Another important impurity of Ti (1.0 wt.% TiO_2 or 0.03 *a.p.f.u.* on average) is more typical for magnetite found in diopsidite, foidolites and apatite-forsterite phoscorite (2–3 wt.% TiO_2 or 0.5–0.1 *a.p.f.u.*). In the above rock sequence, behavior of titanium is opposite to that of magnesium, e.g., titanium content decreases by half from early (apatite)-forsterite phoscorites (2.0 wt.% TiO_2) to intermediate

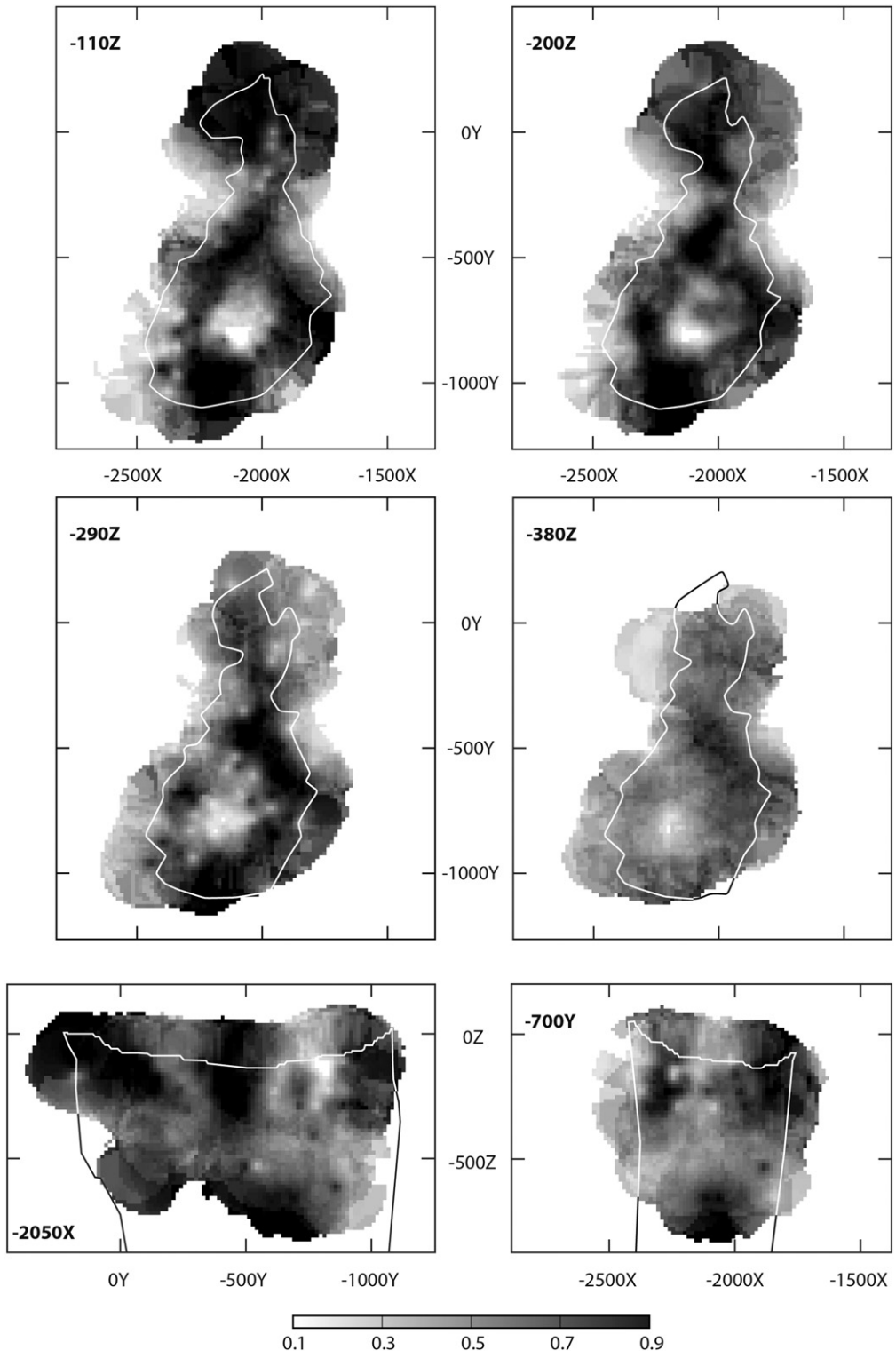

Fig. 6. Distribution of magnetite with oxy-exsolution inclusions of ilmenite–geikielite. Solid lines show the phoscorite–carbonatite pipe boundary.

carbonate-free magnetite-rich phoscorites (1.0 wt.% TiO_2), then slightly rises in the late carbonate-rich phoscorites and carbonatites (1.1 wt.% TiO_2). Impurities of Cr, Mn, Zn and V in magnetite demonstrate the same trend (see Tables 2 and 3).

The rest of magnetite impurities include Si and Sc. Their content decreases gradually from early (apatite)-forsterite phoscorites through carbonate-free magnetite-rich phoscorites to late carbonate-rich phoscorites and carbonatites (see Tables 2 and 3). Conversely, the content of calcium in magnetite increases gradually from early phoscorite varieties to later ones. It is worth noting that presence of Si and Ca in magnetite can be also associated with the nanoinclusions of silicates (in silicate varieties of phoscorites) or carbonates (in carbonate-bearing phoscorites and carbonatites), which have been detected using transmission electron microscopy.

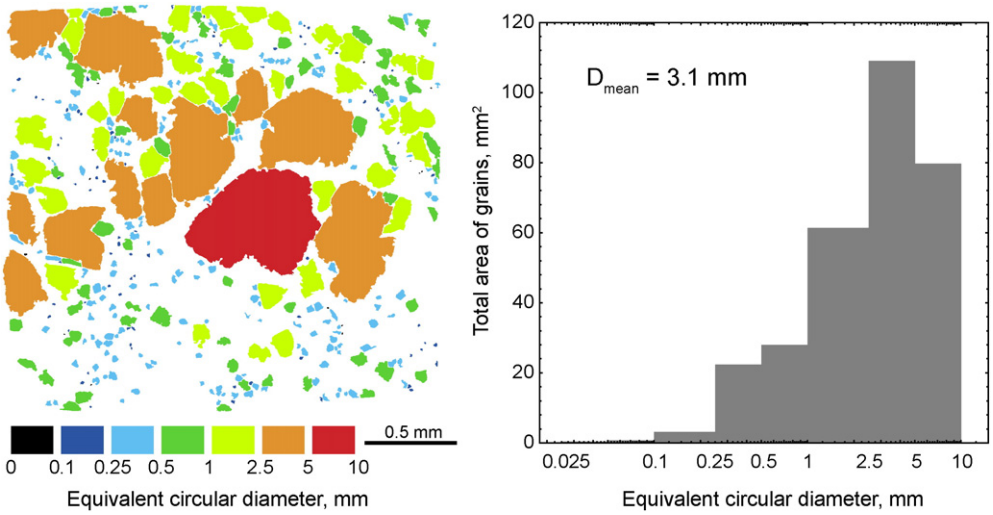

Fig. 7. Estimation of mean grain size of magnetite in dolomite-apatite-magnetite phoscorite 977/191.7.

Due to zonal distribution of the above-mentioned rock assemblages, the peripheral (apatite)-forsterite zone of the phoscorite–carbonatite pipe contains fine-grained magnetite, comparatively rich in Ti, Mn, Si, Cr, Sc and Zn; the intermediate magnetite-(apatite-forsterite) zone accommodates medium- to coarse-grained magnetite with high content of Mg and Al; and the axial carbonate-rich zone of the pipe carries medium-grained magnetite with impurities of V and Ca most frequently found (Figs. 9–11). Surrounding foidolites, diopsidite and glimmerite host magnetite that is comparatively rich in Si, Ti, Mn, Ni and Zn; magnetite–dolomite-phlogopite-serpentine rock carries V-rich magnetite, vein carbonatites contain magnetite enriched in Ca and V (Tables 2 and 3).

Proportion of magnetite grains with the (oxy)-exsolution inclusions of spinel (±quintinite) and/or ilmenite–geikielite grows as content of Al and/or Ti in the magnetite matrix increases (Fig. 12a). Homogeneous grains of Ti-rich magnetite often occur in diopsidite, while non-exsolved Al-rich magnetite grains are typical of carbonate-free phoscorites. Quite expectedly, spinel and geikielite inclusions occur mainly in magnesian magnetite, while lamellae of ilmenite are more typical of low-magnesium magnetite (Fig. 12b).

Chemical composition of spinel inclusions varies insignificantly within the phoscorite–carbonatite pipe and corresponds on average to $(Mg_{0.88}Fe^{2+}_{0.10}\ Zn_{0.02})_{\Sigma 1.00}(Al_{1.86}Fe^{3+}_{0.13}\ Ti_{0.01})_{\Sigma 2.00}O_4$. Iron is the main impurity that replaces Mg and Al during exsolution of Mg–Al-rich magnetite (coefficient of multiple regression of Fe_{total} vs (Mg, Al) is 0.964). Iron-rich spinel inclusions are typical of magnetite that is found in carbonate-free magnetite-rich phoscorites of the intermediate zone of the pipe, while spinel with close to zero iron content occurs in magnetite encountered in axial carbonate-rich phoscorites and carbonatites.

Chemical composition of minerals, belonging to the ilmenite group, widely ranges from pure ilmenite to geikielite and pyrophanite. On average, it corresponds to Mg-rich ilmenite: $(Fe^{2+}_{0.50}Mg_{0.36}Mn_{0.13})_{\Sigma 0.99}(Ti_{0.96}Fe^{3+}_{0.05}Nb_{0.01})_{\Sigma 1.02}O_3$. Geikielite and Mg-rich ilmenite are typical of forsteritite and calcite-(apatite)-magnetite-(forsterite) phoscorite, while Mg-free ilmenite predominantly occurs in surrounding silicate rocks — foidolites, diopsidite and phlogopitite. Within the phoscorite–carbonatite pipe, Mg-rich members of the above series co-exist with iron-free spinel due to exsolution of magnetite with maximum magnesium content. In manganese-rich magnetite of phoscorites (especially MAF), host silicate rocks, magnetite–dolomite-phlogopite-serpentine rock and pyrophanite are sometimes found together with minerals of the ilmenite–geikielite series. The average composition of pyrophanite corresponds to $(Mn_{0.61}Fe^{2+}_{0.27}Mg_{0.11})_{\Sigma 0.99}(Ti_{0.95}Fe^{3+}_{0.06}\ Nb_{0.02}Sc_{0.01})_{\Sigma 1.04}O_3$.

5. Apatite

The apatite group minerals are widespread accessories to rock-forming minerals of the Kovdor massif (Kukharenko et al., 1965; Rimskaya-Korsakova et al., 1968, 1979; Ternovoy et al., 1969; Kurbatova, 1972, 1974, 1986; Kurbatova et al., 1972; Krasnova, 1979; Ivanyuk et al., 2002; Rimskaya-Korsakova and Krasnova, 2002; Krasnova et al., 2004; Mikhailova et al., 2015). Hydroxylapatite (80% of the analyzed samples) and fluorapatite (20%) are the main rock-forming minerals in most phoscorites and phoscorite-related carbonatites and the minor or accessory minerals in foidolites, peridotite, diopsidite, phlogopitite, forsteritite, vein carbonatites and magnetite–dolomite-phlogopite-serpentine rock (Fig. 13, Tables 4-5, Supplementary Data 3).

In foidolite, xenomorphic or elongated prismatic grains of hydroxyl-apatite occur in interstices of rock-forming minerals. They either bear no inclusions (more often) or contain baddeleyite and andradite ingrowths. Hydroxylapatite forms inclusions in phlogopite, diopside, nepheline and calcite. Mean equivalent circle diameter of hydroxylapatite grains in foidolites is 0.1 mm.

In diopsidite, apatite forms irregular grains filling in the interstices of diopside-phlogopite aggregate. Calcite veinlets intersecting the rock carry rounded or elongated prismatic grains of apatite closely associated with forsterite. Apatite inclusions are not typical of diopsidite. Apatite can form inclusions in calcite, phlogopite and diopside. Mean equivalent circle diameter of apatite grains in diopsidite is 0.08 mm.

In phlogopitite, hydroxylapatite and calcite form irregularly shaped clusters in interstices between phlogopite plates. Morphology of individual grains varies from isometric to elongated prismatic. Hydroxylapatite grains are usually fragmented and resorbed with late dolomite on contacts. They contain magnetite, baddeleyite, pyrochlore and sometimes aegirine inclusions, while ingrowths of hydroxylapatite are common in phlogopite, calcite, magnetite and dolomite grains. Mean equivalent circle diameter of hydroxylapatite grains in glimmerite is 0.2 mm.

In all types of phoscorites and phoscorite-related carbonatites, apatite morphology is determined by mineral association. Therefore, apatite is xenomorphic everywhere as opposed to forsterite (Fig. 13a), but it is characterized by a more idiomorphic shape in comparison with magnetite and calcite (Fig. 13b). We observed all stages of growth of magnetite poikilocrysts within apatite-rich matrices – from thin edgings around apatite grains to large poikilitic crystals saturated with prismatic apatite crystals (Fig. 13b). Spatial distribution of apatite in the phoscorites is rather irregular (Rimskaya-Korsakova et al., 1968; Kurbatova, 1974; Krasnova et al., 2004; Mikhailova et al., 2015). It

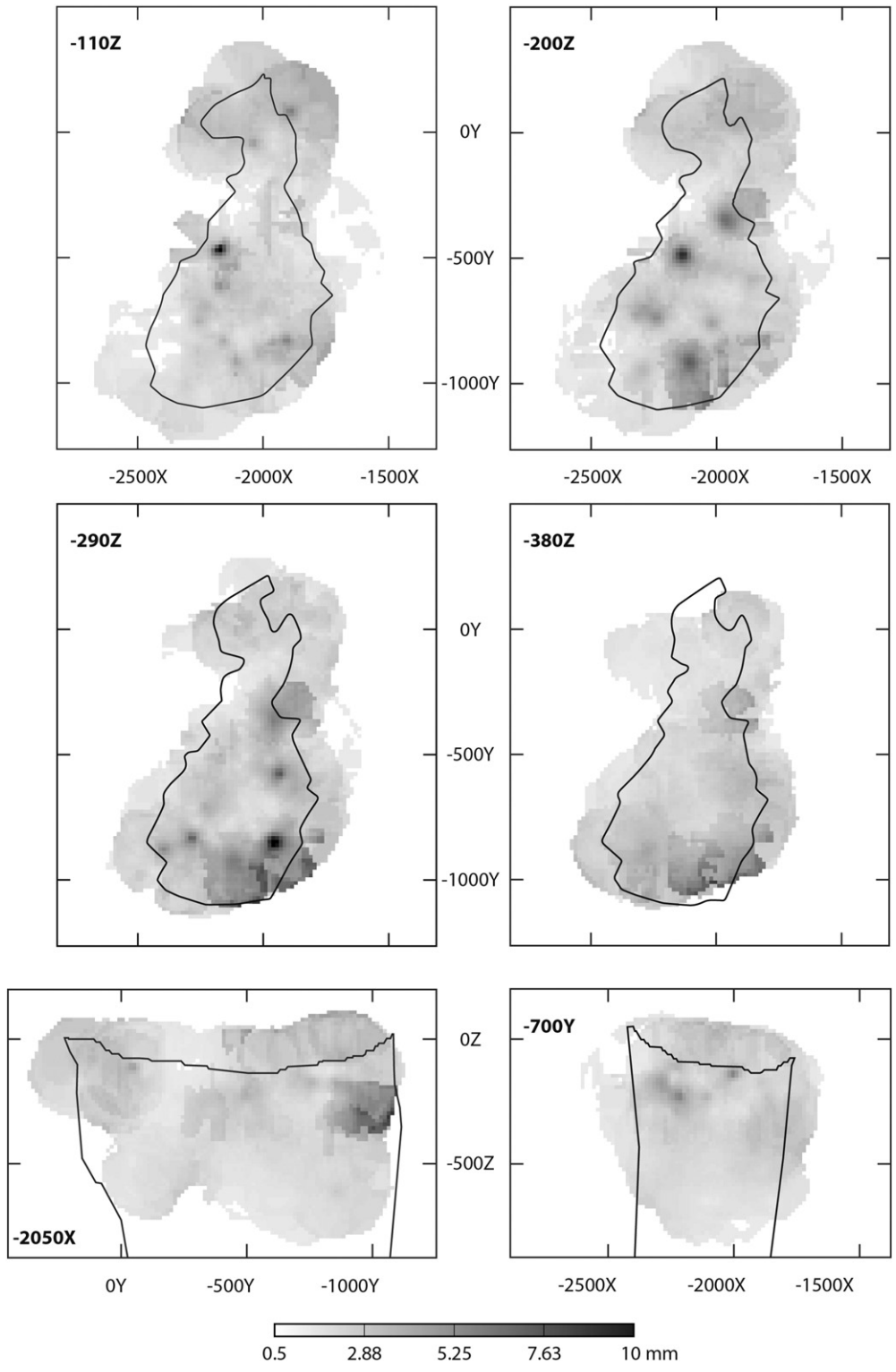

Fig. 8. Distribution of mean equivalent circular diameter of magnetite grains within the phoscorite–carbonatite pipe (black contour).

usually builds up monomineral clusters, lenses and veinlets that consist of polygonal grains of equal size (Fig. 13a). Such segregations are frequently broken into fragments with numerous subparallel fractures that pass from grain to grain. The fractures are filled with serpentine, valleriite and other late minerals. The most typical apatite inclusions are baddeleyite (predominant), magnetite and pyrochlore. Apatite forms inclusions in forsterite, magnetite, baddeleyite (often), calcite, phlogopite and dolomite (sometimes).

Mean equivalent circle diameter of apatite grains in phoscorites and phoscorite-related carbonatites ranges from 0.04 to 0.4 mm (Table 4). Within the phoscorite–carbonatite pipe, apatite grain size varies similarly to that of magnetite (Fig. 14): it grows considerably from early (apatite)-forsterite phoscorites of the marginal zone to intermediate carbonate-free magnetite-rich phoscorites and then slightly decreases in later carbonate-rich phoscorites and phoscorite-related carbonatites. Besides, apatite grain size gradually increases with depth.

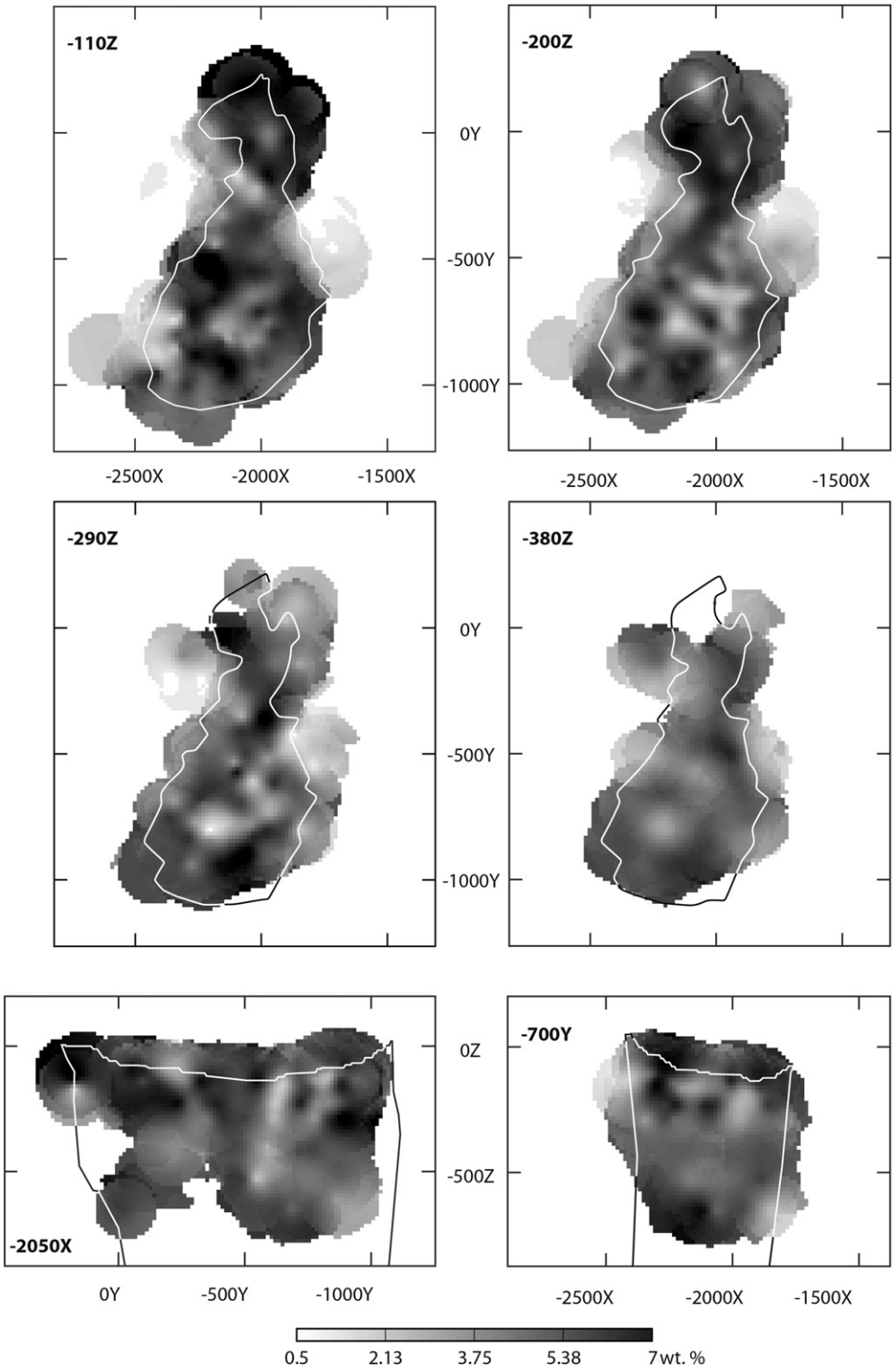

Fig. 9. Distribution of MgO in magnetite within the phoscorite–carbonatite pipe (black/white contour).

In calcitic and dolomitic carbonatite veins, apatite forms isolated or chained grains lying along boundaries of carbonate crystals (Fig. 13c). The grains vary in shape from isometric to oval and elongated prismatic. There are also small lens-like monomineral segregations that consist of polygonal or irregularly shaped apatite grains. Besides, apatite forms inclusions in calcite, magnetite, dolomite and phlogopite grains and contains ingrowths of baddeleyite, calcite, pyrochlore and dolomite. Mean equivalent circular diameter of apatite grains is 0.23 mm in calcitic carbonatite vein and 0.19 mm in dolomitic carbonatite vein.

In magnetite–dolomite-phlogopite-serpentine rock, apatite grains vary in shape from irregular (separated grains) to rounded (inclusions in dolomite and magnetite) and polygonal (in monomineral segregations). Dolomite-serpentine aggregate often carries small grains of newly-formed secondary fluorapatite concentrated in lens and jet-like

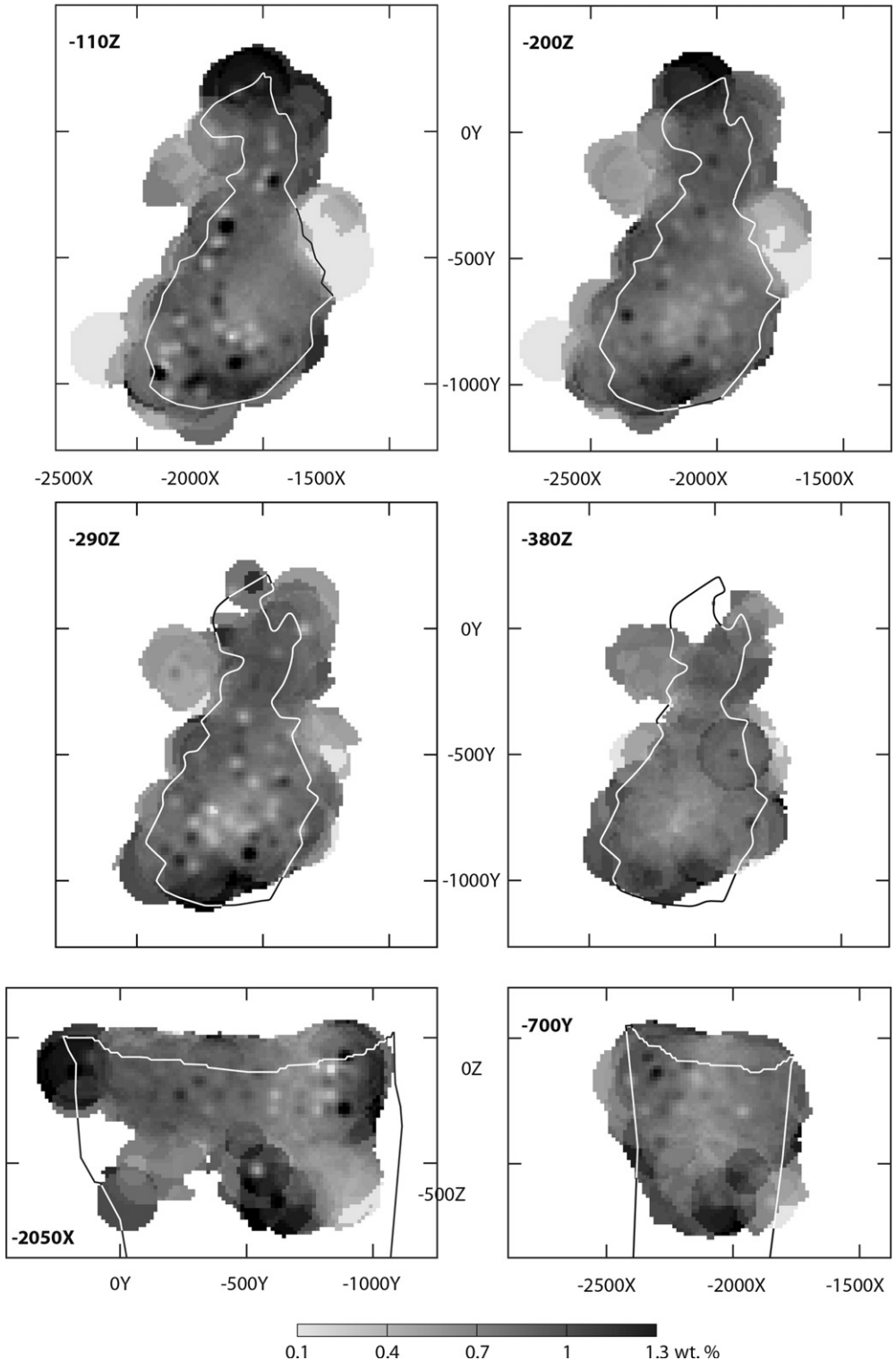

Fig. 10. Distribution of Al_2O_3 in magnetite within the phoscorite–carbonatite pipe (black/white contour).

aggregates (Fig. 13d). Apatite is often found in dolomite, magnetite, phlogopite, serpentine and forsterite grains, and in its turn contains inclusions of baddeleyite, dolomite and phlogopite. Mean equivalent circle diameter of apatite grains in this rock is 0.2 mm.

Results of both microprobe (Tables 4 and 5) and wet chemical analyses of apatite (Rimskaya-Korsakova et al., 1968, 1979; Kurbatova, 1974, 1986) demonstrate stability of its chemical composition and relatively low content of impurities. Therefore, average composition of apatite $(Ca_{4.96}Sr_{0.03}Na_{0.03}Mg_{0.02})_{\Sigma 5.04}[(P_{2.98}Si_{0.01})_{\Sigma 2.99}O_{12}](OH_{0.6}F_{0.4})$ is rather close to its theoretical formula of hydroxylapatite with quite insignificant variations in mineral composition of the natural phoscorite and carbonatite sequence. Nonetheless, the content of Sr, Ln and Ba in apatite tends to increase gradually due to Si, Fe and Mg, from early (apatite)-forsterite phoscorites through carbonate-free magnetite-rich phoscorites to carbonate-rich phoscorites and phoscorite-related carbonatites. The maximum content of Ca and P in apatite is found in apatite-rich phoscorites of the intermediate stage (A-, AF- and MAF-varieties).

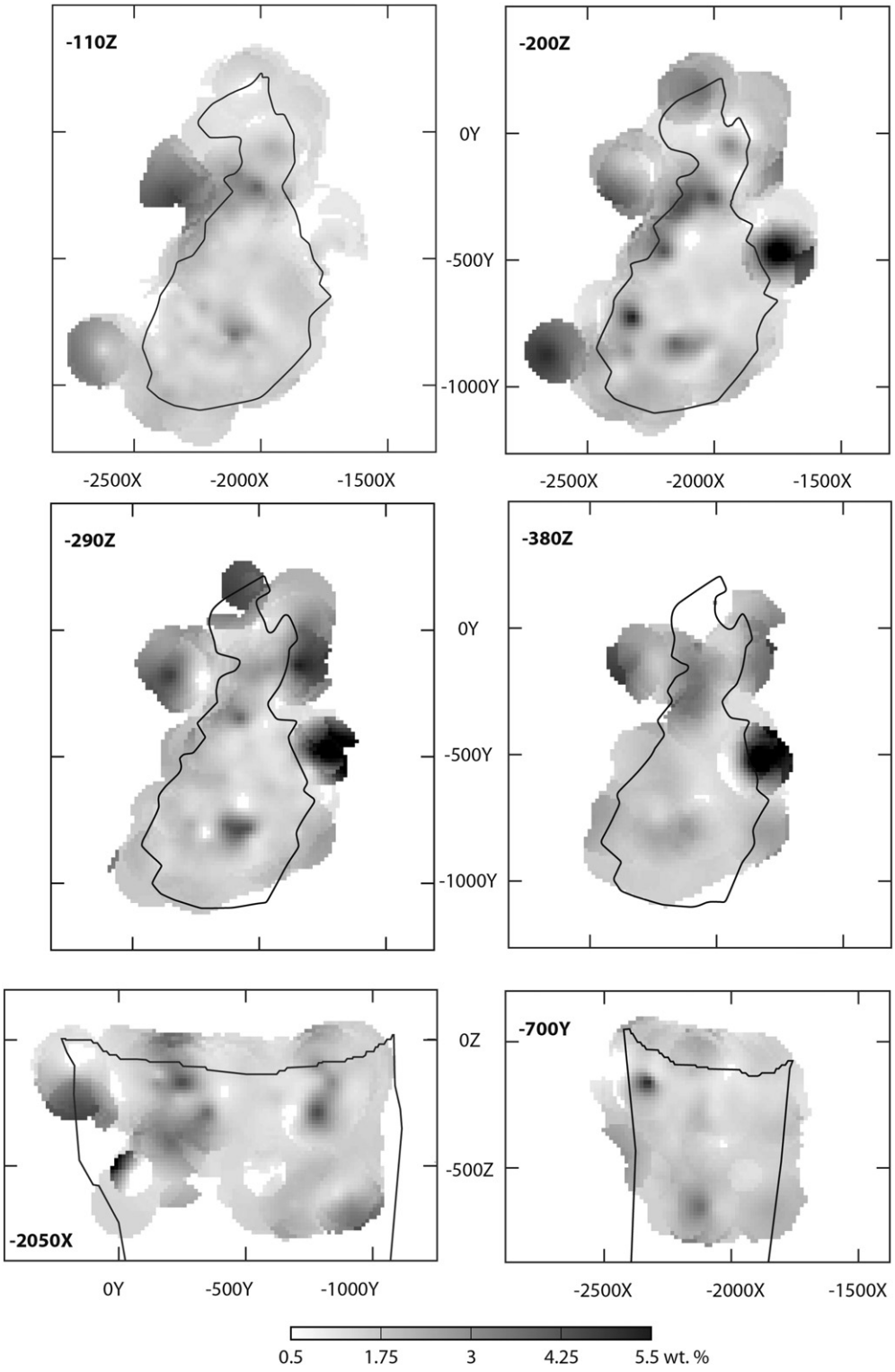

Fig. 11. Distribution of TiO_2 in magnetite within the phoscorite–carbonatite pipe (black contour).

In accordance with the above trend, the radial zonation of the phoscorite–carbonatite pipe can be described in terms of apatite composition with the following chain of isomorphic substitutions (from marginal zone to axis of the pipe): $Mg^{2+} + Fe^{3+} + Si^{4+} \leftrightarrow 2Ca^{2+} + P^{5+} \leftrightarrow Sr^{2+} + Ln^{3+} + Si^{4+}$ (Figs. 15 and 16). REEs are mainly represented by LREEs (in ppm): La 311, Ce 761, Pr 83, Nd 292, Sm 41, Eu 10, Gd 31, Tb 3, Dy 13, Ho 2, Er 4, Tm 0.4, Yb 2, Lu 0.2, Y 41 (average of 40 LA ICP MS assays; Zaitsev et al., 2014; see also Table 4). It should be highlighted that at the later stages of the process, predominant hydroxylapatite was replaced by fluorapatite with increased content of carbon (Kurbatova et al., 1972; Kurbatova, 1974; Rimskaya-Korsakova et al., 1979). As a result of such substitution, a carbonate-bearing fluorapatite (staffelite) was formed. It cemented fragments of phoscorite, carbonatite and fenite in funnel-like explosion bodies located near the present-day surface (Krasnova, 1979; Ivanyuk et al., 2002; Krasnova et al., 2004).

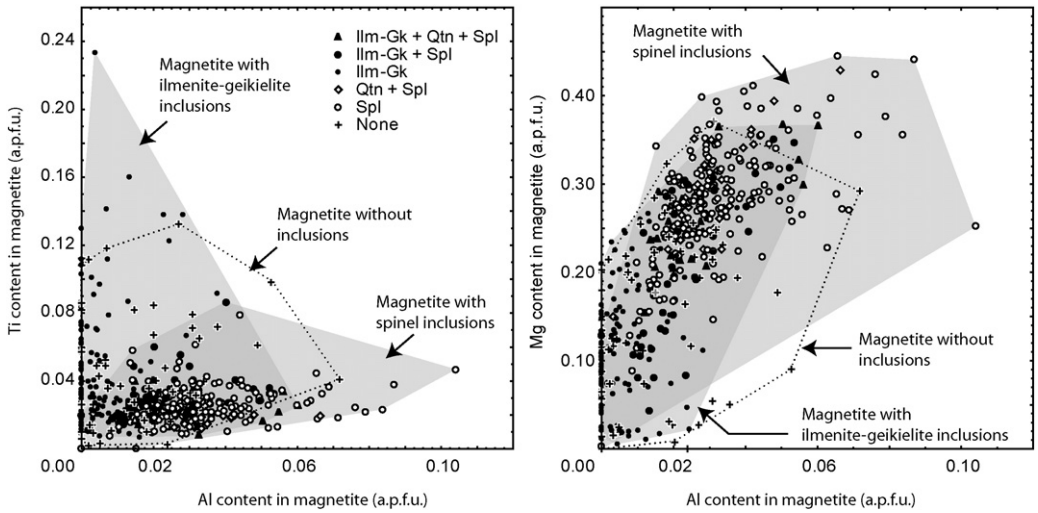

Fig. 12. Proportion of Al, Ti and Mg in magnetite grains with different exsolution inclusions.

Apatite of host silicate rocks (foidolite, diopsidite and phlogopitite) is rather rich in Si, Mn, Na and Ln (Tables 4 and 5) due to substitutions of $Ca^{2+} \leftrightarrow Mn^{2+}$, $2Ca^{2+} \leftrightarrow Ln^{3+} + Na^{+}$, and $Ca^{2+} + P^{5+} \leftrightarrow Ln^{3+} + Si^{4+}$. Calcitic and dolomitic vein carbonatites contain apatite that is comparatively rich in K, Sr and Ln. Magnetite–dolomite-phlogopite-serpentine rocks accommodate apatite with high content of Mg, Ba and, especially, Sr (up to 19 wt.% SrO).

No secondary minerals replace apatite in explicit form. However, rare secondary phosphates mostly remain in regions with pure apatite, which can result from apatite self-cleaning rom impurities at the hydrothermal stage of ore-genesis (Ivanyuk et al., 2002, 2012; Mikhailova et al., 2015). Another possible product of apatite alteration is ancylite-(Ce) that could be formed according to the following reaction:

$$\underset{\text{Sr-Ce-rich hydroxylapatite}}{3(Ca_3SrCe)P_2SiO_{12}(OH)} + \underset{\text{Calcite}}{CaCO_3} + 5CO_2 + 4H_2O$$

$$= \underset{\text{Hydroxylapatite}}{2Ca_5(PO_4)_3(OH)} + \underset{\text{Ancylite-(Ce)}}{3SrCe(CO_3)_2(OH)\cdot H_2O} + 3SiO_2\,.$$

Therefore, there is no surprise that the habitats of ancylite-(Ce) and Ln-rich hydroxylapatite perfectly match (Kalashnikov et al., 2012).

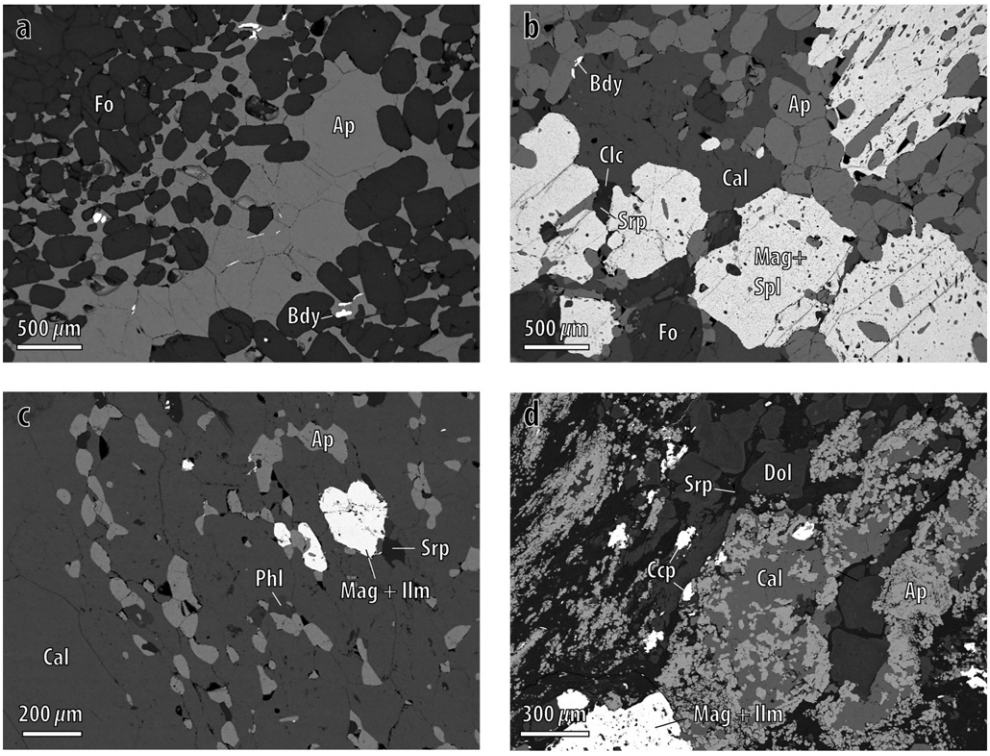

Fig. 13. BSE-images of characteristic apatite aggregates: a — magnetite-apatite-forsterite phoscorite 919/226.2; b — phoscorite-related carbonatite 974/82.5; c — calcitic vein carbonatite 963/123.1; d — magnetite–dolomite-phlogopite-serpentine rock 996/560.9. Ap — apatite, Bdy — baddeleyite, Cal — calcite, Clc — clinochlore, Dol — dolomite, Fo — forsterite, Ilm — ilmenite, Mag — magnetite, Phl — phlogopite, Spl — spinel, Srp — serpentine.

Table 4
Grain size and chemical composition of apatite (mean ± SD/min–max).

Rock (number of analyses)	Content, modal %	D_{eq}, mm	F*	Na_2O	MgO	SiO_2	P_2O_5	CaO	MnO	FeO	SrO	La_2O_3	Ce_2O_3	Nd_2O_3
Foidolite (23)	1 ± 1	0.1 ± 0.1	1.3 ± 0.7	0.2 ± 0.1	0.03 ± 0.05	0.4 ± 0.2	41.4 ± 0.6	54.4 ± 0.5	0.00 ± 0.01	0.02 ± 0.03	0.6 ± 0.2	0.02 ± 0.06	0.3 ± 0.2	0.03 ± 0.05
	0–5	0.01–0.60	0.25–1.82	<0.1–0.32	<0.1–0.19	0.1–1.05	40.24–43.13	53.38–55.09	<0.01–0.06	<0.01–0.12	0.25–0.94	<0.05–0.31	<0.05–0.59	<0.05–0.20
Diopsidite (23)	2 ± 6	0.08 ± 0.06	1.6 ± 0.8	0.2 ± 0.2	0.08 ± 0.08	0.3 ± 0.3	41.5 ± 0.7	55.2 ± 0.6	0.00 ± 0.01	0.03 ± 0.05	0.4 ± 0.1	<0.05	0.1 ± 0.1	<0.05
	0–30	0.01–0.20	0.73–3.17	<0.1–0.67	<0.1–0.31	<0.05–1.00	40.32–42.59	53.82–56.21	<0.01–0.03	<0.01–0.17	0.22–0.71		<0.05–0.41	
Phlogopitite (16)	6 ± 5	0.2 ± 0.2	1.46	0.3 ± 0.2	0.1 ± 0.1	0.2 ± 0.2	41.4 ± 0.8	55 ± 1	0.03 ± 0.09	0.1 ± 0.1	0.5 ± 0.4	0.01 ± 0.02	0.1 ± 0.1	0.01 ± 0.06
	0–15	0.02–0.80		<0.1–0.78	<0.1–0.35	<0.05–0.72	40.17–42.66	52.26–56.27	<0.01–0.36	<0.01–0.53	0.20–1.50	<0.05–0.09	<0.05–0.40	<0.05–0.23
F (10)	2 ± 2	0.08 ± 0.02	1.17	0.22 ± 0.08	0.19 ± 0.07	0.14 ± 0.06	41.9 ± 0.2	55.3 ± 0.4	<0.01	0.04 ± 0.06	0.3 ± 0.2	<0.05	0.03 ± 0.07	<0.05
	0–5	0.06–0.11		0.12–0.35	0.12–0.32	0.05–0.24	41.59–42.30	54.60–55.70		<0.01–0.19	0.14–0.81		<0.05–0.23	
AF (27)	35 ± 26	0.2 ± 0.1	1.6 ± 0.9	0.14 ± 0.09	0.17 ± 0.08	0.11 ± 0.07	41.7 ± 0.5	55.0 ± 0.4	0.00	0.05 ± 0.05	0.30 ± 0.09	<0.05	0.01 ± 0.04	<0.05
	10–80	0.04–0.40	0.86–3.42	<0.1–0.28	<0.1–0.33	<0.05–0.24	40.64–42.55	54.31–56.21	<0.01–0.01	<0.01–0.21	0.17–0.55		<0.05–0.06	
MF (13)	2 ± 2	0.2 ± 0.2	1.2 ± 0.2	0.2 ± 0.3	0.3 ± 0.4	0.2 ± 0.5	41 ± 3	54 ± 3	0.03 ± 0.07	0.1 ± 0.1	0.6 ± 0.7	<0.05	0.03 ± 0.06	<0.05
	0–5	0.04–0.70	0.99–1.50	<0.1–1.15	0.08–1.76	<0.05–2.00	30.89–42.72	44.90–56.09	<0.01–0.23	<0.01–0.47	0.19–2.48		<0.05–0.18	
MAF (122)	35 ± 15	0.3 ± 0.2	1.5 ± 0.8	0.15 ± 0.09	0.14 ± 0.08	0.1 ± 0.2	42.0 ± 0.5	55.2 ± 0.6	<0.01	0.02 ± 0.03	0.4 ± 0.4	<0.05	0.0 ± 0.2	<0.05
	10–70	0.02–1.00	0.69–3.51	<0.1–0.35	<0.1–0.64	<0.05–1.87	39.39–43.26	50.72–57.04		<0.01–0.16	<0.1–4.46		<0.05–1.63	
MA (22)	18 ± 13	0.4 ± 0.3	1.1 ± 0.1	0.2 ± 0.2	0.10 ± 0.07	0.07 ± 0.05	42.0 ± 0.7	55.4 ± 0.8	0.0 ± 0.2	0.02 ± 0.03	0.4 ± 0.1	<0.05	0.04 ± 0.06	<0.05
	5–50	0.10–1.20	0.98–1.35	<0.1–0.83	<0.1–0.23	<0.05–0.15	39.87–42.99	52.78–56.79	<0.01–0.80	<0.01–0.14	0.22–0.58		<0.05–0.15	
M (8)	2 ± 2	0.14 ± 0.09	<0.5	0.10 ± 0.09	0.11 ± 0.06	0.07 ± 0.05	42.1 ± 0.7	55.3 ± 0.3	<0.01	0.1 ± 0.1	0.4 ± 0.1	0.04 ± 0.08	0.07 ± 0.09	<0.05
	0–5	0.02–0.30		<0.1–0.25	<0.1–0.21	<0.05–0.14	40.90–42.75	54.93–55.75		<0.01–0.30	0.28–0.58	<0.05–0.23	<0.05–0.25	
CMAF (72)	27 ± 11	0.3 ± 0.1	1.2 ± 0.5	0.2 ± 0.1	0.09 ± 0.06	0.09 ± 0.06	41.8 ± 0.5	55.3 ± 0.5	<0.01	0.01 ± 0.02	0.4 ± 0.2	0.01 ± 0.05	0.08 ± 0.09	<0.05
	10–60	0.05–0.60	0.32–1.86	<0.1–0.37	<0.1–0.28	<0.05–0.43	40.65–43.00	54.22–56.37		<0.01–0.12	<0.1–0.83	<0.05–0.45	<0.05–0.43	
CMF (8)	1 ± 2	0.2 ± 0.2	0.5 ± 0.1	0.17 ± 0.08	0.2 ± 0.1	0.11 ± 0.08	42.0 ± 0.7	55.4 ± 0.7	<0.01	0.00 ± 0.01	0.4 ± 0.1	<0.05	0.08 ± 0.07	0.01 ± 0.03
	0–5	0.02–0.55	0.34–0.62	<0.1–0.25	<0.1–0.46	<0.05–0.26	40.56–42.71	54.53–56.64		<0.01–0.02	0.24–0.65		<0.05–0.18	<0.05–0.09
CAF (10)	35 ± 13	0.3 ± 0.2	2 ± 1	0.1 ± 0.1	0.2 ± 0.1	0.14 ± 0.09	42.0 ± 0.3	55.3 ± 0.5	<0.01	0.01 ± 0.01	0.35 ± 0.09	<0.05	0.01 ± 0.03	<0.05
	20–55	0.08–0.60	1.05–3.33	<0.1–0.33	<0.1–0.33	<0.05–0.31	41.31–42.45	54.74–55.96		<0.01–0.04	0.19–0.47		<0.05–0.08	
CMA (32)	29 ± 17	0.3 ± 0.2	2 ± 1	0.3 ± 0.4	0.2 ± 0.5	0.08 ± 0.05	41 ± 3	54 ± 3	<0.01	0.02 ± 0.04	1 ± 3	0.01 ± 0.04	0.1 ± 0.2	<0.05
	10–63	0.10–0.80	0.30–3.68	<0.1–1.67	<0.1–1.57	<0.05–0.19	33.44–43.42	43.26–56.24		<0.01–0.16	0.23–10.53	<0.05–0.15	<0.05–0.59	
CA (3)	57 ± 8	0.2 ± 0.1	1.2 ± 0.2	<0.1	0.08 ± 0.01	0.07 ± 0.07	42.0 ± 0.4	55.5 ± 0.2	<0.01	<0.01	0.5 ± 0.2	<0.05	0.08 ± 0.07	<0.05
	50–65	0.15–0.40	1.09–1.39		0.07–0.09	<0.05–0.12	41.61–42.49	55.29–55.72			0.34–0.67		<0.05–0.14	
CM (1)	3 ± 4	0.04	<0.5	0.29	0.07	0.07	42.64	54.39	<0.01	0.37	0.77	<0.05	<0.05	<0.05
	0–5													
Phoscorite-related carbonatite (40)	17 ± 10	0.3 ± 0.1	0.8 ± 0.8	0.2 ± 0.4	0.08 ± 0.07	0.09 ± 0.07	41.8 ± 0.9	55.0 ± 0.8	<0.01	0.04 ± 0.11	0.5 ± 0.2	<0.05	0.12 ± 0.09	<0.05
	2–40	0.10–0.70	0.28–2.25	<0.1–1.95	<0.1–0.32	<0.05–0.33	38.79–42.89	52.13–55.93		<0.01–0.45	0.24–1.17		<0.05–0.35	
Vein carbo-natite (56)	6 ± 4	0.2 ± 0.1	2 ± 1	0.2 ± 0.1	0.07 ± 0.05	0.08 ± 0.07	41.8 ± 0.5	55.2 ± 0.7	0.00 ± 0.01	0.03 ± 0.09	0.6 ± 0.9	0.00 ± 0.01	0.11 ± 0.09	0.00 ± 0.02
	0–15	0.04–0.45	0.25–3.59	<0.1–0.35	<0.1–0.22	<0.05–0.39	40.52–42.90	52.27–56.26	<0.01–0.03	<0.01–0.56	0.14–6.58	<0.05–0.11	<0.05–0.29	<0.05–0.14
Mag–Dol–Phl–Srp rock (35)	8 ± 11	0.2 ± 0.2	2.0 ± 0.8	0.3 ± 0.6	1 ± 1	0.2 ± 0.5	41 ± 2	53 ± 5	0.03 ± 0.07	0.2 ± 0.3	2 ± 5	0.00 ± 0.02	0.1 ± 0.2	<0.05
	0–35	0.01–0.70	1.43–3.53	<0.1–2.32	<0.1–5.25	<0.05–2.24	36.95–42.58	40.95–56.42	<0.01–0.32	<0.01–1.11	0.17–18.81	<0.05–0.12	<0.05–0.68	

* Fluorine are measured by EDS analyses or wet chemistry method. "<n" refers to value below limit of accuracy.
A — apatite, F — forsterite, M — magnetite, C — carbonates (calcite and dolomite); D_{eq} – mean equivalent circular diameter of grains.

Table 5
Apatite formulae (atoms per formula unit) calculated on the basis of O = 12.5 (mean ± SD/min–max).

Rock	Ca	Sr	Na	Mg	Fe	Ce	La	Nd	Mn	P	Si	F
Foidolites	4.94 ± 0.05	0.03 ± 0.01	0.03 ± 0.02	0.00 ± 0.01	0.00	0.01	0.00	0.00	–	2.97 ± 0.03	0.03 ± 0.02	0.3 ± 0.2
	4.82–5.03	0.01–0.05	0.00–0.05	0.00–0.02	0.00–0.01	0.00–0.02	0.00–0.01	0.00–0.01		2.92–3.04	0.00–0.09	0.07–0.48
Diopsidite	4.99 ± 0.05	0.02 ± 0.01	0.03 ± 0.03	0.01 ± 0.01	0.00	0.00	–	–	–	2.96 ± 0.02	0.03 ± 0.02	0.4 ± 0.2
	4.88–5.09	0.00–0.03	0.00–0.11	0.00–0.04	0.00–0.01	0.00–0.01				2.92–3.01	0.00–0.08	0.19–0.84
Phlogopitite	4.99 ± 0.08	0.02 ± 0.02	0.04 ± 0.03	0.01 ± 0.01	0.00 ± 0.01	0.00	–	0.00	0.00 ± 0.01	2.96 ± 0.02	0.01 ± 0.02	0.39
	4.76–5.11	0.01–0.07	0.00–0.13	0.00–0.04	0.00–0.04	0.00–0.01		0.00–0.01	0.00–0.03	2.93–2.99	0.00–0.06	
F	4.97 ± 0.03	0.01 ± 0.01	0.04 ± 0.01	0.02 ± 0.01	0.00	0.00	–	–	–	2.98 ± 0.01	0.01 ± 0.01	0.31
	4.93–5.03	0.01–0.04	0.02–0.06	0.01–0.04	0.00–0.01	0.00–0.01				2.97–2.99	0.00–0.02	
AF	4.98 ± 0.05	0.01	0.02 ± 0.01	0.02 ± 0.01	0.00	–	–	–	0.00	2.98 ± 0.02	0.01 ± 0.01	0.4 ± 0.2
	4.89–5.07	0.01–0.03	0.00–0.05	0.00–0.04	0.00–0.01				0.00–0.01	2.94–3.02	0.00–0.02	0.23–0.91
MF	4.96 ± 0.03	0.03 ± 0.04	0.03 ± 0.06	0.04 ± 0.07	0.00 ± 0.01	0.00	–	–	0.00 ± 0.01	2.96 ± 0.09	0.02 ± 0.05	0.32 ± 0.04
	4.90–5.01	0.01–0.15	0.00–0.23	0.01–0.27	0.00–0.03	0.00–0.01			0.00–0.02	2.66–3.01	0.00–0.20	0.26–0.40
MAF	4.97 ± 0.05	0.02 ± 0.02	0.02 ± 0.02	0.02 ± 0.01	0.00	0.00	–	–	–	2.98 ± 0.02	0.01 ± 0.01	0.4 ± 0.2
	4.58–5.10	0.00–0.22	0.00–0.06	0.00–0.08	0.00–0.01	0.00–0.05				2.81–3.04	0.00–0.16	0.18–0.93
MA	4.99 ± 0.04	0.02	0.03 ± 0.03	0.01 ± 0.01	0.00	–	–	–	0.00 ± 0.01	2.98 ± 0.02	0.01	0.29 ± 0.04
	4.91–5.09	0.01–0.03	0.00–0.14	0.00–0.03	0.00–0.01				0.00–0.06	2.94–3.01	0.00–0.01	0.26–0.36
M	4.96 ± 0.05	0.02 ± 0.01	0.02 ± 0.02	0.01 ± 0.01	0.00 ± 0.01	0.00	0.00	–	–	2.99 ± 0.02	0.01	–
	4.90–5.05	0.01–0.03	0.00–0.04	0.00–0.03	0.00–0.02	0.00–0.01	0.00–0.01			2.96–3.01	0.00–0.01	
CMAF	4.99 ± 0.04	0.02 ± 0.01	0.02 ± 0.02	0.01 ± 0.01	0.00	0.00	0.00	–	–	2.98 ± 0.01	0.01 ± 0.01	0.3 ± 0.1
	4.90–5.07	0.00–0.04	0.00–0.06	0.00–0.03	0.00–0.01	0.00–0.01	0.00–0.01			2.94–3.01	0.00–0.04	0.08–0.49
CMF	4.97 ± 0.05	0.02 ± 0.01	0.02 ± 0.01	0.02 ± 0.02	–	0.00	–	–	–	2.98 ± 0.01	0.01 ± 0.01	0.12 ± 0.03
	4.90–5.06	0.01–0.03	0.00–0.04	0.00–0.06		0.00–0.01				2.96–3.00	0.00–0.02	0.09–0.16
CAF	4.97 ± 0.04	0.02	0.02 ± 0.02	0.02 ± 0.01	–	–	–	–	–	2.98 ± 0.01	0.01 ± 0.01	0.5 ± 0.3
	4.92–5.03	0.01–0.02	0.00–0.05	0.00–0.04						2.96–3.00	0.00–0.03	0.28–0.88
CMA	5.0 ± 0.1	0.1 ± 0.1	0.04 ± 0.08	0.03 ± 0.07	0.00	0.00 ± 0.01	0.00	–	–	2.96 ± 0.07	0.01	0.5 ± 0.3
	4.51–5.10	0.01–0.59	0.00–0.32	0.00–0.23	0.00–0.01	0.00–0.02	0.00–0.01			2.78–3.04	0.00–0.02	0.08–0.98
CA	4.98 ± 0.02	0.02 ± 0.01	–	0.01 ± 0.01	–	–	–	–	–	2.99 ± 0.01	0.01 ± 0.01	0.33 ± 0.06
	4.96–5.00	0.02–0.03		0.00–0.01						2.97–2.99	0.00–0.01	0.29–0.37
CM	4.86	0.04	0.05	0.01	0.03	0.01	–	–	–	3.01	–	–
Phoscorite-related carbonatite	4.97 ± 0.04	0.02 ± 0.01	0.04 ± 0.07	0.01 ± 0.01	0.00 ± 0.01	0.00	–	–	–	2.98 ± 0.03	0.01 ± 0.01	0.2 ± 0.2
	4.55–5.04	0.01–0.06	0.00–0.33	0.00–0.04	0.00–0.03	0.00–0.01				2.91–3.02	0.00–0.03	0.07–0.60
Vein carbonatite	4.97 ± 0.05	0.03 ± 0.04	0.03 ± 0.02	0.01 ± 0.01	0.00 ± 0.01	0.00	–	–	–	2.98 ± 0.02	0.01 ± 0.01	0.4 ± 0.3
	4.79–5.06	0.01–0.33	0.00–0.06	0.00–0.03	0.00–0.04	0.00–0.01				2.94–3.01	0.00–0.03	0.07–0.95
Mag–Dol–Phl–Srp rock	4.8 ± 0.3	0.1 ± 0.3	0.1 ± 0.1	0.1 ± 0.1	0.01 ± 0.02	0.00 ± 0.01	–	–	0.00 ± 0.01	2.95 ± 0.06	0.02 ± 0.05	0.5 ± 0.2
	3.95–5.08	0.01–0.98	0.00–0.40	0.00–0.70	0.00–0.08	0.00–0.02			0.00–0.02	2.75–3.00	0.00–0.20	0.38–0.94

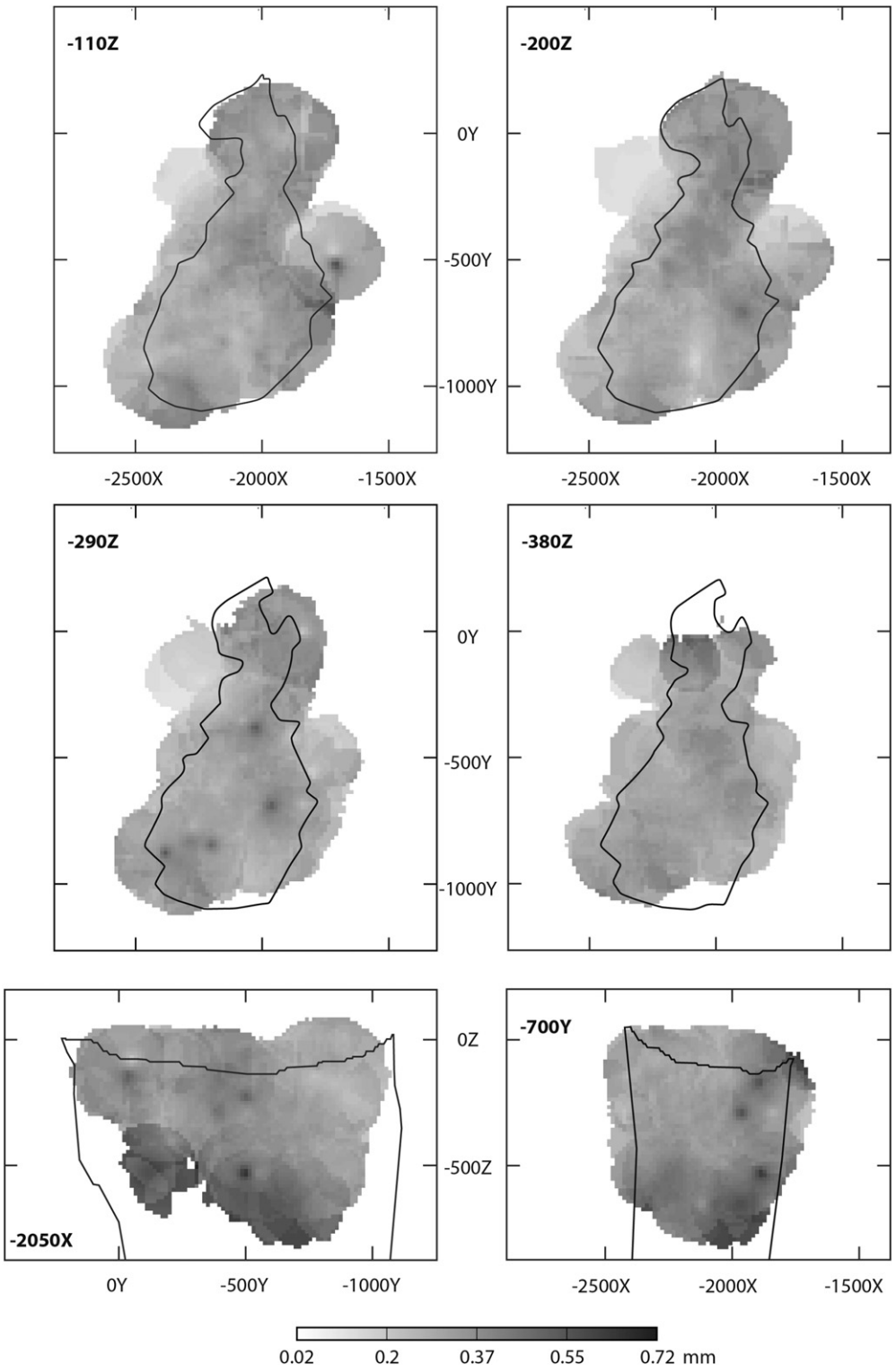

Fig. 14. Size distribution of apatite grains within the phoscorite–carbonatite pipe (black contour).

6. Baddeleyite

Baddeleyite is an accessory mineral of the most rocks in the Kovdor massif. It forms economic concentrations in the phoscorite–carbonatite complex (Rimskaya-Korsakova and Dinaburg, 1964; Kukharenko et al., 1965; Kopylova et al., 1980; Ivanyuk et al., 2002; Krasnova et al., 2004; Mikhailova et al., 2015; Kalashnikov et al., 2016). In foidolites, rare homogeneous prismatic inclusions of baddeleyite (average length is 16 μm) occur in the grains of diopside, titanite, phlogopite, apatite and calcite. In diopsidite, it forms small (up to 50 μm long) flattened prismatic inclusions in magnetite, diopside, forsterite, and phlogopite grains as well as separate short prismatic crystals (up to 150 μm long) in interstices of rock-forming minerals. Zirconolite is a characteristic product of baddeleyite alteration. Complete pseudomorphs of zirconolite after baddeleyite with small relics of the latter are widespread here. The average length of baddeleyite grains in diopsidite is

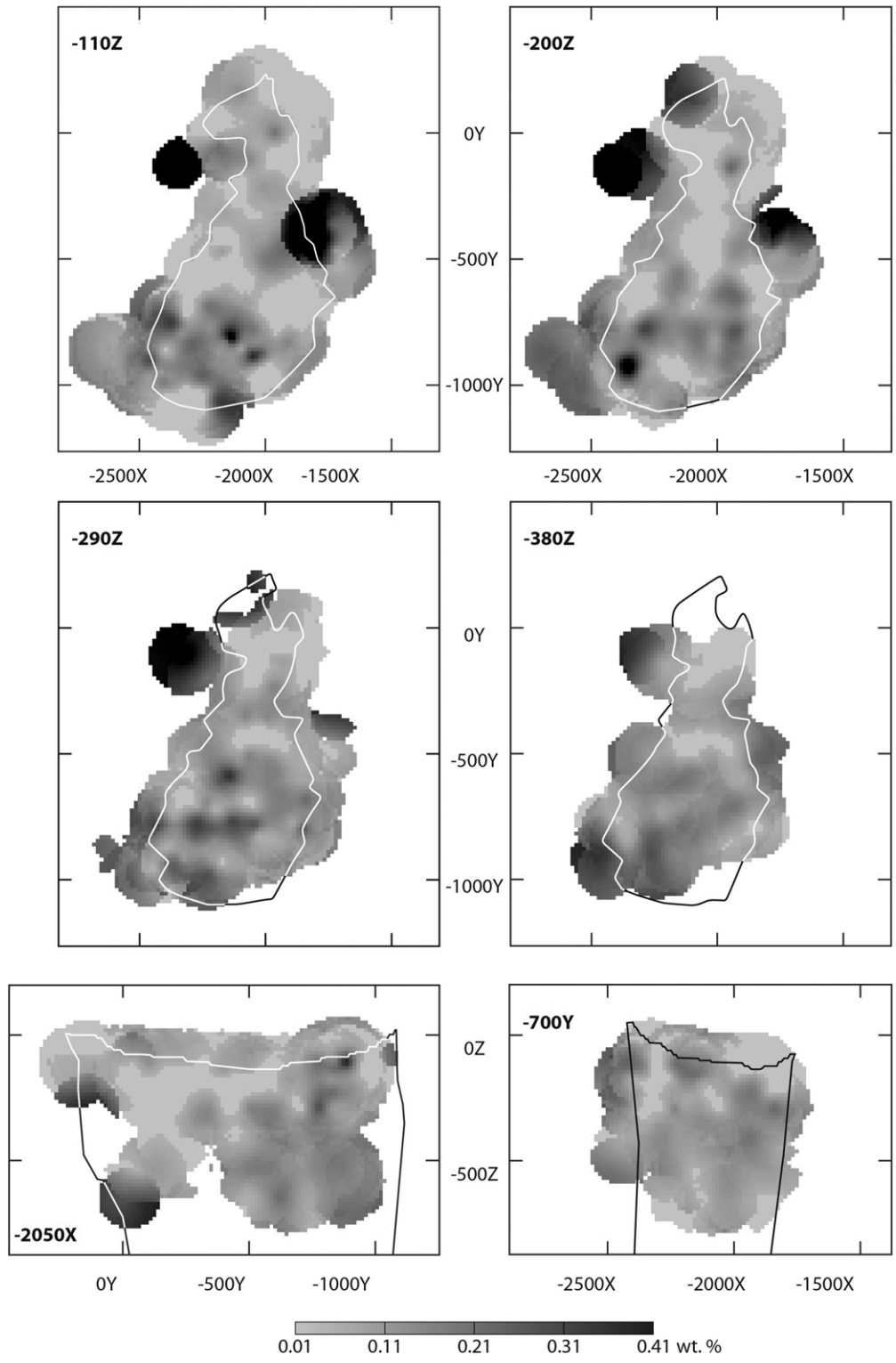

Fig. 15. Distribution of REE_2O_3 in apatite within the phoscorite–carbonatite pipe (black/white contour).

42 μm. Phlogopitite carries separate unaltered prismatic crystals and cross-like twins of baddeleyite (up to 250 μm long) as well as smaller inclusions of baddeleyite remained in phlogopite, magnetite and forsterite grains. The average length of baddeleyite crystals is 46 μm.

In forsterite-dominant and apatite-forsterite phoscorites, baddeleyite usually occurs as irregularly shaped grains and flattened prismatic crystals (up to 200 μm long) in interstices of rock-forming minerals (Fig. 17a). Comparatively large crystals of baddeleyite are often sliced with subparallel fractures filled with serpentine, pyrite and valleriite. Zirconolite and pyrochlore aggregates frequently replace (especially, the former) and cover (especially, the latter) baddeleyite grains (Fig. 17b). The average length of baddeleyite grains in these phoscorites is 34 μm (Table 6).

Comparatively large (up to 300 μm long) baddeleyite poikilitic crystals with numerous inclusions of apatite, forsterite, phlogopite, dolomite and ilmenite most frequently occur in carbonate-free magnetite-rich

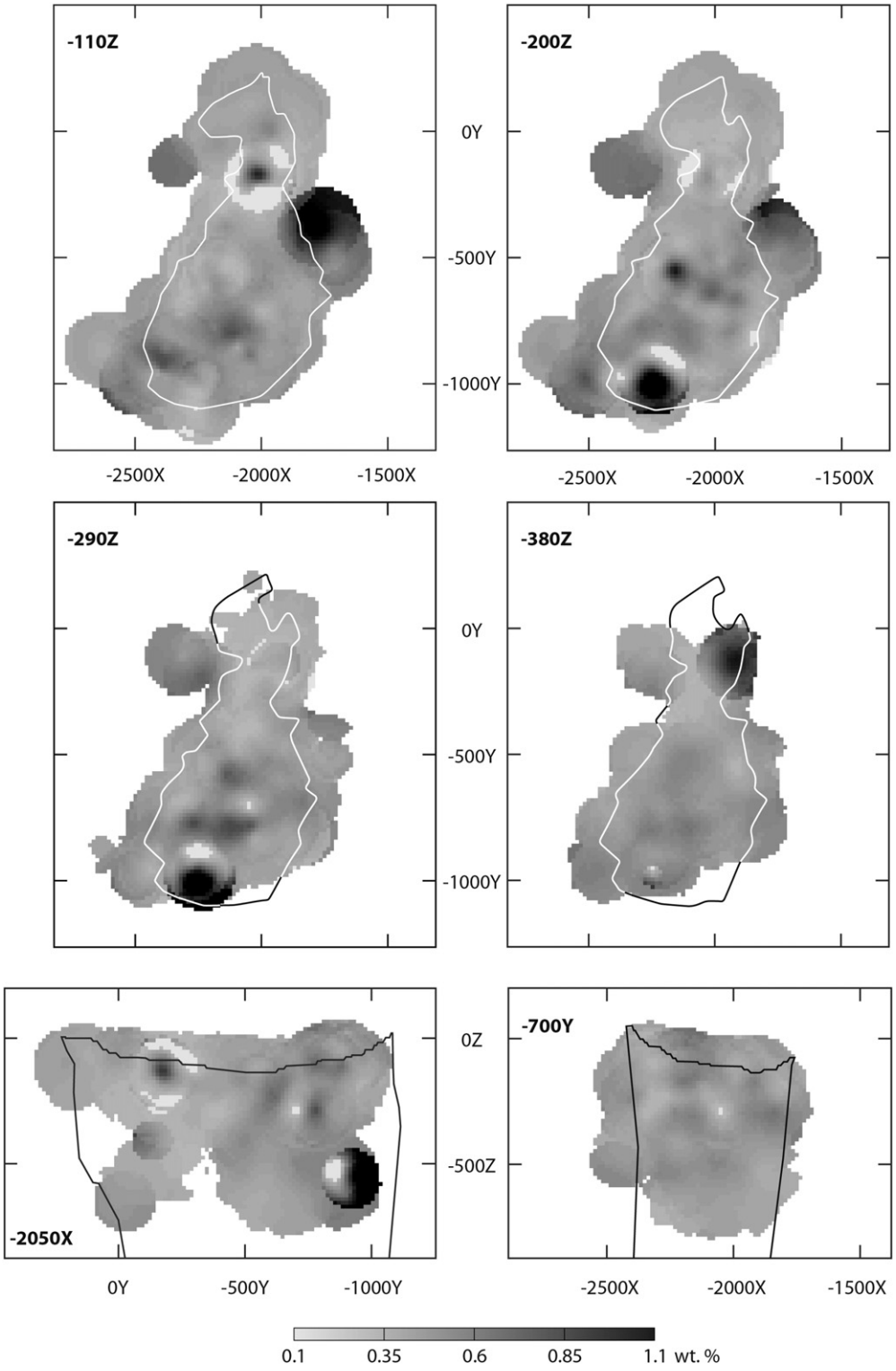

Fig. 16. Distribution of SrO in apatite within the phoscorite–carbonatite pipe (black contour).

phoscorites (M, MA, MF, and MAF; Fig. 17c). Coming second are the prismatic crystals of baddeleyite (up to 200 μm long) that were flattened [100] and assumed rhombic prismatic {110}, {011}, pinacoidal {100} and many other, less developed, shapes (Rimskaya-Korsakova and Dinaburg, 1964; Ivanyuk et al., 2002). Such crystals usually feature polyzonal internal structure that is well manifested due to contrast cathodoluminescence of different zones (Fig. 17d). Characteristic twins, trillings and fourlings along (100), (110) and (101) are widespread too. Besides, baddeleyite forms inclusions in dolomite, phlogopite and serpentine, just as in the rock-forming apatite, forsterite and, especially, magnetite. In the latter instance, baddeleyite usually crystallizes to join spinel (Fig. 17e) due to exsolution of Mg–Al-rich magnetite. Baddeleyite inclusions are much rarer in titanium-rich magnetite carrying ilmenite–geikielite lamellae, although such inclusions also occur within the lamellae. Zirconolite and pyrochlore are typical secondary minerals that replace baddeleyite more intensively as compared to

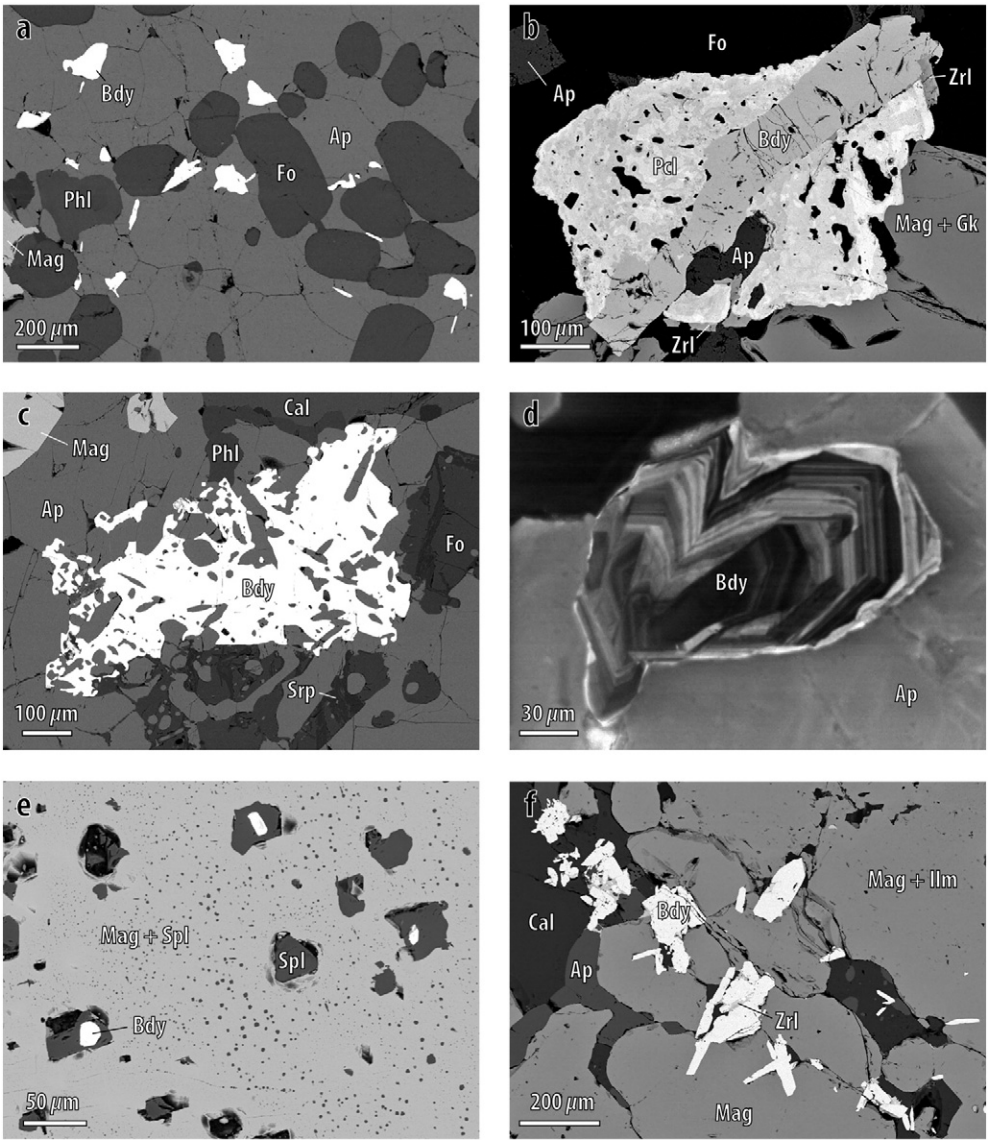

Fig. 17. BSE (a–c, e–f) and cathodoluminescence (d) images of typical morphological varieties of baddeleyite: a — apatite-forsterite phoscorite 964/48.9; b — phlogopitized apatite-forsterite phoscorite 987/99.6; c — magnetite-apatite-forsterite phoscorite 987/227.1; d — magnetite-apatite-forsterite phoscorite 938/92.3; e — phlogipitized magnetite-forsterite phoscorite 1004/496.3; f — calcite–magnetite phoscorite 981/520.0. Ap — apatite, Bdy — baddeleyite, Cal — calcite, Fo — forsterite, Gk — geikielite, Ilm — ilmenite, Mag — magnetite, Pcl — pyrochlore, Phl — phlogopite, Spl — spinel, Srp — serpentine, Zrl — zirconolite.

those in phoscorites of the ore-pipe marginal zone (Rimskaya-Korsakova and Dinaburg, 1964; Ivanyuk et al., 2002; Kalashnikov et al., 2012, 2016; Mikhailova et al., 2015). In the carbonate-free magnetite-rich phoscorites the average length of baddeleyite grains is 83 μm (Table 6).

The following morphological types of baddeleyite (listed in order of abundance) occur in carbonate-rich phoscorites (CA, CM, CMA, CAF, CMF and CMAF) and phoscorite-related carbonatites: irregularly shaped grains (up to 0.7 mm long); flattened prismatic crystals and their twins, trillings and fourlings (up to 0.5 mm long, Fig. 17f); poikilitic crystals with inclusions of apatite (up to 0.7 mm long), pyrochlore and zirconolite; inclusions (up to 50 μm long) in the grains of magnetite, calcite, apatite, forsterite and phlogopite (Rimskaya-Korsakova and Dinaburg, 1964; Ivanyuk et al., 2002; Kalashnikov et al., 2016). Average size of baddeleyite grains in carbonate-rich phoscorites and phoscorite-related carbonatites is 92 μm (Table 6) finalizing the trend towards baddeleyite grains' gradual growth — from silicate host rock to carbonate-rich phoscorites and carbonatites of the ore-pipe axial zone (Fig. 18). We can find here again partial and complete pseudomorphs of pyrochlore and zirconolite after baddeleyite, which mostly occur in carbonate-rich phoscorites and carbonatites along the axis of the phoscorite–carbonatite pipe (Fig. 19).

In calcitic and dolomitic carbonatite vein, baddeleyite usually forms irregularly shaped or tabular grains, flattened prismatic crystals (up to 100 μm long) and cross-like twins of those. Such crystals often contain inclusions of apatite and dolomite, while baddeleyite forms inclusions in grains of the abovementioned minerals and magnetite. Pseudomorphs of zirconolite and pyrochlore after baddeleyite as well as regular intergrowths of pyrochlore with baddeleyite are widely spread (Rimskaya-Korsakova and Dinaburg, 1964; Ivanyuk et al., 2002). Average size of baddeleyite grains in vein carbonatites is 37 μm.

Magnetite–dolomite-phlogopite-serpentine rock accommodates baddeleyite grains of irregular and tabular shapes (up to 220 μm long) in interstices of rock-forming minerals, while smaller prismatic inclusions of baddeleyite are numerous in magnetite, forsterite, dolomite, apatite and phlogopite; and arbitrarily shaped relics are present in grains of zirconolite and pyrochlore (Mikhailova et al., 2015). Average size of baddeleyite grains in the rock is 81 μm.

Table 6
Grain size and chemical composition of baddeleyite (mean ± SD /min–max).

Rock (number of analyses)	*L*, μm	MgO	SiO_2	CaO	Sc_2O_3	TiO_2	Fe_2O_3	ZrO_2	Nb_2O_5	HfO_2	Ta_2O_5
Foidolite (5)	16 ± 16	0.16 ± 0.08	0.01 ± 0.02	0.2 ± 0.2	0.07 ± 0.04	0.04 ± 0.06	0.6 ± 0.5	96.6 ± 0.9	0.2 ± 0.4	1.53 ± 0.07	0.2 ± 0.1
	5–40	<0.1–0.27	<0.05–0.05	<0.03–0.47	0.02–0.14	<0.02–0.12	0.12–1.17	95.21–97.41	<0.05–0.90	1.44–1.63	<0.05–0.30
Diopsidite (14)	42 ± 45	0.15 ± 0.09	0.04 ± 0.05	0.2 ± 0.2	0.09 ± 0.06	0.02 ± 0.05	0.4 ± 0.3	97.1 ± 0.5	0.3 ± 0.5	1.6 ± 0.2	0.2 ± 0.2
	5–150	<0.1–0.32	<0.05–0.12	<0.03–0.67	<0.02–0.21	<0.02–0.16	<0.01–0.99	96.40–98.10	<0.05–1.33	1.26–2.08	<0.05–0.46
Phlogopitite (10)	46 ± 80	0.1 ± 0.1	0.01 ± 0.04	0.2 ± 0.2	0.1 ± 0.1	0.06 ± 0.08	0.3 ± 0.5	97 ± 2	0.2 ± 0.5	1.5 ± 0.2	0.1 ± 0.1
	5–250	<0.1–0.29	<0.05–0.12	<0.03–0.52	<0.02–0.33	<0.02–0.24	<0.01–1.51	92.98–98.45	<0.05–1.51	1.19–1.83	<0.05–0.34
F (7)	18 ± 14	0.2 ± 0.2	0.03 ± 0.05	0.1 ± 0.2	0.03 ± 0.04	0.2 ± 0.3	1 ± 1	97.4 ± 0.8	<0.05	1.7 ± 0.3	0.03 ± 0.07
	5–40	<0.1–0.35	<0.05–0.13	<0.03–0.39	<0.02–0.11	<0.02–0.92	0.08–2.93	96.55–98.43		1.39–2.17	<0.05–0.20
AF (33)	37 ± 41	0.1 ± 0.2	0.03 ± 0.06	0.2 ± 0.2	0.04 ± 0.04	<0.02	0.4 ± 0.5	97.1 ± 0.6	0.1 ± 0.3	1.6 ± 0.3	0.1 ± 0.1
	8–170	<0.1–0.58	<0.05–0.22	<0.03–0.55	<0.02–0.13		<0.01–2.00	95.65–98.21	<0.05–1.34	0.74–2.04	<0.05–0.61
MF (34)	90 ± 80	0.1 ± 0.1	0.01 ± 0.04	0.1 ± 0.1	0.04 ± 0.05	<0.02	0.2 ± 0.2	97.6 ± 0.6	0.0 ± 0.1	1.7 ± 0.2	0.04 ± 0.07
	5–300	<0.1–0.42	<0.05–0.17	<0.03–0.51	<0.02–0.18		<0.01–0.75	96.30–99.06	<0.05–0.56	1.30–2.13	<0.05–0.23
MAF (262)	83 ± 57	0.1 ± 0.1	0.01 ± 0.04	0.2 ± 0.2	0.05 ± 0.06	0.02 ± 0.07	0.3 ± 0.4	97.2 ± 0.8	0.2 ± 0.4	1.7 ± 0.3	0.1 ± 0.1
	8–300	<0.1–0.46	<0.05–0.19	<0.03–0.65	<0.02–0.32	<0.02–0.53	<0.01–2.02	92.40–99.02	<0.05–3.43	0.99–4.16	<0.05–0.80
MA (40)	93 ± 69	0.1 ± 0.1	0.01 ± 0.02	0.2 ± 0.2	0.06 ± 0.06	0.01 ± 0.03	0.3 ± 0.4	97.1 ± 0.8	0.3 ± 0.5	1.7 ± 0.3	0.1 ± 0.2
	8–240	<0.1–0.37	<0.05–0.10	<0.03–0.71	<0.02–0.22	<0.02–0.12	<0.01–1.78	95.42–98.40	<0.05–1.80	1.31–2.40	<0.05–0.53
M (16)	49 ± 37	0.03 ± 0.06	0.01 ± 0.03	0.1 ± 0.2	0.06 ± 0.05	<0.02	0.4 ± 0.5	97.5 ± 0.5	0.1 ± 0.1	1.6 ± 0.4	0.02 ± 0.05
	10–100	<0.1–0.18	<0.05–0.11	<0.03–0.63	<0.02–0.19		<0.01–1.98	96.55–98.43	<0.05–0.26	0.70–2.20	<0.05–0.14
CMAF (163)	95 ± 96	0.1 ± 0.1	0.01 ± 0.04	0.2 ± 0.2	0.10 ± 0.09	0.04 ± 0.08	0.3 ± 0.4	97 ± 1	0.4 ± 0.6	1.7 ± 0.3	0.2 ± 0.2
	10–700	<0.1–0.52	<0.05–0.20	<0.03–0.67	<0.02–0.37	<0.02–0.51	<0.01–2.36	92.97–98.86	<0.05–2.85	1.14–2.90	<0.05–0.90
CMF (49)	113 ± 75	0.08 ± 0.09	0.01 ± 0.03	0.1 ± 0.1	0.09 ± 0.07	0.01 ± 0.03	0.2 ± 0.2	97.5 ± 0.7	0.2 ± 0.3	1.6 ± 0.2	0.07 ± 0.09
	20–280	<0.1–0.42	<0.05–0.12	<0.03–0.49	<0.02–0.33	<0.02–0.18	<0.01–0.87	95.48–98.72	<0.05–1.52	1.18–2.30	<0.05–0.35
CAF (6)	53 ± 77	0.1 ± 0.1	<0.05	0.2 ± 0.2	0.05 ± 0.09	<0.02	0.2 ± 0.3	96.6 ± 0.9	0.2 ± 0.4	1.6 ± 0.3	0.1 ± 0.2
	5–200	<0.1–0.27		<0.03–0.58	<0.02–0.22		<0.01–0.75	95.56–96.79	<0.05–1.06	1.08–2.00	<0.05–0.51
CMA (53)	95 ± 71	0.04 ± 0.07	0.00 ± 0.01	0.3 ± 0.2	0.10 ± 0.08	0.02 ± 0.07	0.3 ± 0.4	96.8 ± 0.8	0.3 ± 0.5	1.6 ± 0.2	0.1 ± 0.2
	20–350	<0.1–0.27	<0.05–0.07	<0.03–0.66	<0.02–0.31	<0.02–0.35	<0.01–1.31	94.31–98.23	<0.05–1.96	1.14–2.37	<0.05–0.63
CA (7)	40 ± 20	0.04 ± 0.08	<0.05	0.5 ± 0.2	0.11 ± 0.03	0.05 ± 0.05	0.1 ± 0.1	96.6 ± 0.6	0.5 ± 0.5	1.7 ± 0.2	0.1 ± 0.1
	20–60	<0.1–0.21		0.27–0.74	0.06–0.15	<0.02–0.11	<0.01–0.38	95.67–97.40	<0.05–1.14	1.35–1.82	<0.05–0.25
CM (4)	25 ± 7	0.03 ± 0.04	<0.05	0.1 ± 0.2	<0.02	<0.02	0.2 ± 0.2	96.9 ± 0.5	0.1 ± 0.2	1.6 ± 0.2	0.1 ± 0.1
	20–30	<0.1–0.10		<0.03–0.45			0.07–0.53	96.15–97.27	<0.05–0.34	1.43–1.78	<0.05–0.24
Phoscorite-related carbo-natite (43)	88 ± 75	0.06 ± 0.08	0.2 ± 0.7	0.3 ± 0.2	0.2 ± 0.4	0.1 ± 0.1	0.3 ± 0.5	96 ± 3	0.5 ± 0.7	2 ± 2	0.2 ± 0.2
	10–280	<0.1–0.35	<0.05–3.47	<0.03–0.85	<0.02–2.38	<0.02–0.52	<0.01–2.54	82.14–98.21	<0.05–2.94	1.10–12.02	<0.05–0.76
Vein carbo-natite (52)	37 ± 30	0.1 ± 0.1	0.02 ± 0.04	0.4 ± 0.3	0.1 ± 0.1	0.1 ± 0.1	0.4 ± 0.4	96 ± 1	0.7 ± 0.8	1.7 ± 0.4	0.3 ± 0.2
	2–100	<0.1–0.48	<0.05–0.19	<0.03–1.00	<0.02–0.43	<0.02–0.58	<0.01–1.80	93.16–98.18	<0.05–3.47	<0.2–3.37	<0.05–0.99
Mag–Dol–Phl–Srp rock (71)	81 ± 60	0.10 ± 0.08	0.01 ± 0.03	0.2 ± 0.2	0.1 ± 0.1	0.1 ± 0.2	0.3 ± 0.3	96.9 ± 0.9	0.4 ± 0.6	1.7 ± 0.3	0.2 ± 0.2
	5–220	<0.1–0.33	<0.05–0.13	<0.03–0.56	<0.02–0.29	<0.02–0.85	<0.01–1.48	93.66–98.46	<0.05–2.49	1.17–2.36	<0.05–1.00

A — apatite, F — forsterite, M — magnetite, C — carbonates (calcite and dolomite); *L* — mean length of grains. "<n" refers to value below limit of accuracy.

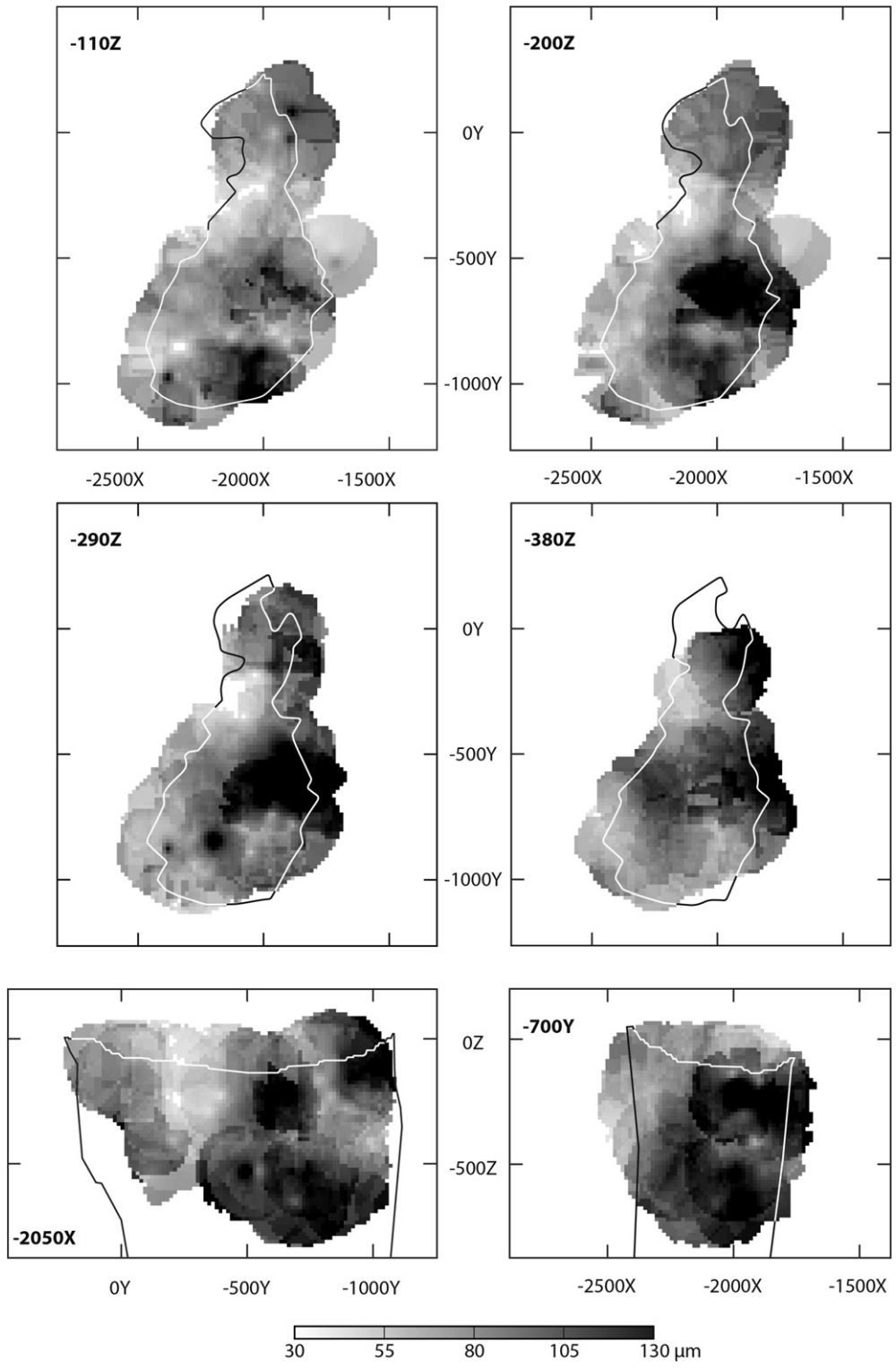

Fig. 18. Grain size distribution of baddeleyite within the phoscorite–carbonatite pipe (black/white contour).

Microprobe analyses of baddeleyite (Polyakov and Polezhaeva, 1991; Ivanyuk et al., 2002, 2013; Mikhailova et al., 2015; Kalashnikov et al., 2016) show low content of impurities, mainly, Hf, Nb, Fe^{3+} and Sc. Along the natural sequence of rocks – from early (apatite)-forsterite phoscorites through intermediate magneitite-(apatite-forsterite) phoscorites to late carbonate-(magnetite-apatite-forsterite) phoscorites and phoscorite-related carbonatites – baddeleyite gradually becomes richer in Hf, Nb, Ta and Sc due to Ti, Fe, Mg and Mn (Tables 6 and 7, Supplementary Data 4). Silicon is a typical component of baddeleyite in both early and late phoscorites (phoscorite-related carbonatites), while baddeleyite from intermediate low-carbonate magnetite-rich phoscorites carries minimal amounts of impurities.

The maximum content of most foreign inclusions in baddeleyite is accumulated in vein carbonatites: Ti, Ta, Nb, Sc, Ca and Sr. The latter two are probably associated with fine carbonate inclusions in baddeleyite. In the same way, the highest content of Mg in baddeleyite

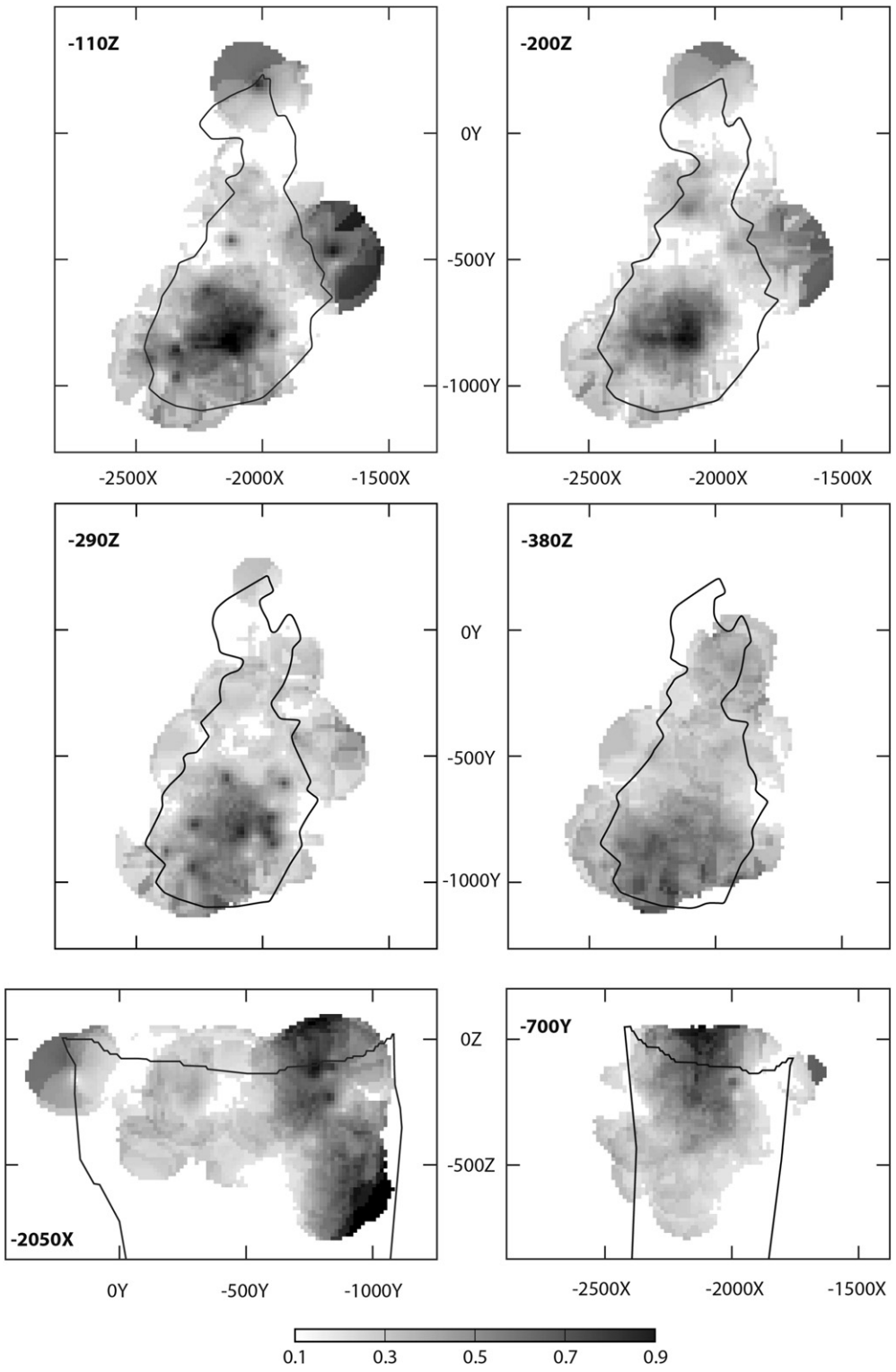

Fig. 19. Distribution of pyrochlore-baddeleyite intergrowths within the phoscorite–carbonatite pipe (black contour).

from host silicate rocks can be associated with the finest inclusions of Mg-silicates.

The spatial orderliness of baddeleyite composition reflects the basic patterns of isomorphism: $Zr^{4+} \leftrightarrow (Hf, Ti, Si)^{4+}$ and $2Zr^{4+} \leftrightarrow (Nb, Ta)^{5+} + Sc^{3+}$ (Figs. 20 and 21). The latter is especially important as it results in baddeleyite enrichment in Sc and accumulation of the secondary Sc-phosphates. Indeed, juonniite ($CaMgSc(PO_4)_2(OH)\cdot 4H_2O$) and some other secondary phosphates of scandium occur in large quantities in voids within phoscorites and carbonatites of the ore-pipe axial zone (Liferovich et al., 1997; Ivanyuk et al., 2002; Kalashnikov et al., 2016), especially in the regions with pure (self-refined) baddeleyite (Ivanyuk et al., 2012).

So the phoscorite–carbonatite pipe features distinct zoning in terms of grain sizes, composition and alteration of baddeleyite: early (apatite)-forsterite phoscorites of the marginal zone contain fine grains of baddeleyite rich in Si, Fe, Mg and Mn; carbonate-free magnetite-rich

Table 7
Baddeleyite formulae (atoms per formula unit) calculated on the basis O = 2 (mean ± SD/min–max).

Rock	Zr	Hf	Nb	Ta	Ti	Fe^{3+}	Sc	Si	Ca	Mg
Foidolite	0.97 ± 0.01	0.01	0.00	–	–	0.01 ± 0.01	–	–	0.00	0.01
	0.96–0.98	0.01–0.01	0.00–0.01			0.00–0.02			0.00–0.01	0.00–0.01
Diopsidite	0.98 ± 0.01	0.01	0.00	–	–	0.01 ± 0.01	–	–	0.00	0.00
	0.96–0.99	0.01–0.01	0.00–0.01			0.00–0.02			0.00–0.01	0.00–0.01
Phlogopitite	0.98 ± 0.01	0.01	0.00	–	–	0.00 ± 0.01	0.00	–	0.00	0.00
	0.95–0.99	0.01–0.01	0.00–0.01			0.00–0.02	0.00–0.01		0.00–0.01	0.00–0.01
F	0.98 ± 0.01	0.01	–	–	0.00 ± 0.01	0.01 ± 0.01	–	–	0.00	0.00
	0.96–0.98	0.01–0.01			0.00–0.01	0.00–0.04			0.00–0.01	0.00–0.01
AF	0.98 ± 0.01	0.01	0.00	–	–	0.01 ± 0.01	–	–	0.00	0.00
	0.95–0.99	0.00–0.01	0.00–0.01			0.00–0.03			0.00–0.01	0.00–0.02
MF	0.98	0.01	0.00	–	–	0.00	–	–	0.00	0.00
	0.98–0.99	0.01–0.01	0.00–0.01			0.00–0.01			0.00–0.01	0.00–0.01
MAF	0.98 ± 0.01	0.01	0.00	–	0.00	0.00 ± 0.01	0.00	–	0.00	0.00
	0.91–0.99	0.01–0.02	0.00–0.03		0.00–0.01	0.00–0.03	0.00–0.01		0.00–0.01	0.00–0.01
MA	0.98 ± 0.01	0.01	0.00	–	–	0.00 ± 0.01	–	–	0.00	0.00
	0.95–0.99	0.01–0.01	0.00–0.02			0.00–0.03			0.00–0.02	0.00–0.01
M	0.98 ± 0.01	0.01	–	–	–	0.01 ± 0.01	–	–	0.00	0.00
	0.96–0.99	0.00–0.01				0.00–0.03			0.00–0.01	0.00–0.01
CMAF	0.97 ± 0.01	0.01	0.00 ± 0.01	0.00	0.00	0.00 ± 0.01	0.00	–	0.01	0.00
	0.92–0.99	0.01–0.02	0.00–0.03	0.00–0.01	0.00–0.01	0.00–0.04	0.00–0.01		0.00–0.01	0.00–0.02
CMF	0.98 ± 0.01	0.01	0.00	–	–	0.00	0.00	–	0.00	0.00
	0.96–0.99	0.01–0.01	0.00–0.01			0.00–0.01	0.00–0.01		0.00–0.01	0.00–0.01
CAF	0.98 ± 0.01	0.01	0.00	–	–	0.00	–	–	0.01	0.00
	0.96–0.99	0.01–0.01	0.00–0.01			0.00–0.01			0.00–0.01	0.00–0.01
CMA	0.98 ± 0.01	0.01	0.00	–	0.00	0.01 ± 0.01	0.00	–	0.01	0.00
	0.95–0.99	0.01–0.01	0.00–0.02		0.00–0.01	0.00–0.02	0.00–0.01		0.00–0.01	0.00–0.01
CA	0.97 ± 0.01	0.01	0.00	–	–	0.01	–	–	0.01	0.01
	0.96–0.99	0.01–0.01	0.00–0.01			0.00–0.01			0.01–0.02	0.00–0.01
CM	0.98	0.01	–	–	–	0.00	–	–	0.00	–
	0.98–0.99	0.01–0.01				0.00–0.01			0.00–0.01	
Phoscorite-related carbonatite	0.97 ± 0.03	0.01 ± 0.01	0.00 ± 0.01	–	0.00	0.01 ± 0.01	0.00 ± 0.01	0.00 ± 0.01	0.01 ± 0.01	0.00
	0.83–0.99	0.01–0.07	0.00–0.03		0.00–0.01	0.00–0.04	0.00–0.04	0.00–0.07	0.00–0.02	0.00–0.01
Vein carbonatite	0.97 ± 0.01	0.01	0.01 ± 0.01	0.00	0.00	0.01 ± 0.01	0.00	–	0.01 ± 0.01	0.00
	0.92–0.98	0.00–0.02	0.00–0.03	0.00–0.01	0.00–0.01	0.00–0.03	0.00–0.01		0.00–0.02	0.00–0.01
Mag–Dol–Phl–Srp rock	0.97 ± 0.01	0.01	0.00 ± 0.01	0.00	0.00	0.00 ± 0.01	0.00		0.00	0.00
	0.92–0.99	0.01–0.01	0.00–0.02	0.00–0.01	0.00–0.01	0.00–0.02	0.00–0.01		0.00–0.01	0.00–0.01

phoscorites of the intermediate zone carry medium-sized grains of pure baddeleyite; late carbonate-rich phoscorites and carbonatites of the axial zone accommodate large-sized grains of Hf–Nb–Ta–Sc-rich baddeleyite partially or completely replaced by zirconolite and pyrochlore, and accompanied by the secondary scandium phosphates.

Chemical composition of the secondary zirconolite and pyrochlore widely varies by almost all components (Williams, 1996; Subbotin and Subbotina, 2000; Ivanyuk et al., 2002) and generally corresponds to $(Ca_{0.76}Ce_{0.09}La_{0.02}\ Mg_{0.06}Th_{0.04}Nd_{0.03}Mn_{0.02}Na_{0.02}Sr_{0.02}U_{0.01})_{\Sigma 1.07}Zr_{0.90}(Ti_{1.07}Nb_{0.54}Fe^{3+}_{0.34}Ta_{0.05}Si_{0.02})_{\Sigma 2.02}O_7$ for zirconolite; $(Ca_{0.69}U_{0.17}Ce_{0.07}Th_{0.06}Mg_{0.02}Sr_{0.02}Mn_{0.01}Ba_{0.01}Y_{0.01}La_{0.01})_{\Sigma 1.07}(Nb_{1.22}Ti_{0.38}Ta_{0.21}\ Fe^{3+}_{0.11}Zr_{0.04}Si_{0.02}\ Al_{0.01})_{\Sigma 1.99}O_6(OH)$ for pyrochlore. The natural rock series – from host foidolite, diopsidite and glimmerite through phoscorite to carbonatite – is distinguished by gradual growth of impurity content, which makes carbonate-rich phoscorites and carbonatites of the ore-pipe axial zone richer in U–La-rich pyrochlore and zirconolite. Presence of both minerals forms a higher radioactivity halo known as the Anomalous Zone (Ivanyuk et al., 2002). It should be noted that both pyrochlore and zirconolite are considered as harmful impurities that must be removed during acidic purification of the baddeleyite concentrate (Lebedev et al., 2006).

7. Ore processing optimization

Accurate product quality management requires information on spatial distribution of the parameters of economic, potentially economic and harmful minerals. The most important parameters are shown in Table 8.

Grain size of the economic minerals determines grinding parameters that provide a balance between a liberation degree and losses (Wills and Napier-Munn, 2006). Limits on MgO content in magnetite are specified according to the metallurgical conditions at the Cherepovets Steel Mill (PAO Severstal, Vologda Region, Russia) processing the Kovdor's magnetite concentrate. Aluminum and titanium found in magnetite are the alloying metals for steel, which can influence the metallurgical process. Tiny inclusions of spinel and ilmenite–geikielite in magnetite can, firstly, change physical and chemical properties of magnetite and, consequently, its behavior in mineral processing flow, and, secondly, disturb chemical composition of magnetite concentrate spoiling metallurgical process. The same can also be said about the intergrowths related to baddeleyite. Besides, the most widespread minerals intergrowing with baddeleyite are U-rich pyrochlore and zirconolite, which cause a need for deactivation of the baddeleyite concentrate. Strontium is a harmful impurity for phosphoric fertilizers, which are a final product of the apatite treatment. Apatite is also known as a concentrator of REEs, e.g., the world's largest apatite deposits in Khibiny (Murmansk Region, Russia) contain a huge amount of REE resources (Khramov, 2014). Therefore, estimation of REE content and its spatial distribution at the Kovdor deposit can show perspectives of the REE recovery here. Similarly, scandium and niobium in baddeleyite can be by-products of zirconium production (Kalashnikov et al., 2016).

The data obtained from the analyses provide an adequate basis for real-time and long-term forecasting of the ore quality, optimization of the ore processing and complex utilization of mineral resources. This data can be used for characterization of the general spatial trends as well as prediction of mineralogical characteristics and grain-size distribution of ore in any mining block. Prediction can be fulfilled with two independent methods that should ensure a cross-check. The first approach is based on geostatistical analysis of the key parameters: variography reveals correlation between the values variation within the deposit, then Kriging is used to predict variables between sampling points (i.e., interpolation). The second method enables us to identify

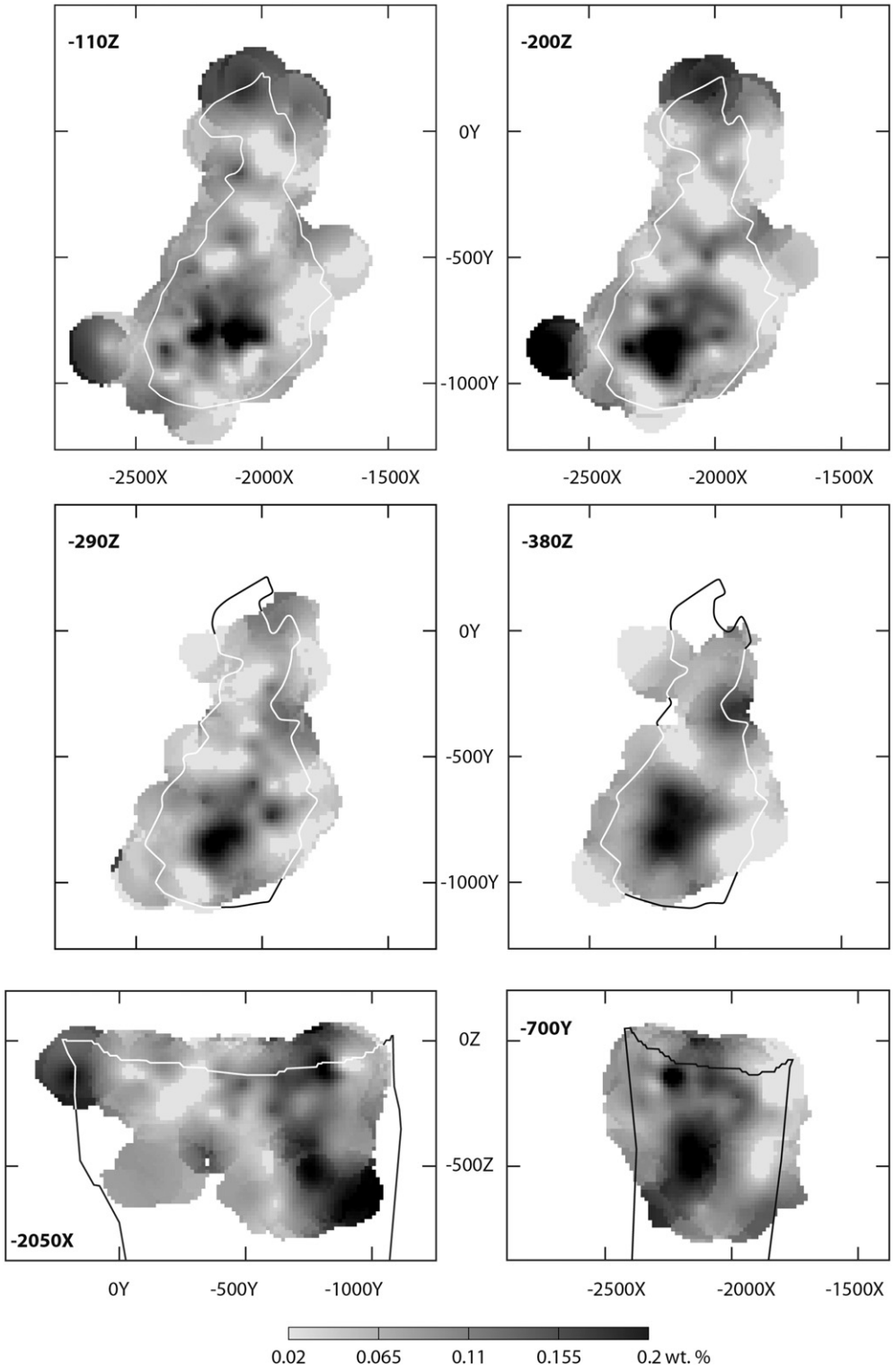

Fig. 20. Distribution of Sc_2O_3 in baddeleyite within the phoscorite–carbonatite pipe (black/white contour).

correlations between ordinary sampling data (supplementary exploration data) and mineralogical variables with multiple regressions.

The first method based on geostatistics employs a direct approach, which constitutes its main advantage. Accuracy of interpolation can be specified numerically by cross-checking, and taken into consideration during estimation of the ore properties. The disadvantage is a limited amount of mineralogical samples due to high cost and slowness. The volume of mineralogical samples is usually by an order of magnitude lesser than the volume of ordinary samples, and conventional exploration activities fail to enhance the accuracy of the ore characterization.

The second (regression-based) method has more advantages as it enables us to re-calculate regression formulae automatically, which ensures accuracy on a permanent basis and enhances efficiency of forecasts for a specific mining block. The disadvantage lies in approximation of multiple regression formulae, especially when it comes to comparatively small sets of variables in ordinary sampling. At JSC Kovdorskiy

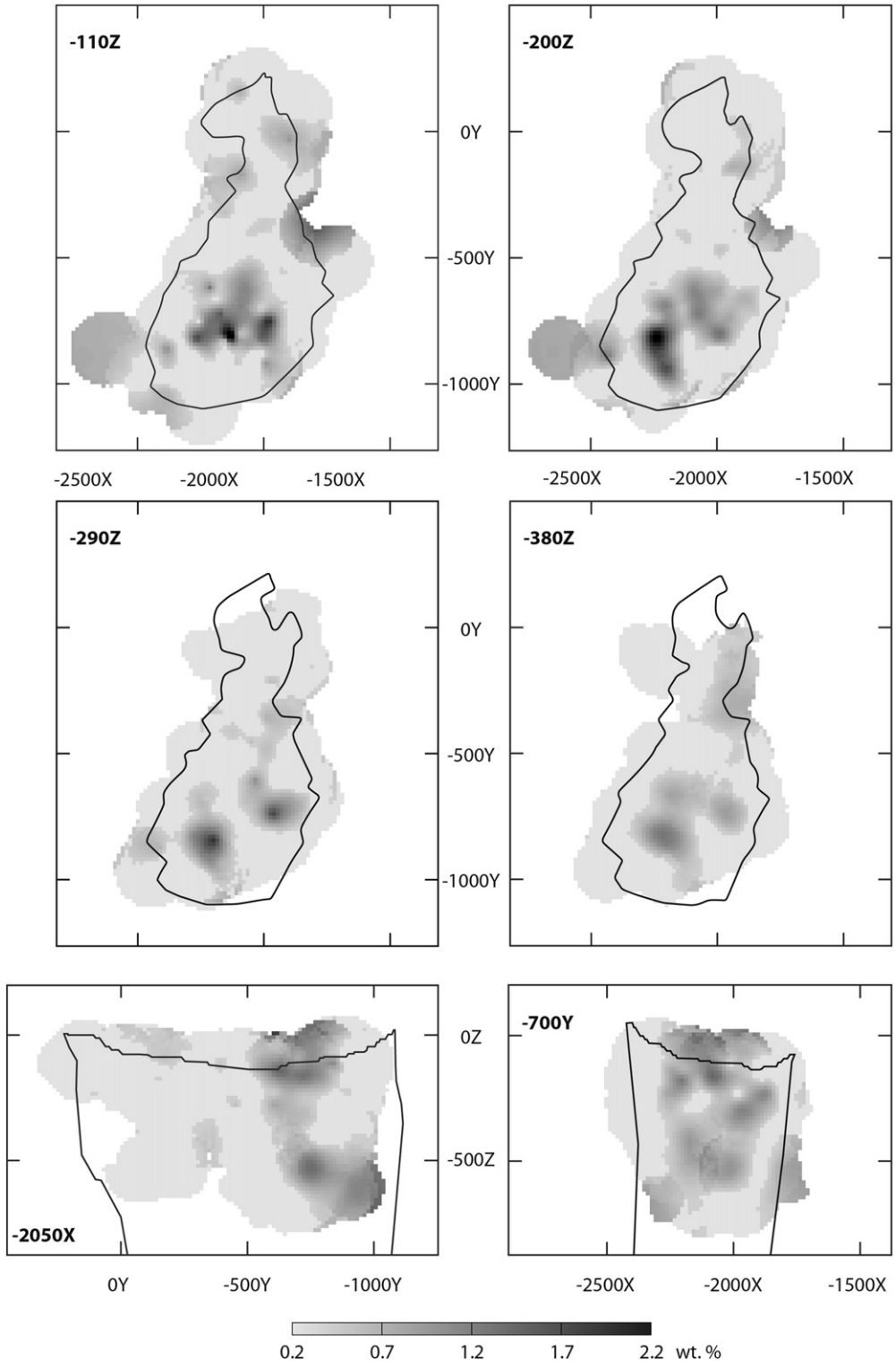

Fig. 21. Distribution of Nb_2O_5 in baddeleyite within the phoscorite–carbonatite pipe (black contour).

GOK, this set includes an analysis for 13 bulk rock components (SiO_2, TiO_2, ZrO_2, Al_2O_3, Fe_{total}, Fe_{Mag}, MgO, CaO, Na_2O, K_2O, P_2O_5, CO_2, S_{total}), and 6 components of magnetic fraction (TiO_2 m.f., Fe_{total} m.f., MgO m.f., ZnO m.f., P_2O_5 m.f. and S_{total} m.f.).

The most important application of the 3D mineralogical mapping of the Kovdor deposit becomes a prediction of magnesium content in magnetite, because it has significant influence on the metallurgical process. Metallurgical product of the highest quality requires a content of 3–5 wt.% MgO, required by the Cherepovets Steel Mill (PAO Severstal, Vologda Region, Russia) for Kovdor's magnetite concentrate. Deviations (both above and below these parameters) result in deterioration of the product quality or even metallurgical process failures. At the same time MgO content in magnetite can reach 8 wt.% (Table 1). Therefore, by knowing the spatial distribution of MgO in magnetite in the whole deposit, we can adjust the ore blending flow sheets to maintain the content within the required limits.

Table 8
Parameters of the economic minerals, important for mineral processing and end product technologies.

Mineral	Parameter	Cause
Magnetite	Grain size	Determines grinding limits
	MgO	Metallurgical condition
	Al_2O_3	Alloying dopant
	TiO_2	Alloying dopant
	Inclusions: mineral species and presence probability	Cause losses of magnetite
Apatite	Grain size	Determines grinding limits
	SrO	Harmful impurity
	REE_2O_3	Outlooks of by-product recovery
Baddeleyite	Grain size	Determines grinding limits
	Sc_2O_3	Outlooks of by-product recovery
	Nb_2O_3	Outlooks of by-product recovery
	Intergrowths: mineral species and presence probability	Cause losses of baddeleyite; may carry harmful impurities (uranpyrochlore)

The multiple regression equation for prediction of MgO content in magnetite is:

$$\begin{aligned}MgO_{Mag} = {} & -2.901 - 0.025(SiO_2) + 0.303(TiO_2) + 0.537(ZrO_2) \\ & + 0.314(Al_2O_3) - 0.027(Fe_{total}) + 0.078(Fe_{Mag}) + 0.075(MgO) \\ & + 0.052(CaO) - 0.310(Na_2O) - 0.114(K_2O) + 0.045\,(P_2O_5) \\ & + 0.016(CO_2) - 0.192(S_{total}) - 0.339(TiO_2\,m.f.) - 0.004(Fe_{total}\,m.f.) \\ & + 0.627(MgO\ m.f.) + 26.607(ZnO\ m.f.) - 2.021(P_2O_5\,m.f.) \\ & - 0.002(S_{total}\,m.f.).\end{aligned}$$

Quality of the forecast is estimated with the correlation coefficient $r = 0.71$. Consequently, spatial distribution of MgO in magnetite, predicted according to the above-mentioned equation in 250,000 mining blocks (Fig. 22), is close to that obtained by Kriging interpolation of real data (Fig. 9).

Similarly, calculation of the multiple regression for the forecast of REE_2O_3 content in apatite and Nb_2O_5 content in baddeleyite results in the following equations ($r = 0.69$ and 0.73, correspondingly):

$$\begin{aligned}REE_2O_{3\ Ap} = {} & 0.583 + 0.002(SiO_2) + 0.357(TiO_2) + 0.076(ZrO_2) \\ & + 0.066(Al_2O_3) - 0.005(Fe_{total}) + 0.002(Fe_{Mag}) + 0.006(MgO) \\ & + 0.009(CaO) - 0.086(Na_2O) - 0.133(K_2O) - 0.005\,(P_2O_5) - 0.001(CO_2) \\ & - 0.019(S_{total}) + 0.002(TiO_2\,m.f.) - 0.009(Fe_{total}\,m.f.) \\ & - 0.034(MgO\ m.f.) - 4.030(ZnO\ m.f.) - 0.040(P_2O_5\,m.f.) \\ & + 0.050(S_{total}\,m.f.);\end{aligned}$$

$$\begin{aligned}Nb_2O_{5\ Bdy} = {} & -0.525 - 0.028(SiO_2) + 1.367(TiO_2) + 0.415(ZrO_2) \\ & - 0.136(Al_2O_3) + 0.042(Fe_{total}) - 0.044(Fe_{Mag}) + 0.026(MgO) \\ & + 0.006(CaO) + 0.177(Na_2O) + 0.241(K_2O) + 0.012(CO_2) \\ & + 0.066(S_{total}) + 0.061(TiO_2\,m.f.) - 0.009(Fe_{total}\,m.f.) \\ & + 0.037(MgO\ m.f.) + 1.811(ZnO\ m.f.) - 0.104(P_2O_5\,m.f.) \\ & + 0.109(S_{total}\,m.f.).\end{aligned}$$

These and similar equations enable us to predict nearly all essential mineralogical characteristics of multicomponent ores with relatively high confidence, using the above-mentioned chemical data. Thus, the final block model of the Kovdor baddeleyite-apatite-magnetite deposit contains data on chemical composition of ores, rock-forming and accessory minerals, their grain-size distribution and other key variables (Table 8) for each of 250,000 blocks. Importantly, the simulated spatial distributions can be even more realistic and detailed than those obtained by Kriging interpolation of the real data as the scope of ordinary sampling is much larger.

8. Discussion

8.1. Origin of the pipe zonation

There are two main points of view on genesis of concentric zonation of the Kovdor phoscorite–carbonatite pipe. Most researchers believe that its zonation is the result of gradual crystallization of forsterite-phoscorites, magnetite-rich ones and then carbonatite-rich phoscorites and phoscorite-related carbonatites, directed from the pipe walls to its inner zone due to both cooling and degassing (pressure drop) of the fluid-rich magmatic column (Rimskaya-Korsakova, 1963; Kukharenko et al., 1965; Ternovoy et al., 1969; Kapustin, 1980; Dunaev, 1982; Ivanyuk et al., 2002; Afanasyev, 2011; Mikhailova et al., 2015). During crystallization, the volume of apatite and magnetite first gradually increases due to the earlier forsterite and then decreases due to development of carbonates, and every earlier mineral has been preserved as an inclusion or relict within grains and aggregates of later minerals (Rimskaya-Korsakova, 1963; Mikhailova et al., 2015). According to the alternative hypothesis, the pipe is considered to consist of steeply dipping and chaotically oriented veins of various rocks, with sharp contacts between them and insufficient influence of the later rock on the earlier ones (Krasnova and Kopylova, 1988; Rimskaya-Korsakova and Krasnova, 2002; Krasnova et al., 2004).

The first, "traditional" point of view on zonation of the Kovdor phoscorite–carbonatite pipe was confirmed by Mikhailova et al. (2015) based on our large petrographic and geological dataset. In particular, our studies showed clear intrusive relations between phoscorites and vein carbonatites, as well as gradual transition between all types of phoscorites and phoscorite-related carbonatites. We also believe that gradual concentric zonation of the pipe was formed due to both cooling and rapid degassing of a fluid-rich magmatic column and, then, by pneumatolytic and hydrothermal processes especially active within the axial zone of the pipe.

As you can see on Sections 4–6, the properties and composition of all economic minerals vary within the phoscorite–carbonatite pipe in accordance with the pipe regular petrographic zonation. In particular, comparatively fine grains of Mn–Ti-rich magnetite (with exsolution inclusions of ilmenite) of marginal (apatite)-forsterite phoscorites are replaced with coarse-to-giant grains of Mg–Al-rich magnetite (with exsolution inclusions of spinel) found in intermediate apatite-magnetite-(forsterite) phoscorites, with the latter being further replaced by moderately medium-to-coarse-grained Ti–V-rich magnetite (with exsolution inclusions of geikielite and Mg-rich ilmenite) of carbonate-rich phoscorites and phoscorite-related carbonatites.

By analogy, comparatively finely grained apatite with high content of impurities occurs in marginal (apatite)-forsterite phoscorites and axial carbonate-rich rocks, while medium-grained pure apatite is common to intermediate apatite-magnetite-(forsterite) phoscorites. Finally, comparatively fine grains of Fe–Ti-rich baddeleyite, found in

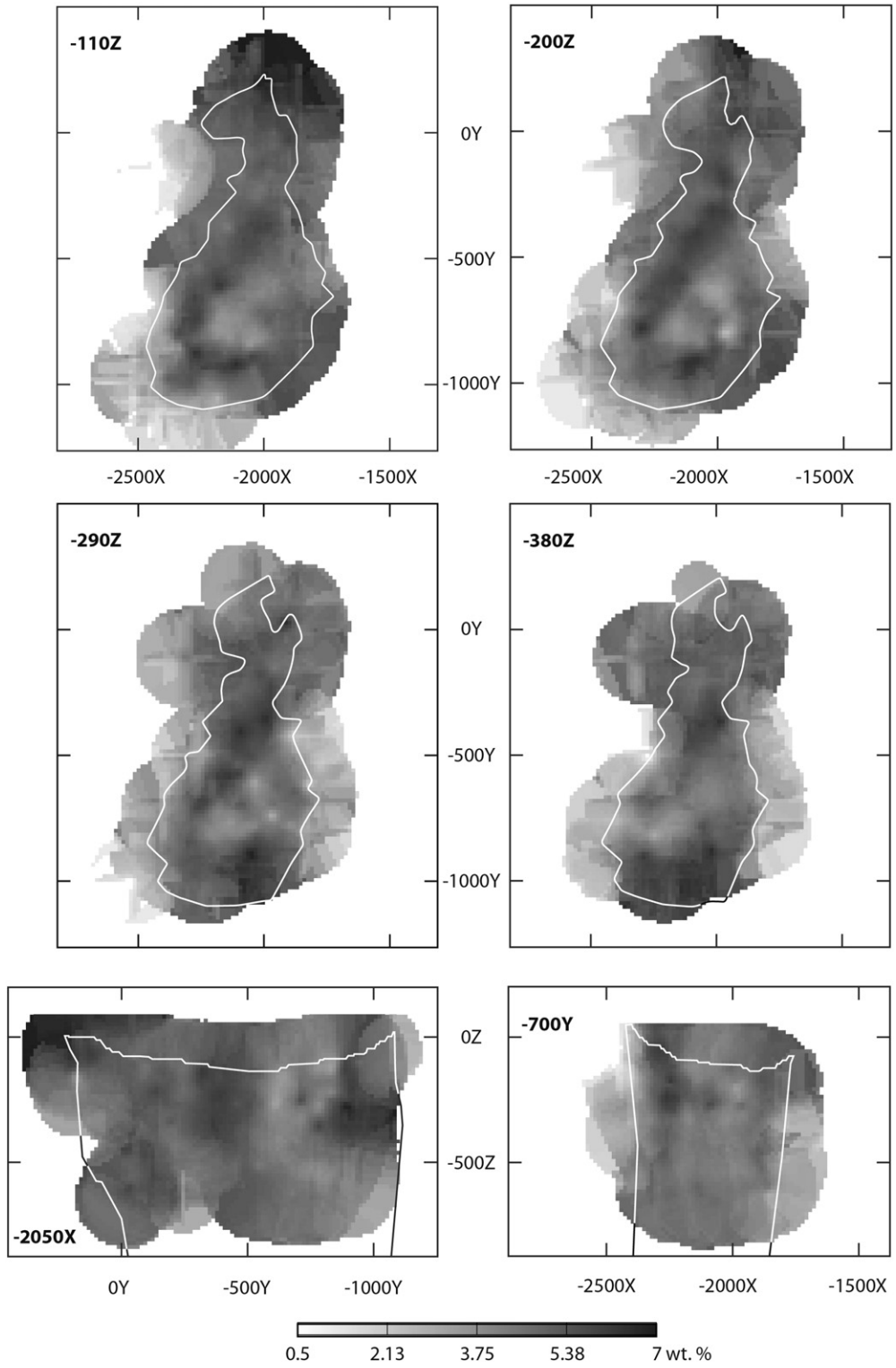

Fig. 22. Distribution of MgO in magnetite using results of multiple regression with regard to exploitation block samples. Solid lines show the phoscorite–carbonatite pipe boundary.

the ore-pipe marginal zone, become larger and purer in the intermediate zone, turning even larger and richer in Hf, Sc and Nb in the axial zone. Such mineralogical zonation is obviously caused by self-refining of rock-forming and accessory minerals from impurities, which is why all localities of the rare secondary minerals (quintinite, juonniite, numerous endemic phospates) lie within rocks characterized by the simplest modal composition and purest (without impurities and closest to theoretical composition) rock-forming and accessory minerals (Ivanyuk et al., 2012; Mikhailova et al., 2015).

8.2. Mineral processing

Recovery of economic minerals (especially apatite and baddeleyite) depends on many parameters such as grain size distribution, chemical

composition, presence of inclusions or intergrowths with other minerals and others (Bogdanovich and Pogankina, 1987). Solutions of some processing problems can be directly found in the mineralogical database and the 3D models. However, development of detailed interrelations between the properties of ore *in situ*, and parameters of mineral processing require additional studies. The 3D mineralogical mapping and database constitute a representative basis for further mapping intended to specify process flows for each mining block.

In the 1980s, the Kovdorskiy GOK developed methods connecting chemical composition of the ore and concentrate properties: regression equations based on Fe_{total}, $Fe_{magnetic}$, P_2O_5 and CO_2 content was derived for prediction of magnetite and apatite concentrate yields, Fe content in the magnetite concentrate and P_2O_5 content in apatite concentrate, and magnetite recovery factor (Riko et al., 1987). As a result, six types of ores were recognized, and, consequently, six processing flow sheets were developed. It allows a real-time adjustment of milling and flotation circuits, and, as a result, decreases losses of magnetite and apatite. However, processing parameters of the ore types do overlap, and regression parameters were not so accurate as the bulk chemical composition of the ores is not directly connected with physical properties of magnetite and apatite. Besides, properties of baddeleyite (or ZrO_2 in ore) were not taken into account in this system of equation. Nevertheless, combination of the above approach with 3D mineralogical mapping can overcome these disadvantages.

Direct advantages of the suggested 3D mineralogical mapping approach enable us, for example, to define the spatial distribution of MgO content in magnetite allowing to avoid a loss in magnetite concentrate quality. One more example is the specification of potentially commercial concentration of scandium. The suggested approach allows us to evaluate resources of the metal associated with baddeleyite and to identify the zones with Sc-rich baddeleyite and, probably, juonnaiite (Kalashnikov et al., 2016). Similarly, we can assess prospects of other elements contained in the currently recoverable minerals,e.g., niobium and hafnium in baddeleyite, REEs in apatite.

Apart from the Kovdor baddeleyite-apatite-magnetite deposit, there are some other deposits and occurrences of such type in the Murmansk Region related to the Seblyavr (Central Zone deposit), Vuoriyarvy (Tukhta-Vara and Neske-Vara deposits) and Sallanlatva alkaline-ultrabasic massifs (Afanasyev, 2011). All deposits are characterized by diverse mineralogy, especially mineralogy of rare metals, and by variable concentration of economic components. Implementation of the 3D mineralogical mapping alongside with the deposits exploration would allow us to increase its value and ensure more efficient use of mineral resources. We believe that application of the 3D mineralogical mapping can increase mining efficiency in most endogenous ore deposits with complex structure and heterogeneous composition. In addition, a large scope of geological, petrographic, geochemical, mineralogical and crystallographic data will ensure a sustainable foundation for constrained genetic reconstructions for any ore deposit.

9. Conclusions

The 3D mineralogical mapping of the Kovdor apatite-magnetite-baddeleyite deposit showed concentric zonation of the phoscorite–carbonatite pipe in terms of modal and chemical composition of rocks, grain size distribution, morphology, anatomy and chemical composition of extractable minerals (as described herein). Specifically, the marginal zone consists of (apatite)-forsterite phoscorites carrying fine grains of Mn–Ti–Si-rich magnetite with ilmenite exsolution lamellae, fine grains of apatite enriched in Fe and Mg and finest grains of baddeleyite with Mg, Fe, Si and Mn. The intermediate zone accommodates carbonate-free magnetite-rich phoscorites that carry medium to coarse grains of Mg–Al-rich magnetite with exsolution inclusions of spinel, medium-grained pure apatite and medium-sized crystals of pure baddeleyite. The axial zone hosts carbonate-rich phoscorites and phoscorite-related carbonatites, bearing medium-grained Ti–V–Ca-rich magnetite with exsolution inclusions of geikielite–ilmenite, fine grains of Ba–Sr-REE-rich apatite and comparatively large grains of baddeleyite, rich in Hf, Ta, Nb and Sc.

The study results allow us:

- to predict the variations in chemical and physical properties of ore and accessory minerals and to select the mineralogically suitable ores in accordance with the dressing technology requirements;
- to identify concentration zones of prospective components where by-product can be mined, in particular, scandium in baddeleyite and REEs in apatite;
- to develop a feasibility studies for other deposits of such type in the Murmansk Region (Seblyavr, Vuoriyarvy, Sallanlatva).

Future studies will be aimed to directly correlate physical and chemical properties of the ore in situ and the mineral processing methods.

Supplementary data to this article can be found online at http://dx.doi.org/10.1016/j.oregeorev.2016.02.008.

Acknowledgments

The research was undertaken as part of additional exploration of deep levels of the Kovdor deposit implemented by JSC Kovdorskiy GOK in 2007–11. The authors also received support from the Presidium of the Russian Academy of Sciences (Program #27), the Russian Foundation for Basic Research and the Murmansk Region Government (grant 12-05-98802) and Laplandia Minerals Ltd. (Apatity, Russia). The comments by anonymous reviewers and, particularly, Alexander Yakubchuk helped us to significantly improve this paper. We would also like to thank Prof. Franco Pirajno for his editorial assistance and encouragement.

References

Afanasyev, B.V., 2011. Mineral Resources of Alkaline-Ultrabasic Massifs of the Kola Peninsula. Roza Vetrov Publishing, Saint-Petersburg (in Russian). 152 p.

Amelin, Y., Zaitsev, A.N., 2002. Precise geochronology of phoscorites and carbonatites: the critical role of U-series disequilibrium in age interpretations. Geochim. Cosmochim. Acta 66, 2399–2419. http://dx.doi.org/10.1016/S0016-7037(02)00831-1.

Bayanova, T.B., Kirnarsky, Yu.M., Levkovich, N.V., 1997. U–Pb study of baddeleyite from Kovdor massif rocks. Dokl. Earth Sci. 356, 509–511 (in Russian).

Bogdanovich, V.V., Pogankina, T.N., 1987. Technological mineralogy for complex utilization of ores of the Kovdor deposit. Gorniy Zhurnal. 7, 9–12 (in Russian).

Chernysheva, L.V., Gaydukova, V.S., 1973. About late magnetite of carbonatites of the Kovdor deposit. Geologiya rudnykh mestorozhdeny 15, 106–109 (in Russian).

Dunaev, V.A., 1982. Structure of the Kovdor deposit. Geol. Ore Deposits 3, 28–36 (in Russian).

Eurochem, 2014. Annual report and accounts 2013. http://www.eurochemgroup.com/wp-content/uploads/2014/04/EuroChem-Annual-Report-2013-ENG1.pdf.

Gaydukova, V.S., Sokolov, S.V., Dubinchuk, V.T., Sidorenko, G.A., Il"yasov, A.M., 1984. About multistage decomposition of magnetite from iron ores of the Kovdor deposit. Mineralogichesky Zhurnal 6, 64–70 (in Russian).

Ivanyuk, G.Y., Yakovenchuk, V.N., Pakhomovsky, Y.A., 2002. Kovdor. Laplandia Minerals, Apatity (343 p).

Ivanyuk, G.Yu., Yakovenchuk, V.N., Pakhomovsky, Ya.A., 2012. Where are new minerals hiding? The main features of rare mineral localization within alkaline massifs. In: Krivovichev, S.V. (Ed.), Minerals as Advanced Materials II. Springer-Verlag, Berlin-Heidelberg, pp. 13–24 http://dx.doi.org/10.1007/978-3-642-20018-2_2.

Ivanyuk, G.Yu, Kalashnikov, A.O., Sokharev, V.A., Pakhomovsky, YaA., Bazai, A.V., Mikhailova, YuA., Konopleva, N.G., Yakovenchuk, V.N., Goryainov, P.M., 2013. Three-Dimensional Mineralogical Model of the Kovdor Magnetite-apatite-Baddeleyite Deposit. Vestnik of the Kola Science Centre of the Russian Academy of Sciences 4, 44–57 (in Russian).

Kalashnikov, A.O., Sokharev, V.A., Ivanyuk, G.Yu., Mikhailova, Yu.A., Pakhomovsky, Ya.A., Konopleva, N.G., Yakovenchuk, V.N., Bazai, A.V., 2012. The 3D mineralogical mapping of the Kovdor carbonatite-phoscorite complex. Proceedings of the IX Fersman's Scientific Session. K&M, Apatity, pp. 332–334 URL http://geoksc.apatity.ru/images/stories/Print/Fersman_2012.pdf (in Russian).

Kalashnikov, A.O., Yakovenchuk, V.N., Pakhomovsky, Y.A., Bazai, A.V., Sokharev, V.A., Konopleva, N.G., Mikhailova, J.A., Goryainov, P.M., Ivanyuk, G.Y., 2016. Scandium of the Kovdor baddeleyite–apatite–magnetite deposit (Murmansk Region, Russia): Mineralogy, spatial distribution, and potential resource. Ore Geol. Rev. 72, 532–537. http://dx.doi.org/10.1016/j.oregeorev.2015.08.017.

Kapustin, Yu.L., 1980. Mineralogy of Carbonatites. Amerind Publishing, New Delhi (288 p).

Khramov, D.G. (Ed.), 2014. On Condition and Use of Mineral Resources of the Russian Federation in 2013, State Report. Ministry of Natural Resources of the Russian

Federation, Moscow (URL http://www.mnr.gov.ru/regulatory/detail.php?ID=140744. (in Russian) 384 p).
Kopylova, L.N., Krasnova, N.I., Martovitskaya, N.A., Poritskaya, L.G., 1980. Typical chemical features of calcite and baddeleyite of the Kovdor complex deposit. Shchelochnoi Magmatizm I apatitonosnost' Severa Sibiri (Alkaline Magmatism and Apatite in the North Siberia). Nauka, Leningrad, pp. 124–138 (in Russian).
Kopylova, L.N., Krasnova, N.I., Sulimov, B.I., 1985. A new type of ores of the Kovdor complex deposit. Petrologiya I Minerageniya Shchelochno-Ultraosnovnykh I Karbonatitovykh Kompleksov Karelo-Kol'skogo Regiona (Petrology and Mineragеny of Alkaline-Ultrabasic and Carbonatite Complexes of the Karelia-Kola Region). Kol'sky filial AN SSSR Publishing, Apatity, pp. 69–76 (in Russian).
Krasnova, N.I., 1979. Geology, mineralogy and problem of genesis of apatite-francolite rocks of the Kovdor massif. Veshchestvenny Sostav Phosphoritov (Composition of Phosphorites). Nauka, Novosibirsk, pp. 164–172 (in Russian).
Krasnova, N.I., Kopylova, L.N., 1988. The geologic basis for mineral-technological mapping at the Kovdor ore deposit. Int. Geol. Rev. 30, 307–319. http://dx.doi.org/10.1080/00206818809466011.
Krasnova, N.I., Krezer, Yu.L., 1995. New data on the nature of fine and ultrafine lamellae in titanomagnetite. Eur. J. Mineral. 7, 1361–1372.
Krasnova, N.I., Balaganskaya, E.G., Garcia, B., 2004. Kovdor — classic phoscorites and carbonatites. In: Wall, F., Zaitsev, A.N. (Eds.), Phoscorites and Carbonatites from Mantle to Mine: the Key Example of the Kola Alkaline ProvinceMineralogical Society Series 10. Mineralogical Society, London, pp. 99–132.
Krivovichev, S.V., Yakovenchuk, V.N., Zhitova, E.S., Zolotarev, A.A., Pakhomovsky, Ya.A., Ivanyuk, G.Yu., 2010a. Crystal chemistry of natural layered double hydroxides. 1. Quintinite-2*H*-3*c* from Kovdor alkaline massif, Kola peninsula, Russia. Mineral. Mag. 74, 821–832. http://dx.doi.org/10.1180/minmag.2010.074.5.821.
Krivovichev, S.V., Yakovenchuk, V.N., Zhitova, E.S., Zolotarev, A.A., Pakhomovsky, Ya.A., Ivanyuk, G.Yu., 2010b. Crystal chemistry of natural layered double hydroxides. 2. Quintinite-1M: first evidence of monoclinic polytype in M^{2+}–M^{3+} layered double hydroxides. Mineral. Mag. 74, 833–840. http://dx.doi.org/10.1180/minmag.2010.074.5.833.
Kukharenko, A.A., Orlova, M.P., Bulakh, A.G., Bagdasarov, E.A., Rimskaya-Korsakova, O.M., Nefedov, E.I., Il'inskiy, G.A., Sergeev, A.S., Abakumova, N.B., 1965. The Caledonian Complex of the Ultrabasic, Alkaline Rocks and Carbonatites of the Kola Peninsula and Northern Karelia (Geology, Petrology, Mineralogy and Geochemistry). Nedra, Moscow (in Russian). 772 p.
Kurbatova, G.S., 1972. Apatitization of olivinite and ijolite of the Kovdor massif. Materialy Po Mineralogii Kol'skogo Poluostrova (Data on the Mineralogy of the Kola Peninsula) 9. Nauka, Leningrad, pp. 53–58 (in Russian).
Kurbatova, G.S., 1974. Typomorphic features of apatite of the Kovdor massif. Shchelochnye Porody Kol'skogo Poluostrova (Alkaline Rocks of the Kola Peninsula). Nauka, Leningrad, pp. 129–139 (in Russian).
Kurbatova, G.S., 1986. Apatite of complex ores from deep horizons of the Kovdor apatite-magnetite deposit. Non-Metallic Raw Material Deposits of the Kola Peninsula. Kola Branch of the USSR Academy of Sciences Publishing, Apatity, pp. 39–43 (in Russian).
Kurbatova, G.S., Gannibal, L.F., Dudkin, O.B., 1972. Composition and genesis of francolite breccia of the Kovdor massif. Dokl. Akad. Nauk SSSR 207, 1208–1211 (in Russian).
Lebedev, V.N., Lokshin, E.P., Barmin, I.S., Akhmetshina, L.N., Zabal'sky, D.V., 2006. Baddeleyite concentrate cleaning with diluted acids. Obogashchenie Rud 5, 16–19 (in Russian).
Le Maitre, R.W. (Ed.), 2002. Igneous Rocks. A Classification and Glossary of Terms. Recommendations of the International Union of Geological Sciences Subcommission on the Systematics of Igneous Rocks. Cambridge University Press, New York.
Liferovich, R.P., Yakovenchuk, V.N., Pakhomovsky, Ya.A., Bogdanova, A.N., Britvin, S.N., 1997. Juonniite, a new mineral of scandium from calcite–dolomite carbonatites of the Kovdor massif. Zap. Vses. Mineral. O-va. 126, 56–63 (in Russian).
Lotter, N.O., Kowal, D.L., Tuzun, M.A., Whittaker, P.J., Kormos, L., 2003. Sampling and flotation testing of Sudbury Basin drill core for process mineralogy modelling. Miner. Eng. 16, 857–864. http://dx.doi.org/10.1016/S0892-6875(03)00207-3.
Mercus, H.G., 2009. Particle Size Measurements – Fundamentals, Practice, Quality. Springer.
Mikhailova, Yu.A., Krasnova, N.I., Kretser, YuL, Wall, F., Pakhomovsky, Ya.A., 2002. Inclusions in minerals of the Kovdor intrusion of ultrabasic, alkaline rocks and carbonatites as indicators of the endogenic evolution processes. In: Vladykin, N.V. (Ed.), Deep-Seated Magmatism, Magmatic Sources and the Problem of Plumes. Siberian Branch of RAS, Irkutsk–Vladivostok, pp. 296–320 (in Russian).
Mikhailova, J.A., Kalashnikov, A.O., Sokharev, V.A., Pakhomovsky, Y.A., Konopleva, N.G., Yakovenchuk, V.N., Bazai, A.V., Goryainov, P.M., Ivanyuk, G.Y., 2015. 3D mineralogical mapping of the Kovdor phoscorite–carbonatite complex (Russia). Mineral. Deposita 51, 131–149. http://dx.doi.org/10.1007/s00126-015-0594-z.
Polyakov, K.I., Polezhaeva, L.I., 1991. Peculiarity of chemical composition and physical properties of baddeleyite from Kovdor deposit. New Data in the Field of Rare-Element Mineralogy of the Kola Peninsula. Kola Science Centre of the Academy of Science of the USSR Publishing, Apatity, pp. 45–48 (in Russian).
Riko, V.T., Shaposhnikov, V.A., Anikeeva, T.F., 1987. Geologic-technologic mapping of the Kovdor deposit of complex ore. Gorniy Zhurnal. 7, 9–12 (in Russian).
Rimskaya-Korsakova, O.M., 1950. A question about regular intergrowths of spinel with magnetite. 89, 178–190 (in Russian).
Rimskaya-Korsakova, O.M., 1963. On Question about Genesis of the Kovdor Iron-Ore Deposit, in: Problems of Magmatism and Metamorphism. Leningrad State University Publishing, Leningrad, pp. 125–142 (in Russian).
Rimskaya-Korsakova, O.M., Dinaburg, I.B., 1964. Baddeleyite in massifs of ultrabasic and alkaline rocks of the Kola Peninsula. Mineralogy and Geochemistry 1. Leningrad State University Publishing, Leningrad, pp. 13–30 (in Russian).
Rimskaya-Korsakova, O.M., Krasnova, N.I., 2002. Geology of the Deposits of Kovdor Massif. St. Petersburg University Press (in Russian). 146 p.
Rimskaya-Korsakova, O.M., Vasil'eva, Z.V., Ryzhova, R.I., Sokolova, E.P., 1968. Apatites of the Kovdor massif. Mineralogiya I Geokhimiya (Mineralogy and Geochemistry) 3. Leningrad State University Publishing, Leningrad, pp. 82–86 (in Russian).
Rimskaya-Korsakova, O.M., Krasnova, N.I., Kopylova, L.N., 1979. Typical chemical features of apatite of the kovdor complex deposit. Mineralogiya I Geokhimiya (Mineralogy and Geochemistry) 6. Leningrad State University Publishing, Leningrad, pp. 58–70 (in Russian).
Rodionov, N.V., Belyatsky, B.V., Antonov, A.V., Kapitonov, I.N., Sergeev, S.A., 2012. Comparative in-situ U–Th–Pb geochronology and trace element composition of baddeleyite and low-U zircon from carbonatites of the Palaeozoic Kovdor alkaline–ultramafic complex, Kola Peninsula, Russia. Gondwana Res. 21, 728–744. http://dx.doi.org/10.1016/j.gr.2011.10.005.
Streckeisen, A., 1974. Classification and nomenclature of plutonic rocks recommendations of the IUGS subcommission on the systematics of Igneous Rocks. Geol. Rundsch. 63, 773–786. http://dx.doi.org/10.1007/BF01820841.
Subbotin, V.V., Subbotina, G.F., 2000. Minerals of the Pyrochlore Group in Phoscorites and Carbonatites of the Kola Peninsula. Vestnik of the Murmansk State Technical University 3, 273–284 (in Russian).
Ternovoy, V.I., 1977. Carbonatite Massifs and their Ores. Leningrad State University Publishing, Leningrad (in Russian). 168 p.
Ternovoy, V.I., Afanasyev, B.I., Sulimov, B.I., 1969. Geology and Exploring of the Kovdor Vermiculite–Phlogopite Deposit. Nedra, Leningrad (in Russian). 287 p.
Volotovskaya, N.A., 1952. Petrology of Kovdorozerskiy Massif of Ultrabasic, Alkaline and Carbonate Rocks Unpublished Ph.D. theses Leningrad State University (in Russian).
Volotovskaya, N.A., 1958. The Kovdorskiy Massif. In: L.Ya., Kharitonov (Ed.)Geology of USSR XXVII, pp. 419–428 (in Russian).
Wall, F., Zaitsev, A.N. (Eds.), 2004. Phoscorites and Carbonatites from Mantle to Mine: the Key Example of the Kola Alkaline ProvinceMineralogical Society Series 10. Mineralogical Society, London (498 pp).
Williams, C.T., 1996. The occurrence of niobian zirconolite, pyrochlore and baddeleyite in the Kovdor carbonatite complex, Kola Peninsula, Russia. Min. Mag. 60, 639–646.
Wills, B.A., Napier-Munn, T., 2006. Wills' Mineral Processing Technology. seventh ed. Elsevier Science & Technology Books (444 p).
Yegorov, L.S., 1993. Phoscorites of the Maymecha-Kotuy ijolite–carbonatite association. Int. Geol. Rev. 35, 346–358. http://dx.doi.org/10.1080/00206819309465533.
Zaitsev, A.N., Terry Williams, C., Jeffries, T.E., Strekopytov, S., Moutte, J., Ivashchenkova, O.V., Spratt, J., Petrov, S.V., Wall, F., Seltmann, R., Borozdin, A.P., 2014. Rare earth elements in phoscorites and carbonatites of the Devonian Kola Alkaline Province, Russia: examples from Kovdor, Khibina, Vuoriyarvi and Turiy Mys complexes. Ore Geol. Rev. 61, 204–225. http://dx.doi.org/10.1016/j.oregeorev.2014.02.002.
Zhitova, E.S., Yakovenchuk, V.N., Krivovichev, S.V., Zolotarev, A.A., Pakhomovsky, Ya.A., Ivanyuk, G.Yu., 2010. Crystal chemistry of natural layered double hydroxides. 3. The crystal structure of Mg, Al-disordered quintinite-2H. Mineral. Mag. 74, 841–848. http://dx.doi.org/10.1180/minmag.2010.074.5.841.